

Aus dem Zentrum für Innere Medizin der Universität zu Köln  
Klinik und Poliklinik für Innere Medizin I  
Direktor: Universitätsprofessor Dr. med. M. Hallek

# **Effects of Genotoxic Stress on Macrophage Phenotype and Phagocytic Capacity**

Inaugural-Dissertation zur Erlangung der Doktorwürde  
der Medizinischen Fakultät  
der Universität zu Köln

vorgelegt von  
Henning Dieter Feldkötter  
aus Ibbenbüren

promoviert am 29.02.2024



Dekan: Universitätsprofessor Dr. med. G. R. Fink  
1. Gutachter: Universitätsprofessor Dr. med. C. Pallasch  
2. Gutachter: Professor Dr. rer. nat. L. Eichinger

## Erklärung

Ich erkläre hiermit, dass ich die vorliegende Dissertationsschrift ohne unzulässige Hilfe Dritter und ohne Benutzung anderer als der angegebenen Hilfsmittel angefertigt habe; die aus fremden Quellen direkt oder indirekt übernommenen Gedanken sind als solche kenntlich gemacht.

Bei der Auswahl und Auswertung des Materials sowie bei der Herstellung des Manuskriptes habe ich keine Unterstützungsleistungen erhalten.

Weitere Personen waren an der Erstellung der vorliegenden Arbeit nicht beteiligt. Insbesondere habe ich nicht die Hilfe einer Promotionsberaterin/eines Promotionsberaters in Anspruch genommen. Dritte haben von mir weder unmittelbar noch mittelbar geldwerte Leistungen für Arbeiten erhalten, die im Zusammenhang mit dem Inhalt der vorgelegten Dissertationsschrift stehen.

Die Dissertationsschrift wurde von mir bisher weder im Inland noch im Ausland in gleicher oder ähnlicher Form einer anderen Prüfungsbehörde vorgelegt.

Die in dieser Arbeit angegebenen Experimente sind nach entsprechender Anleitung durch Frau Dr. rer. nat. Daniela Vorholt von mir selbst ausgeführt worden. Vor der Aufnahme der mikroskopischen Bilder wurde ich von Herrn Dr. Christian Jüngst in die Bedienung des Mikroskops eingewiesen und Herr Peter Zentis hat mich bezüglich der Auswertung der Aufnahmen beraten. Zur Auswertung der mikroskopischen Bilder wurden die Programme ImageJ und Fiji benutzt. Für die Berechnung der Signifikanzen und Darstellung der Diagramme wurde das Programm GraphPad PRISM benutzt.

## Erklärung zur guten wissenschaftlichen Praxis:

Ich erkläre hiermit, dass ich die Ordnung zur Sicherung guter wissenschaftlicher Praxis und zum Umgang mit wissenschaftlichem Fehlverhalten (Amtliche Mitteilung der Universität zu Köln AM 132/2020) der Universität zu Köln gelesen habe und verpflichte mich hiermit, die dort genannten Vorgaben bei allen wissenschaftlichen Tätigkeiten zu beachten und umzusetzen.

Köln, den 03.09.2022

Unterschrift: .....

# Acknowledgment

Many people helped and supported me throughout this work, without whom I could not have achieved my goals.

First and foremost, I would like to thank Prof. Dr. Christian Pallasch for giving me the opportunity to work on this interesting and challenging project. With his great scientific knowledge and calm as well as encouraging nature, he always was a great support.

Furthermore, I am very grateful for the support and mentoring by Dr. Daniela Vorholt, who taught me a lot about scientific work, in practical as well as theoretical regards. Thank you for your enlightening ideas and great patience while supervising me.

A special thank you is due to Dr. Stuart Blackemore, who helped me during my writing process with his experience and great notes. I will always appreciate the time you took to support me with my writing, although we only worked briefly together in the laboratory.

In addition, I would like to express my gratitude for Prof. Dr. Michael Hallek for providing me the chance to work in his laboratory.

I thank the remaining members of AG Pallasch for always sharing their ideas and creating a great atmosphere in our working group. Also, I wish to thank the members of AG Hallek, AG Frenzel and AG Krause for the nice atmosphere at work as well as the great times we had inside and outside of the laboratory.

Also, I would like to mention the CECAD imaging facility, especially Dr. Christian Jüngst and Peter Zentis. Thank you for your support and insight regarding microscopy and image analysis.

Finally, I thank my family and friends for their ongoing support and encouragement. Especially I would like to thank my brother, Daniel Feldkötter, for his continues support throughout my time in the laboratory and during the writing process, as well as my former roommates, Sinika Henschke and René Neuhaus, for their support during the challenging times of my work.

# Table of content

<b>Abbreviations</b>	<b>8</b>
<b>1 Abstract of Dissertation</b>	<b>14</b>
<b>2 Zusammenfassung</b>	<b>15</b>
<b>3 Introduction</b>	<b>16</b>
3.1 Immune system	16
3.1.1 Innate immune system	16
3.1.2 Adaptive immune system	18
3.2 Macrophages	21
3.2.1 Heterogeneity and Polarisation	21
3.2.2 Phagocytosis	24
3.3 Cancer	26
3.3.1 Tumor microenvironment	27
3.3.2 Tumor associated macrophages	30
3.4 DNA Damage Response	32
3.5 Immunological effects of chemotherapy	37
3.6 Aim of Research	39
<b>4 Materials and Methods</b>	<b>40</b>
4.1 Materials	40
4.1.1 Devices	40
4.1.2 Disposable Materials	42
4.1.3 Chemicals and substances	43
4.1.3.1 General	43
4.1.3.2 Western Blot	44
4.1.3.3 Confocal Microscopy	45
4.1.3.4 Cell culture	45
4.1.4 Buffer, Media and Solution composition	46
4.1.5 Kits	47
4.1.6 Agents	47
4.1.6.1 Chemotherapeutics	47
4.1.6.2 MDM2 Inhibitor	47
	4

4.1.7	Antibodies	47
4.1.7.1	Primary Antibodies	47
4.1.7.2	Secondary Antibodies	48
4.1.7.3	Fluochrome Conjugated Antibodies	48
4.1.8	Cell Lines and Bacterial Strains	48
4.1.8.1	Cell Lines	48
4.1.8.2	Bacterial Strains	48
4.1.9	Software	48
4.2	Methods	50
4.2.1	Cell culture	50
4.2.2	CellTiter-Glo viability assay	50
4.2.3	Measurement of protein levels	51
4.2.3.1	Generation of cell lysates	51
4.2.3.2	Measuring protein amount by Pierce BCA protein assay kit	51
4.2.3.3	SDS polyacrylamide gel electrophoresis (SDS-PAGE)	51
4.2.3.4	Western blotting (WB)	52
4.2.4	Confocal Microscopy	53
4.2.4.1	Preparation of conditions	53
4.2.4.2	Analysis	54
4.2.5	Phagocytosis assays	55
4.2.5.1	Non-opsonised phagocytosis assay based on Mycobacterium bovis strain Bacille Calmette-Guérin (BCG)	55
4.2.5.2	Opsonised Fc-independent phagocytosis assay based on pH-sensitive beads	56
4.2.5.3	Evaluation of the bacteria to macrophage and bead to macrophage impact on the phagocytosis rate	57
4.2.5.4	Modification to the BCG and pH-sensitive bead phagocytosis assay	58
4.2.5.5	Generation of conditioned medium	58
4.2.6	Statistical analysis and data illustration	59
<b>5</b>	<b>Results</b>	<b>60</b>

5.1	Murine macrophage viability decreases dose-dependently when treated with Mafosfamide or Doxorubicin	60
5.2	Mafosfamide and Doxorubicin induced p53 expression and phosphorylation	61
5.3	Mafosfamide and Doxorubicin induce phenotypical and phagocytic changes in murine macrophages	64
5.4	High concentrations of Mafosfamide and Doxorubicin increase the non-opsonised phagocytic capacity of murine macrophages	69
5.5	The phagocytosis rate was dependent on the bacteria to macrophage ratio	70
5.6	Lower concentrations of Mafosfamide and Doxorubicin seem to have a positive effect on non-opsonised phagocytosis of murine macrophages	71
5.7	Modification of the BCG-phagocytosis assay resolves bacteria to macrophage differences	73
5.8	Positive effect on non-opsonised phagocytic capacity of Doxorubicin was conveyed by soluble factors	75
5.9	Phagocytosis rate was dependent on pH-sensitive bead to macrophage ratio	76
5.10	Phagocytosis of pH-sensitive beads was enhanced by Mafosfamide and Doxorubicin	77
5.11	In a modified pH-sensitive bead phagocytosis assay, Mafosfamide and Doxorubicin have a positive effect on phagocytic capacity	80
<b>6</b>	<b>Discussion</b>	<b>82</b>
6.1	Chemotherapy treatment induced phenotypical changes in macrophages which suggested a more phagocytically active phenotype.	83
6.2	Direct chemotherapy treatment increased opsonised and non-opsonised Fc-independent phagocytic capacity of macrophages.	85
6.3	Soluble factors conveyed the positive effect of Doxorubicin, suggesting the induction of a secretory phenotype in macrophages	92
6.4	Outlook	96
<b>7</b>	<b>References</b>	<b>98</b>
<b>8</b>	<b>Appendices</b>	<b>125</b>
8.1	Supplemental Data	125
8.1.1	Supplemental WB	125
8.1.2	Supplemental figure of bacteria to macrophage ratio dependency	126
8.1.3	Supplemental figure of bead to macrophage ratio dependency	126
8.1.4	Modification to the BCG-phagocytosis assay	127
8.1.4.1	Method	127
8.1.4.2	Results	127

8.1.4.3	Discussion	130
8.2	List of Tables	132
8.3	List of Figures	133

## Abbreviations

ADCP	Antibody-dependent cellular phagocytosis	BCR	B cell receptor
ALL	Acute lymphocytic leukaemia	BER	Base excision repair
AML	Acute myeloid leukaemia	BSA	Bovine Serum Albumin
AMP	Anti-microbial peptide	CAFs	Cancer-associated fibroblasts
ANG2	Angiopoietin 2	CBP/p300	CREB-binding protein
APPs	Acute phase proteins	CCL2	CC-chemokine ligand 2
APS	Ammonium Persulfate	CD	Cluster of differentiation
Arg	Arginase	Cdc25A/B/C	Cell division cycle 25 A/B/C
ASAP	acute secretory activating phenotype	CDK2	Cyclin-dependent kinase 2
AT	Ataxia Telangiectasia	CHK1/2	Checkpoint kinase 1/2
ATM	Ataxia-telangiectasia mutated kinase	CHOP scheme	Cyclophosphamide, Doxorubicin, Vincristine and Prednisolone scheme
ATR	Ataxia- and Rad3-related kinase	CLL	Chronic lymphocytic leukaemia
ATRIP	Ataxia- and Rad3-related kinase interacting protein	cm	Centimeter
BAX	bcl-2-like protein 4	CML	Chronic myeloid leukaemia
BCG	Bacille Calmette-Guerin	CO <sub>2</sub>	Carbon dioxide

CR	Complement receptors	DMSO	Dimethylsulphoxide
CRISPR/ Cas method	Clustered Regularly Interspaced Short Palindromic Repeats/CRIPSR- associated method	DNA	Deoxyribonucleic acid
		DPBS	Dulbecco's Balanced Salt Solution
		DSBs	Double-strand breaks
CRP	C-reactive protein	DTT	1.4-Dithiothreit
CS	Cockayne syndrome	ECM	Extracellular matrix
CSCs	cancer stem cells	EDTA	Ethylendiamine Tetra Acetic Acid
CSF-1	Colony stimulating factor 1	EGF	Epithelial growth factor
CTLs	Cytolytic T lymphocytes	EMT	Epithelial-to- mesenchymal transition
DAMPs	Danger-associated molecular patterns	ERK	Extracellular signalregulated kinase
DANN-PK	DNA-dependent protein kinase	FACS	Fluorescence- activated cell sorting
DAPI	4',6'-Diamidin-2- phenylindol	FBS	Fetal Bovine Serum
DCs	Dendritic cells	FC scheme	Fludarabine and Cyclophosphamide scheme
DDR	DNA damage response	FcR	Fc-receptor
DLBCL	Diffuse large B-cell lymphoma	FGF2	Fibroblast growth factor 2
DMEM	Dulbecco's Modified Eagle Medium		

FITC	Fluorescein-5- isothiocyanat	hMB	humanized mouse model MYC/Bcl2
FSC	Forward-scatter	hMof	Human males absent on the first
FSC-H	Forward-scatter hight	HR	Homologues recombination
FSC-W	Forward-scatter width	HSF1	Heat shock factor 1
GADD45	Growth-arrest and DNA-damage- inducible protein 45	ICD	Immunogenic cell death
G-CSF	Granulocyte-colony stimulating factor	ICL	Interstrand crosslinks
GFP	Green fluorescent protein	ICs	Immune complexes
GG-NER	Global genome nucleotide excision repair	Ig	Immunoglobulin
GM-CSF	Granulocyte- macrophage- colony stimulating factor	IGF1	Insulin-like growth factor 1
HAT	Histone acetyltransferases	IIC	Infiltrating immune cells
HDM2	Human double minute protein 2	IL	Interleukins
HGF	Hepatocyte growth factor	ILCs	Innate lymphoid cells
HLA I	Class I human leukocyte antigen	INF	Interferons
		iNOS	inducible Nitric oxide synthase
		IR	Ionizing radiation
		ITAM	Immunoreceptor tyrosine-based activation

LIMP2	Lysosomal integral membrane protein 2	MRN	MRE11/Rad50/NBS1
		NaCl	Sodium Chloride
LOX1	Lectin-like oxidized LDL receptor 1	NER	Nucleotide excision repair
LPS	Lipopolysaccharides	NETs	Neutrophil extracellular traps
MAPK	Mitogen-activated protein kinase	NFκB	nuclear factor κ-lightchain-enhancer of activated B cells
MAPK	Mitogen-activated protein kinase		
M-CSF	Macrophage-colony stimulating factor	NHEJ	Nonhomologous end joining
MDM2/4/X	Mouse double minute protein 2/4/X	NHLs	Non-Hodgkin lymphomas
MDSCs	Myeloid derived suppressor cells	NHS	N-hydroxysuccinimide
		NKs	Natural killer cells
MFG-E8	milk-fat globule-epidermal growth factor-VIII	NO	Nitric oxide
MHC-II	Major histocompatibility complex-II	NOXA	Phorbol-12-myristate-13-acetate-induced protein 1
		PAA	Polyacrylacid
MK2	Mitogen-activated protein kinase - activated protein kinase 2	PAMPs	Pathogen-associated molecular patterns
		PARP	Poly (ADP-ribose) polymerase
ml	Milliliter	PBS	Phosphate buffered saline
MMR	Mismatch repair		

PD-1	Programmed cell death protein-1	Rac1	Ras-related C3 botulinum toxin substrate 1
PDGF-C	Platelet-derived growth factor-C	R-CHOP	Rituximab plus CHOP scheme
PD-L1	Programmed cell death protein-1 ligand	RIPA buffer	Radioimmuno-precipitation assay buffer
PDL2	Programmed death ligand 2	ROI	Reactive oxygen intermediates
PE	Phycoerythrin	ROS	Reactive oxygen species
PEDF	Pigmented epithelial-derived factor	RPA	Replication protein A
PIKKs	Phosphatidylinositol 3-kinase-like protein kinase	rpm	revolutions per minute
PKB $\alpha$	Protein kinase B $\alpha$	SD	Standard deviation
pp53	Phosphorylated p53	SDF1/ CXCL12	Stroma cell-derived growth factor-1
PPAR $\gamma$	Peroxisome proliferator activated receptor- $\gamma$	SDS	Sodium Dodecyl Sulfate
PRRs	Pattern-recognition receptors	SDS-PAGE	Sodium Dodecyl Sulfate polyacrylamide gel electrophoresis
PS	Penicillin/Streptomycin	SHM	Somatic hypermutation
PTM	Posttranslational modification	shRNA	small hairpin RNA
PUMA	p53 upregulated modulator of apoptosis	SSBs	Single-strand brakes
		SSC	Sight scatter

ssDNA	single stranded DNA	TLRs	Toll-like receptors
STAT1/6	Signal transducer and activator of transcription 1/6	TME	Tumor microenvironment
Syk	Spleen tyrosine kinase	TMEM	Tumor microenvironment of metastasis
TAMs	Tumor associated macrophages	TNF	Tumor necrosis factors
Tao kinases	Thousand and one amino acid kinases	T <sub>reg</sub> cells	Regulatory T cells
TBS	Tris-buffered saline	TSGs	Tumor suppressor genes
TBS-T	Tris-buffered saline with Tween20	UV-light	Ultraviolet-light
TC-NER	Transcription-coupled nucleotide excision repair	VEGF	Vascular endothelial growth factor
TCR	T cell receptor	WB	Western Blot
TEMED	Tetramethylethylendiamin	Wip1	Wild-type p53-induced phosphatase 1
T <sub>fh</sub> cells	Follicular T <sub>h</sub> cells	XP	Xeroderma pigmentosum
TGF	Transforming growth factors	μl	Mikroliter
TGF-β	Transforming growth factor-β	μm	Mikrometer
T <sub>h</sub> 1/2 cell	T helper 1/2 cell	μM	Mikromolar
TI	Trained immunity		

# 1 Abstract of Dissertation

The tumor microenvironment (TME) plays an important role in the genesis, progression and metastasis of malignancies. One of the key players in the TME are macrophages, referred to as tumor associated macrophages (TAMs). As macrophages are a very heterogenic group, their impact on disease progression and outcome varies strongly depending on the tumor entity. In most cases, TAMs are mainly associated with a poor prognosis in regard to tumor progression, therapy efficacy and disease relapse after treatment.

Previous work from this laboratory could show that the application of genotoxic stress in form of a low dose treatment with a alkylating agent, Mafosfamide, induced an increase in the phagocytic capacity of macrophage cell lines as well as primary murine macrophages *in vitro*. This stimulatory effect was observed in an assay, which evaluated opsonised Fc-receptor (FcR) mediated phagocytosis, utilizing Phycoerythrin (PE) labelled latex beads as well as green fluorescent protein (GFP) labelled humanized lymphoma cells as engulfment targets. Opsonization was ensured through the addition of monoclonal therapeutic antibodies. In addition, it was observed that stressed macrophages undergo morphological changes, which upon treatment with Mafosfamide and Doxorubicin led to an increase in size as well as granularity, detected by confocal microscopy and flow cytometry.

In this work, an increase in opsonised FcR-independent as well as non-opsonised phagocytic capacity of macrophages *in vitro*, caused by chemotherapy treatment, was observed. Interestingly, this effect was induced by either Mafosfamide or Doxorubicin treatment, mirroring the effect both chemotherapeutics had on opsonised FcR-dependent phagocytosis. Furthermore, for Mafosfamide this seemed to be caused by direct effects of the chemotherapeutic on the macrophages. The mechanism of action observed under Doxorubicin treatment differed from Mafosfamide in that it induced increased phagocytosis via both direct and indirect treatment.

## 2 Zusammenfassung

Das Tumormikromilieu spielt eine entscheidende Rolle bei der Entstehung, dem Fortschreiten und der Metastasierung von malignen Erkrankungen. Makrophagen sind eine der zentralen Zellen im Tumormikromilieu und werden als Tumor-assoziierte Makrophagen (TAMs) bezeichnet. Makrophagen sind ein hoch heterogener Zelltyp, dessen Einfluss auf Fortschritt und Ausgang einer Krebserkrankung stark von der jeweiligen Art der malignen Erkrankung abhängt. Jedoch sind TAMs meistens mit einer schlechten Prognose bezüglich Krankheitsentwicklung, Therapieeffektivität und Wiederauftreten der malignen Erkrankung assoziiert.

Interessanterweise konnte die Arbeitsgruppe von Prof. Dr. Pallasch nachweisen, dass die Schädigung der DNA durch niedrig dosierte Alkylanzien, wie Mafosfamide, eine höhere Phagozytoserate in Makrophagen-Zelllinien, sowie primären murinen Makrophagen induziert. Diese Stimulation wurde in einem Experiment, welches opsonierte Fc-Rezeptor (FcR) vermittelte Phagozytose misst, beobachtet. In diesem Experiment wurden PE markierte Latexkügelchen und GFP markierte humanisierte Lymphom Zellen als Phagozytoseziele benutzt, sowie, um die Opsonierung zu garantieren, monoklonale Antikörper hinzugefügt. Ebenso wurde beobachtet, dass behandelte Makrophagen sich morphologisch verändern. Unter der Behandlung mit Mafosfamide oder Doxorubicin nahm die Zellgröße und -granularität zu, was mittels eines Konfokalmikroskops und Durchflusszytometrie nachgewiesen wurde.

In dieser Arbeit wurde gezeigt, dass opsonierte FcR-unabhängige Phagozytose und nicht opsonierte Phagozytose, durch Makrophagen, ebenfalls mittels Chemotherapie erhöht werden kann. Dieser Effekt wurde durch Mafosfamide- und Doxorubicinbehandlung hervorgerufen, wie es auch für opsonierte Fc-abhängige Phagozytose beobachtet wurde. Bei Mafosfamide war dieser Effekt abhängig von der direkten Behandlung von Makrophagen mit dem Chemotherapeutikum. Der Effekt von Doxorubicin wurde jedoch bei direkter, sowie indirekter Behandlung, mittels konditioniertem Mediums, beobachtet.

## 3 Introduction

### 3.1 Immune system

The immune system is composed of cellular and humoral factors, which protect the body against pathogenic organisms, their toxins, as well as insect poisons. To accomplish this, the immune system carries out four major tasks: recognition of pathogens, performance of immune effector functions, immunoregulation and formation of an immunological memory<sup>1</sup>. In recent years, it has become apparent, that the immune system also performs anti-tumor functions and plays a key role in tumorigenesis (see 1.3.1). The immune system is subdivided into the innate immune system and the adaptive immune system, which will be discussed in 1.1.1 and 1.1.2.

#### 3.1.1 Innate immune system

The innate immune system is first to react against pathogenic organisms, preventing infection and preserving homeostasis<sup>2</sup>. The recognition of pathogens is mediated through pattern-recognition receptors (PRRs), which bind pathogen-associated molecular patterns (PAMPs) displayed on the surface of pathogenic organisms<sup>3</sup>. Epithelial and endothelial cells, as well as humoral and cellular mechanisms contribute to the innate immune system<sup>1</sup>.

Epithelial cells are connected via tight junctions, forming a barrier against pathogens and dehydration, called the epidermis. In addition, the epidermis is protected by secreted cytokines, a weakly acid pH in its outer layer, desquamation, the natural microbiome and anti-microbial peptides<sup>4</sup>. Linked by tight junctions, endothelial cells form the mucosa membrane, which covers the body cavities and protects them from invasion by pathogens. Low pH, internal mucosa layer, hydrolytic enzymes and bioactive molecules, e.g. from the anti-microbial peptide (AMP) family, facilitate the barrier function of the mucosa membrane<sup>5</sup>.

Humoral factors play an important role in the innate immune system. Being proteins, these factors are secreted by different cell types, like glandular cells,

macrophages, epithelial cells, neutrophils and hepatocytes. Lysozyme lyses bacteria when secreted by cells, e.g. macrophages in the airways. Furthermore, AMP, such as  $\beta$ -defensins or neutrophil peptides, perform antibacterial, antifungal and antiparasitic functions<sup>6</sup>. Other crucial humoral factors are acute phase proteins (APPs), which affect different mechanisms, like recognition of pathogens, agglutination, complement activation, opsonization and immunomodulation. Prominent examples of APPs are C-reactive protein (CRP), haptoglobin, transferrin, serum amyloid A and P<sup>7</sup>. Moreover, cytokines play an important role in the communication between cells and a coordinated immune response. They are differentiated into classes, including interleukins (IL), interferons (INF), tumor necrosis factors (TNF) and transforming growth factors (TGF)<sup>8</sup>. The complement system, also a humoral factor of the innate immune system, consists of more than 30 proteins, which after initiation activate each other through a proteolytic cascade. Performing broad functions, like lysis of targets, priming the immune system and opsonizing targets, the complement system also resembles a link between innate and adaptive immune system, affecting T and B cells<sup>9</sup>.

The cellular compartment of the innate immune system is usually the first subset of the immune system to react against pathogens, which have breached the physical barrier composed of epithelial or endothelial cells. Macrophages, being at the forefront of the reaction, phagocytose the invading organisms and initiate an immune reaction<sup>1</sup>. A prolonged activation state of macrophages, after contact with certain pathogens, represents one mechanism of the innate immune system to develop an immunologic memory, in this case termed trained immunity (TI)<sup>10,11</sup>. Macrophages are discussed in greater detail in 1.2.1 and 1.2.2. Dendritic cells (DCs), like macrophages, phagocytose pathogens, process them intracellularly and then present their antigens via major histocompatibility complex-II (MHC-II) molecules to naïve T-cells to initiate an adaptive immune response, resembling a connection between innate and adaptive immune system<sup>12</sup>. Another phagocytic cell type are neutrophil granulocytes or neutrophils, which enter the locus of inflammation within minutes after cytokine release by macrophages<sup>13</sup>. Neutrophils exhibit anti-microbial mechanisms beyond phagocytosis, they can release neutrophilic granules, which are

important for neutrophil migration and elimination of pathogens, and form neutrophil extracellular traps (NETs), representing an extracellular defense against bacteria and fungi<sup>14,15</sup>. In recent years NETs were also associated with autoimmune diseases and have been shown to be performed simultaneously with phagocytosis<sup>16,17</sup>. Two more granulocyte subsets are known, basophils, which react to target bound immunoglobulin (Ig) E and are associated with allergic reactions, and eosinophils, which also react to target bound IgE and are important for antiparasitic responses<sup>13</sup>. Myeloid derived suppressor cells (MDSCs) are also part of the innate immune system. They can dampen immune responses by suppressing natural killer cells (NKs), T- and B-cell reactions<sup>18,19</sup>. Cells of the neutrophil and the monocytic lineage contribute to the MDSC population<sup>20</sup>. NKs are of lymphoid origin, distinguishing them from the myeloid cell types described above. Being able to sense a change in MHC-I molecule expression on cells, NKs can discriminate between normal cells and infected or cancer cells. After engaging infected or abnormal cells, NKs eliminate these cells by releasing cytolytic granular or forcing them into apoptosis via death receptor engagement<sup>1</sup>. NKs are subsumed under the group of innate lymphoid cells (ILCs), which belong to the innate immune system, although being of lymphoid heritage, because they are lacking somatically recombinant antigen receptors. Besides NKs three more groups of ILCs are known: ILC1, which are similar to T helper (T<sub>h</sub>) 1 cells and secret INF $\gamma$ , ILC2, producing cytokines associated with T<sub>h</sub> 2 cells, and ILC3, being a source of IL17 and IL22<sup>21</sup>. Different ILC groups also exhibit the ability to differentiate into memory-like cells<sup>22,23</sup>. In concert with macrophages, this represents the ability of the innate immune system to form an immunological memory.

### 3.1.2 Adaptive immune system

If the innate immune system cannot control a pathogen, which has entered the organism, the more finetuned and better equipped adaptive immune system attends to the intruder<sup>1</sup>. The adaptive immune system consists of T cells, which provide the cellular immune response, and B cells, which produce the humoral immune response<sup>24</sup>.

Based on the expression of certain coreceptors, T-cells can be divided into two main groups, CD8<sup>+</sup> and CD4<sup>+</sup> T cells. T cells expressing CD8 are called CD8<sup>+</sup> T cells or cytolytic T lymphocytes (CTLs). CTLs recognise infected or mutated cells, which express foreign or abnormal proteins on their MHC-I molecules, via the interaction between these molecules and their T cell receptor (TCR)<sup>1</sup>. Releasing intracellular granules and interacting with the Fas receptor on the target cells, CTLs induce apoptosis in infected or mutated cells<sup>25</sup>. CD4 expressing or CD4<sup>+</sup> T cells are further subdivided into different groups, mainly based on their cytokine profile. Activated through the interaction between MHC-II molecules, on antigen presenting cells, and TCR on the CD4<sup>+</sup> T cells, they differentiate under the influence of certain cytokines<sup>24</sup>. The first subset are T helper (T<sub>h</sub>) 1 cells, which are induced by IL-12 and secrete IL-2 and IFN $\gamma$ . They activate macrophages, CTLs and NKs, hence fostering a cellular immune response, especially against intracellular bacteria and viruses. Differentiated under IL-4 signalling, the second subset, T<sub>h</sub> 2 cells, produce IL-4, IL-5, IL-10 and IL-13. They induce antibody production and have a key role in anti-parasite and hypersensitivity reactions. In addition, there are memory T<sub>h</sub> cells, called follicular T<sub>h</sub> (T<sub>fh</sub>) cells, which can stimulate B cells. They are part of the immunological memory<sup>25</sup>. Another subset of CD4<sup>+</sup> T cells are T<sub>h</sub> 17 cells, which differentiate under the influence of IL-6 and TGF- $\beta$  and secrete IL-17. Inducing autoimmunity, T<sub>h</sub> 17 cells are capable of stimulating an inflammatory reaction<sup>26</sup>. Opposing this, are regulatory T cells (T<sub>reg</sub> cells), which represent a heterogeneous group of T cells, all of which have regulatory functions in regard to immune reactions, often mediated by IL-10<sup>27</sup>. One last subset of CD4<sup>+</sup> T cells discussed here, are T<sub>h</sub> 9 cells. They differentiate under the influence of IL-4 and TGF- $\beta$ . Producing IL-9, they are important for immune reactions against helminths<sup>28</sup>.

B cells are in charge of producing the humoral adaptive immune response via the secretion of antibodies. After the B cell receptor (BCR) has bound an antigen, the B cell is partially activated. It internalizes the antigen to process and then present it, on the cell surface bound to an MHC-II molecule, for a T cell to recognise and then trigger further actions by the B cell<sup>1</sup>. Some antigens are capable of inducing a B cell driven humoral adaptive immune response

without the necessity of T cell interaction<sup>29</sup>. Activated B cells either become plasma cells, which start producing antibodies, or establish a germinal center in a follicle. In the germinal center two important mechanisms take place: the B cells can switch the Ig type, they are producing, e.g. from IgM to IgG, this process is called class-switching and through the acquisition of point mutations in the Ig variable regions, a process called somatic hypermutation (SHM), the affinity of the produced Igs can be increased<sup>30,31</sup>. B cells can also form memory cells, which react faster to a subsequent exposure to the same antigen<sup>25</sup>.

## 3.2 Macrophages

### 3.2.1 Heterogeneity and Polarisation

Being part of the myeloid lineage of the hematopoietic system, macrophages, DCs, monocytes and their bone-marrow precursors compose the mononuclear-phagocytic system<sup>32</sup>. Resident tissue macrophages originate in the embryonic period from progenitor cells, formed in the yolk sack or the fetal liver, and replenish themselves, under steady state conditions, throughout the adult life<sup>33-36</sup>. Recruitment of monocytes, out of the bloodstream, can also elevate tissue macrophage numbers in case of inflammation, cancer or severe depletion<sup>37-39</sup>. Cytokines involved in recruiting monocytes are described in 1.3.2.

Tissue macrophages resemble a highly heterogenic group of cells with specialized members like Kupffer cells in the liver, osteoclasts in the bone, microglia in the central nervous system and Langerhans cells in the skin<sup>40-44</sup>. This heterogeneity can also be observed within the same organ. Homing three different kinds of macrophage subpopulations (red pulp, marginal-zone and marginal-zone metallophilic macrophages), the spleen resembles a great example for this diversity<sup>45</sup>. Because of their great plasticity, macrophages can be conditioned by their microenvironment and perform a variety of functions, like phagocytosing debris, dead cells or pathogens, producing extracellular matrix (ECM), resorbing bone tissue, repairing and healing wounds, producing bilirubin et cetera<sup>46,47</sup>.

Besides their heterogeneity, macrophages show a great diversity in their activation state, also referred to as polarisation. In line with the CD4<sup>+</sup> T<sub>h</sub> cells classification of T<sub>h</sub> 1 and T<sub>h</sub> 2 cells, macrophages are classified in a spectrum ranging from M1 to M2, with M1 and M2 being the extremes of a continuum of activation states<sup>48</sup>. Through the exposure to INF $\gamma$ , which is secreted by T<sub>h</sub> 1 cells or NKs, lipopolysaccharides (LPS) or TNF macrophages are classically activated, referred to as M1 polarisation<sup>49,50</sup>. The signalling is transduced by signal transducer and activator of transcription 1 (STAT1), nuclear factor  $\kappa$ -light-chain-enhancer of activated B cells (NF $\kappa$ B) and the Notch signalling pathway<sup>51-53</sup>. The functional characteristics of M1 macrophages include secretion of pro-

inflammatory cytokines, endorsement of  $T_h$  1 immune responses, tumoricidal and microbicidal effects by induction of reactive oxygen species (ROS) and nitric oxide production, thus fostering their cytotoxic abilities, as well as phagocytosis of tumor cells and bacteria<sup>54-57</sup>. Especially associated with opsonised Fc-dependent phagocytosis, through the upregulation of certain FcRs, M1 macrophages are described to have the higher phagocytic capacity compared to M2 macrophages<sup>58-61</sup>. Therefore a tight regulation of M1 macrophages is important, because they can also contribute to excessive tissue damage and autoimmune diseases<sup>62</sup>. M2 polarisation of macrophages, which is associated with wound healing, tissue repair, anti-inflammatory effects and effective phagocytosis of dead cells and debris, resembles the opposite pole on the continuum of activation states<sup>63</sup>. The M2 macrophages subsume a heterogenic group of macrophages with different subgroups. Through IL-4 and IL-13 signalling, via transcription factors like STAT6, peroxisome proliferator activated receptor- $\gamma$  (PPAR $\gamma$ ) and PPAR $\delta$ , alternative M2 macrophage activation is induced, which is also referred to as M2a macrophages<sup>48,59,64-66</sup>. They produce less pro-inflammatory cytokines as well as ROS and nitric oxide than M1 macrophages and show less efficient elimination of intracellular pathogens. But they play a vital part in fostering  $T_h$  2 responses, immune reactions against parasites and the secretion of ECM, which enables them to immunoregulatory functions as well as tissue repair, this is why they are also referred to as wound-healing macrophages<sup>59,67,68</sup>. A second subset of M2 macrophages are activated under the simultaneous influence of immune complexes (ICs) and agonists of Toll-like receptors (TLRs), like LPS, which are termed M2b macrophages or type II activated macrophages<sup>59,69</sup>. These are part of the macrophage subset introduced by Flemming and Mosser, called regulatory macrophages, which subsumes macrophages activated by TLR agonists and a co-stimulus, like ICs, apoptotic cells, prostaglandin E2 (PGE2) or TGF- $\beta$ <sup>62</sup>. An important role in the polarisation of regulatory macrophages is played by the mitogen-activated protein kinase (MAPK) extracellular signal-regulated kinase (ERK), which is activated by many of the mentioned co-stimuli and is proven to enable access to the promoter of the IL-10 gene<sup>70</sup>. High IL-10 secretion is one of the main characteristics of this macrophage subset, besides triggering a  $T_h$  2 immune response and acting as immunoregulators, although

still secreting pro-inflammatory cytokines like IL-1 or IL-6<sup>59</sup>. The last subset of M2 macrophages, which is going to be introduced in this chapter, is called M2c macrophages or deactivated macrophages. These are induced through IL-10 and macrophage-colony stimulating factor (M-CSF) or glucocorticoid signalling, with IL-10 signalling being dependent on STAT3<sup>59,71,72</sup>. This subset is especially associated with suppressing immune reactions and remodelling tissues, e.g. by secreting transforming growth factor- $\beta$  (TGF- $\beta$ ) and phagocytosing apoptotic cells and debris<sup>59,72,73</sup>. Another M2 subset are M2d macrophages, which are characterised in 3.3.2. Besides their diversity in cytokine production and function, different macrophage polarisation states can be identified by expression of surface markers, some typical surface markers are displayed in Figure 1<sup>74</sup>. In general, one must bear in mind, that the different polarisation states of macrophages are not fully understood yet and the approach to fit them into a strict system always includes oversimplifications.

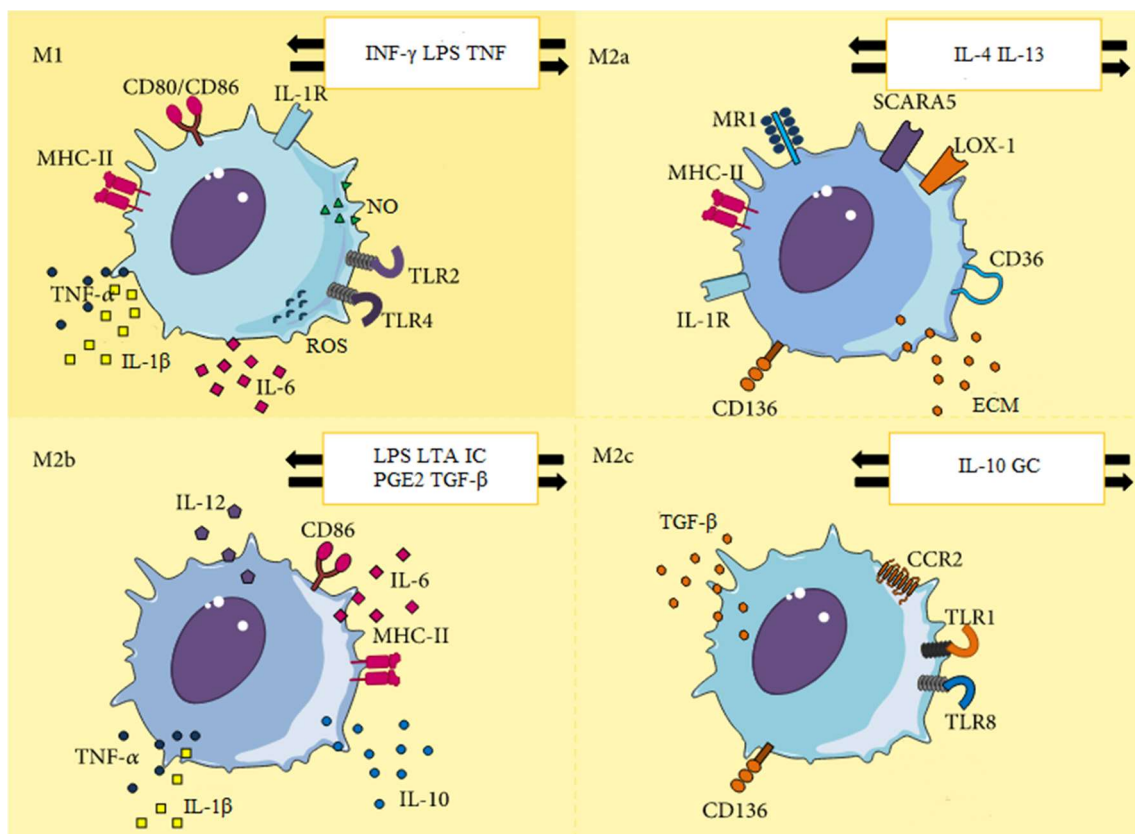


**Figure 1: Polarisation states of macrophages (modified from<sup>74</sup>)**

Macrophages can be polarized and thus activated through different stimuli, which is described by the M1 and M2 polarisation scheme (see 3.2.1). The expressions of different surface markers and receptors as well as cytokines for different polarisation states are shown in this figure.

### 3.2.2 Phagocytosis

Phagocytosis describes the cellular process of ingesting particles which exceed a diameter of  $0.5\mu\text{m}$ <sup>75</sup>. In a multicellular organism phagocytosis is mainly carried out by professional phagocytes, e.g. macrophages, neutrophils and dendritic cells, but can also be performed by non-professional phagocytes, e.g. fibroblasts, epithelial cells and endothelial cells. The internalisation of microbial pathogens, only carried out by professional phagocytes, is a crucial part of the innate and, through antigen presentation, of the adaptive immune system. In addition, phagocytosis is crucial for tissue homeostasis and remodelling via the clearance of apoptotic and dead cells as well as debris, which is performed by professional and non-professional phagocytes<sup>76,77</sup>.

To initiate phagocytosis the target of interest must be recognised by the phagocyte. This can be conveyed by non-opsonic receptors, like CD36, lysosomal integral membrane protein 2 (LIMP2), lectin-like oxidized LDL receptor 1 (LOX1), CD163, mannose receptor or Dectin-1, which can detect PAMPs of microbial pathogens or danger-associated molecular patterns (DAMPs) of e.g. apoptotic cells<sup>78-80</sup>. Non-opsonic receptors are a subgroup of the PRRs, which also include the Toll-like receptors (TLRs)<sup>81</sup>. TLRs are not able to initiate phagocytosis on their own, but they can induce an immune response as well as prime phagocytes and their receptors for an efficient target engagement in a p38-dependant manner<sup>76,82</sup>. Besides non-opsonic receptors, specialized phagocytes also express opsonic receptors, which recognise phagocytic targets after they were tagged by an opsonin, like Igs or complement factors<sup>83,84</sup>. The most prominent opsonic receptors are FcRs, which bind the Fc portion of target-bound IgG and IgA and are essential for opsonised Fc-dependent phagocytosis. Additional opsonic receptors are complement receptors (CR), which bind to e.g. target-bound iC3b and play a role in opsonised Fc-independent phagocytosis<sup>85-87</sup>. Interestingly CR3 has also been proven to be involved in non-opsonised phagocytosis of mycobacteria and zymosan<sup>88</sup>.

Signalling pathways, which induce phagocytosis after receptor engagement, are best described for FcR and CR, but are poorly understood for non-opsonic

receptors. FcRs cluster after target binding, which leads to phosphorylation of the immunoreceptor tyrosine-based activation (ITAM) motif by Src-family kinases<sup>89</sup>. This leads to the engagement of the spleen tyrosine kinase (Syk), which recruits additional signalling proteins<sup>90</sup>. The signalling pathway leads to membrane remodelling and changes in the actin cytoskeleton, which are both essential for phagocytosis<sup>91</sup>. The signalling required for CR-mediated or Fc-independent phagocytosis shows differences to FcR-mediated or Fc-dependent phagocytosis, e.g. CR-mediated signalling is not dependent on Syk and CR-mediated phagocytoses requires the actin and microtubule cytoskeleton<sup>92,93</sup>. After phagocytosis is initiated via signalling pathways, phagosome formation and maturation follow to end the process<sup>91</sup>.

### 3.3 Cancer

Cancer subsumes a distinct group of related diseases, defined by uncontrolled proliferation of a subset of cells, which have lost the capability to form tissues of orderly form and function. The cause of this being mutations in genes, which are critical for normal tissue homeostasis<sup>94</sup>. These genes are further differentiated into oncogenes and tumor suppressor genes (TSGs). Oncogenes usually develop through gain-of-function mutations of proto-oncogenes, which promote cellular proliferation, growth and evasion of apoptosis. In addition, loss-of-function mutations in TSGs can contribute to the development of cancer<sup>95</sup>. The distinction between gatekeeper genes and caretaker genes is of importance for TSGs. Gatekeeper genes control the cell cycle and proliferation, whilst caretaker genes preserve the genome integrity by being involved in processes like the DNA damage response (DDR)<sup>96</sup>.

Histopathologically the distinction between benign and malignant cancers is based on invasion into surrounding tissues. Malignant cancers are characterised by invasive growth and the formation of metastasis and benign cancers displace the surrounding tissue without invading it. Furthermore, histopathological differentiation of cancers can be executed regarding their tissue of origin. Four main groups are used to discriminate between most cancers. The largest group originates from epithelial cells and is called carcinoma, which is further divided into squamous cell carcinomas and adenocarcinomas. Cancers derived from mesenchymal cells, like fibroblasts, myocytes, osteoblasts or chondrocytes, are termed sarcomas. Hematopoietic cells can degenerate into leukaemia or lymphoma cells. Leukaemias are formed by degenerated cells in the bone marrow which proliferate unregulated and spill into the blood stream. Myeloid precursor cells cause acute myeloid leukaemia (AML) or chronic myeloid leukaemia (CML), while degeneration of lymphoid precursors results in acute lymphocytic leukaemia (ALL) or chronic lymphocytic leukaemia (CLL)<sup>94</sup>. Although CLL is historically assigned to leukaemias, today it is classified as an indolent non-Hodgkin lymphoma<sup>97</sup>. Lymphomas are derived from lymphoid cells and are mainly located in lymphoid organs<sup>94</sup>. Two main types of lymphomas are discriminated, non-Hodgkin lymphomas (NHLs), like

CLL or large B cell lymphoma, and Hodgkin lymphomas, which are characterised by Reed-Sternberg cells, which resemble multinucleated, peculiar, large B lymphocytes<sup>97,98</sup>. The last main group comprises neuroectodermal tumors which originate from cells of the peripheral and central nervous system. A few cancers do not fit the major groups described above, e.g. melanomas, small-cell lung carcinomas or teratomas<sup>94</sup>

To further elucidate the complexity of cancers Hanahan and Weinberg proposed eight hallmarks of cancer. These consist of evading growth suppressors, sustaining proliferative signalling, evading apoptosis, enabling replicative immortality, reprogramming the energy metabolism, inducing angiogenesis, resisting immune destruction, activating invasion and metastasis. Genome instability, inflammation and the tumor microenvironment underlie and cultivate these hallmarks<sup>99</sup>.

### 3.3.1 Tumor microenvironment

In the past two decades cancer research has undergone a paradigm change by not only focusing on the cancer cells and their genetic aberrations, but also the surrounding microenvironment, the TME, and the interactions between the two<sup>99</sup>. Nowadays it is well recognised that cancer cells recruit and stimulate different cell types, which form the TME, as well as that through the communication in-between cancer cells and the TME the hallmarks of cancer, as mentioned in 1.3, are facilitated and fostered<sup>100</sup>. Leukaemic cells undergo apoptosis within days *in vitro*, when cultured in the absence of certain players of the TME, which illustrates their dependency on those players quite drastically<sup>101</sup>. The TME consists of endothelial cells, pericytes, cancer-associated fibroblasts (CAFs), adipocytes, the ECM and immune cells, like TAMs, different subpopulations of T cells, NKs, B cells, mast cells, neutrophils, DCs and MDSCs. The exact composition and activity of the TME are dependent on the cancer type, which further complicates the comprehension of cancer<sup>102</sup>.

Like in normal tissues vessels in solid tumors, which supply nutrients and oxygen through the blood stream, are composed of endothelial cells and pericytes<sup>103</sup>. Through angiogenesis cancer cell proliferation is fostered and

hyperplasia can be transitioned into neoplasia, a phenomenon called “angiogenic switch”<sup>104,105</sup>. Endothelial cells secrete growth-promoting factors, e.g. granulocyte-colony stimulating factor (G-CSF), granulocyte-macrophage-CSF (GM-CSF), nitric oxide (NO) and pigmented epithelial-derived factor (PEDF), which further promote proliferation and progression of cancer through paracrine signalling<sup>106</sup>. Caused by constitutively active vascular endothelial growth factor (VEGF) signalling, provided by cancer and stroma cells of the TME, endothelial cells in this microenvironment display looser tight junctions as well as less coverage of and association with pericytes, which contributes to the formation of metastasis<sup>100</sup>.

One of the largest cell populations in the TME are CAFs, which stimulate tumorigenesis and tumor progression<sup>102</sup>. Via secreting a variety of growth factors, like members of the epithelial growth factor (EGF) family, hepatocyte growth factor (HGF), stroma cell-derived growth factor-1 (SDF1/CXCL12) and insulin-like growth factor 1 (IGF1), cancer cell proliferation is enhanced by CAFs<sup>100</sup>. In addition, they are associated with the epithelial-to-mesenchymal transition (EMT) of cancer cells by secreting TGF- $\beta$  and, along with activated adipocytes, recruit immune infiltrating cells to the TME<sup>107-109</sup>. Production and secretion of TGF- $\beta$  as well as CXCL12 is initiated by the transcription factor heat shock factor 1 (HSF1) and its activation is one of many characteristics which differ between normal fibroblasts and CAFs<sup>110</sup>. Through initiating EMT of cancer cells and modifying the ECM of the TME by secreting distinct ECM proteins and remodelling enzymes, CAFs foster invasion into adjacent tissue and metastasis<sup>111</sup>. Supporting tumor angiogenesis, by providing proangiogenic factors like VEGF, fibroblast growth factor 2 (FGF2) and platelet-derived growth factor C (PDGF-C), resembles another protumor function of CAFs<sup>100</sup>. Even the energy metabolism of cancer cells and CAFs was proven to be intertwined, showing that one cell type can use the lactate produced by the other cell type as an energy source<sup>112,113</sup>.

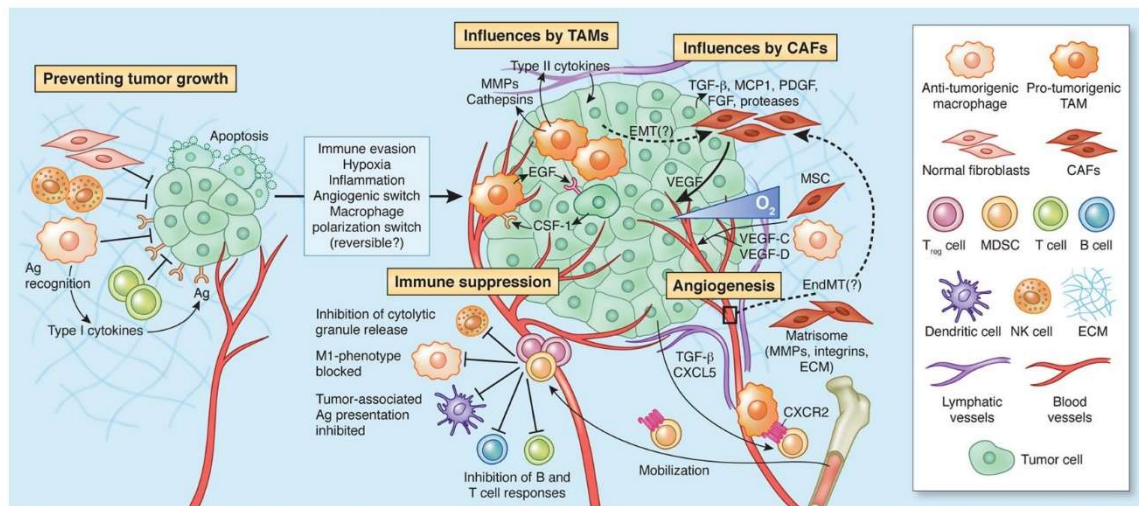


**Figure 2: Role of the TME in preventing tumors, tumorigenesis and tumor progression<sup>102</sup>**

After escaping intrinsic apoptosis mechanisms, cancer cells are recognised and destroyed by cells of the immune system. Especially antigen-presenting cells, like macrophages, identify cancer cells via cancer cell-specific antigens and present them to CTLs, thus activating them. Macrophages are also capable of eliminating cancer cells on their own. Fibroblast can also inhibit tumor cell progression. After evading immune surveillance, the cancer cells shape their environment into a tumor-supportive TME. The immune system is suppressed by recruited MDSCs and Treg cells, which inhibit antigen presentation by DCs, M1 polarisation of macrophages as well as NK, T and B cell function. TAMs and CAFs foster tumor progression, metastasis and angiogenesis via the secretion of proteases, cytokines and growth factors<sup>102</sup>.

The immune system plays a dual role regarding tumorigenesis, either it can stop cancer occurrence by eliminating atypical cells, called cancer immunosurveillance, or via immunoediting it can generate less immunogenic cancer cells or tumors with a stronger inhibitory effect on anti-tumor immune responses<sup>114-116</sup>. Once the tumor is established, it is mostly supported by infiltrating immune cells (IIC). An anti-tumor function is shown by CD8<sup>+</sup> T cells and a subpopulation of NKs, CD56<sup>dim</sup> NKs, via cytotoxic effects<sup>117,118</sup>. NKs show special relevance in eliminating intravasated cancer cells and thus preventing metastasis<sup>119</sup>. CD4<sup>+</sup> T<sub>h</sub> 1 cells were usually associated with an anti-tumor immune function and CD4<sup>+</sup> T<sub>h</sub> 2 cells were characterised as pro-tumorigenic, but there are studies showing a contradictory correlation between T<sub>h</sub> 1 associated cytokines and poor prognosis in B cell NHL as well as T<sub>h</sub> 2 associated cytokines and better prognosis in follicular lymphoma<sup>120-122</sup>. MDSCs are immunosuppressive, immature myeloid cells which are recruited to developing

tumors and support tumor angiogenesis<sup>123</sup>. Furthermore, they repress anti-tumor immune responses by inhibiting CD4<sup>+</sup> and CD8<sup>+</sup> T cell activation, antigen presentation by DCs, M1 polarisation of macrophages and cytotoxicity of NKs<sup>124-127</sup>. T<sub>reg</sub> cells are also associated with suppression of an immune response against cancer cells, by inhibiting CD8<sup>+</sup> T cell activity and antigen presentation as well as inhibiting CD4<sup>+</sup> T cells through binding of the programmed cell death protein 1(PD-1) on CD4<sup>+</sup> T cells to PD-1 ligand (PD-L1), which is expressed on T<sub>reg</sub> cells after T cell receptor activation<sup>128,129</sup>. But clinical studies showed conflicting correlations between T<sub>reg</sub> cell populations and prognosis for different types of cancer<sup>129-131</sup>. Another important immune cell in the TME are TAMs which will be discussed in 1.3.2.

### 3.3.2 Tumor associated macrophages

Being one of the most frequent cells in the TME, TAM infiltration in cancer is usually associated with a poor prognosis for patients, but was also associated with a better prognosis under immunochemotherapy<sup>132,133</sup>. Circulating monocytes, which also resemble a negative prognostic factor in diffuse large B-cell lymphoma (DLBCL) and CLL, are most likely the main source of TAMs in many cancer types<sup>134-139</sup>. These monocytes are recruited to the TME, where they differentiate into TAMs, which is initiated by cancer cells through the secretion of colony stimulating factor 1 (CSF-1), resembling the most important factor, VEGF-A, IL-34 and CC-chemokine ligand 2 (CCL2)<sup>140-143</sup>. The polarisation of macrophages impacts their effect on cancer cells with M1 macrophages being anti-tumorigenic and M2 macrophages showing pro-tumorigenic functions, but it was shown that TAMs do not resemble classical M1, nor M2 polarized macrophages<sup>50,134</sup>. This led to the introduction of a new M2 subset, which subsumes TAMs, called M2d. This polarisation is induced by the above-mentioned factors as well as the costimulation of the A2 adenosine receptor and the TLR or IL-6 stimulation<sup>144-146</sup>.

By secreting proinflammatory mediators like TNF- $\alpha$ , reactive oxygen intermediates (ROI), IL-6 and IL-1 $\beta$ , macrophages are associated with

promoting DNA damage, inflammation-induced carcinogenesis and proliferation of cancer cells<sup>147,148</sup>. The secretion of TNF- $\alpha$  and IL-6 is triggered by an activation of NF- $\kappa$ B<sup>149,150</sup>. Once the tumor is established, TAMs show an immunosuppressive phenotype by secreting anti-inflammatory cytokines, like IL-10 and TGF- $\beta$ <sup>151,152</sup>. Through the secretion of chemokines, like CCL20 or CCL22, TAMs attract T<sub>reg</sub> cells to the TME which suppress anti-cancer immune responses<sup>153,154</sup>. T cell function is also inhibited via the secretion of arginase I by TAMs, leading to the depletion of L-argininen in the TME, which is essential for T cell function<sup>155,156</sup>. Also, TAMs directly suppress T cell responses by cell-cell interaction via the expression of PD-L1 and B7-H4<sup>157,158</sup>. PD-L1 is upregulated in TAMs, because of the activation of hypoxia inducible factor 1 alpha (HIF-1 $\alpha$ ), which is caused by the hypoxic conditions in the TME<sup>132,159</sup>. HIF-1 $\alpha$  also induces the expression of angiogenic factors, like VEGF, in TAMs. They also secrete other angiogenic factors, like EGF and IL 8<sup>132</sup>. A special subset of TAMs was proven to be especially pro-angiogenic, Tie2<sup>+</sup> macrophages<sup>160</sup>. Aligning along blood vessels, caused by the expression of angiopoietin 2 (ANG2) on endothelial cells, Tie2<sup>+</sup> macrophages foster intravasation of cancer cells and thus metastasis<sup>161,162</sup>. The migration, invasion and metastasis of cancer cells is supported by a CSF-1-EGF paracrine loop in between cancer cells and TAMs as well as by the secretion of TGF- $\beta$  which fosters EMT<sup>163,164</sup>. In addition TAMs remodel the ECM of the TME by secreting different proteases, which support tumor cell invasion and metastasis<sup>165</sup>. Being part of the tumor microenvironment of metastasis (TMEM), macrophages are also associated with homing cancer cells at ectopic sites<sup>166</sup>. TAMs can also have a restrictive effect on anti-cancer therapies, like chemotherapy, irradiation or anti-vascular therapy, by different mechanisms, but were shown to have a beneficial effect on certain immunochemotherapies<sup>133,167-170</sup>.

### 3.4 DNA Damage Response

DNA damage can be induced endogenously via spontaneous DNA alterations through depurination or deamination as well as via oxidation by ROS, generated by normal metabolism. Exogenously induced DNA damage on the other hand is caused by ultraviolet light (UV-light), ionizing radiation (IR), smoking or chemotherapeutics<sup>171</sup>. In the case of chemotherapeutics the induction of DNA damage is a key mechanism to promote growth arrest and apoptosis in cancer cells and thus disease regression<sup>172</sup>. Through endogenously induced DNA damage as well as exogenously induced DNA damage by UV-light the estimated DNA lesions per cell each day are around  $10^5$ <sup>173</sup>. This illustrates, why a well-functioning and tightly regulated DDR is crucial for survival and preservation of correct genetic information for following generations.

Different mechanisms contribute to the DDR, depending on the specific cause and type of DNA lesion. Replication errors, like mismatches or small deletions, are repaired through mismatch repair (MMR). The base excision repair (BER) restores small chemical alterations of bases, caused by ROS, spontaneous deamination or hydrolysis and single-strand breaks (SSBs), induced by IR, ROS or chemotherapeutics, like anthracycline (e.g. Doxorubicin)<sup>174</sup>. SSBs are also repaired through nucleotide excision repair (NER), which also restores bulky adducts, evoked by IR and smoking, and intrastrand crosslinks induced by chemotherapeutics, like nitrogen mustards (e.g. Cyclophosphamide)<sup>175</sup>. Two modes of NER were described, the transcription-coupled NER (TC-NER) and the global genome NER (GG-NER). The TC-NER is activated by lesions which delay transcription and the GG-NER acts on lesions anywhere in the genome. Double-strand breaks (DSBs) are evoked like SSBs, but are repaired through more complex mechanisms. One of them being homologues recombination (HR), which is performed in S and G<sub>2</sub> phase of the cell cycle. Nonhomologous end joining (NHEJ) resembles the second option, which acts in G<sub>1</sub> phase and post-mitotic cells<sup>176</sup>. Interstrand crosslinks (ICL), which are induced by environmental factors like air pollutants and chemotherapeutics like Cyclophosphamide, are restored by ICL repair. A mechanism which involves key players of other DNA damage repair mechanisms like NER and HR as well

as other proteins like Fanconi anemia proteins, but is yet to be fully elucidated<sup>177,178</sup>. Although the different DNA damage repair mechanisms are mainly seen as separate units, one has to bear in mind that they share many key players and overlap significantly<sup>176</sup>.

The regulation of the DDR is mainly performed by the poly (ADP-ribose) polymerase (PARP) family and the phosphatidylinositol 3-kinase-like protein kinase (PIKKs) family, which includes the ataxia- and Rad3-related kinase (ATR), the ataxia-telangiectasia mutated kinase (ATM) and the DNA-dependent protein kinase (DNA-PK). ATR is activated by a complex of Replication protein A (RPA) and single stranded DNA (ssDNA) via ATR interacting protein (ATRIP). After being activated ATR phosphorylates and thus initiates activity of Checkpoint kinase 1 (CHK1). Upon the recognition of DSBs through the MRE11/Rad50/NBS1 (MRN) complex activity of ATM is promoted, which initiates recruitment of essential proteins for the DNA damage repair as well as activates Checkpoint kinase 2 (CHK2)<sup>176,179,180</sup>. DNA-PK, which is also activated by DSBs via the Ku70/Ku80 hetero-dimer, phosphorylates different proteins involved in NHEJ and through downstream targets one of the DNA damage response key players, p53. PIKKs regulate the DNA damage repair enzymes and stall the cell cycle to guarantee correct DNA repair before replication<sup>176,181</sup>. Different signalling cascades are activated by PIKKs to delay the cell cycle. CHK2, after being activated by ATM, phosphorylates and thus inactivates cyclin-dependent kinase 2 (CDK2), which leads to cell cycle arrest further downstream. Furthermore CHK1 and CHK2 deactivate cell division cycle 25 A, B and C (Cdc25A, Cdc25B and Cdc25C), so that these members of the Cdc25 family cease to dephosphorylate CDK2, thus staying inactive<sup>180</sup>. One of the most important steps to induce cell cycle arrest and shield the organism from altered genomic information, caused by DNA damage, via PIKKs is the stabilization of p53 through the phosphorylation of mouse double minute protein 2 (MDM2/HDM2 in humans). ATM and ATR directly inhibit MDM2 via phosphorylation and DNA-PK mediates its effect through the activation of Protein kinase B  $\alpha$  (PKB $\alpha$ ) and its downstream targets<sup>182-184</sup>. Activated CHK1 and CHK2 also phosphorylate p53, thus stabilizing it and regulating its activity<sup>185</sup>.

One of the key players of the DDR is p53, which can induce cell cycle arrest, senescence and apoptosis. It is mainly regulated through ubiquitylation by MDM2, promoting proteasomal degradation of p53<sup>186</sup>. Many different kinases, like the ones mentioned above, the wild-type p53-induced phosphatase 1 (Wip1) which induces MDM2 activity through phosphorylation or CREB-binding protein (CBP)/p300, which inhibits MDM2 via acetylation, influence the interaction between MDM2 and p53 and thus stabilize or destabilize p53<sup>187,188</sup>. The stabilization of p53 is considered the first step of p53 activation<sup>189</sup>. Another important regulator of p53 is mouse double minute protein 4/X (MDM4/MDMX), on one hand it promotes function of MDM2 and on the other hand together with MDM2 it can form a protein complex with p53, which is located at promoters of p53 target genes to inhibit transcription<sup>189,190</sup>. This repression of transcription can be overcome by acetylation of p53 which is carried out e.g. by the histone acetyltransferases (HAT), CBP/p300, Tip60 or human males absent on the first (hMof). This is the second step of p53 activation and it is called antirepression<sup>189</sup>. The last step of p53 activation is the promoter specific activation, which is achieved through posttranslational modification (PTM). PTMs include phosphorylation, acetylation, ubiquitylation, sumoylation, neddylation and methylation, which are carried out by different proteins, like the above-mentioned ATM, CHK2, CBP/p300, CHK1 and others. The promoter specific activation leads to recruitment of cofactors, regulation of p53 activity, association with transcription factors, different subcellular localizations of p53 and regulation of the influence by other signalling pathways. Through this mechanism the different responses to p53 activation can be controlled, which include apoptosis, senescence, cell-cycle arrest and DNA repair<sup>189,191</sup>. After being activated p53 acts as a transcription factor, which either induces or represses transcription of the target genes. These include MDM2, which acts as a negative feedback loop for p53 activation, p21, growth-arrest and DNA-damage-inducible protein 45 (GADD45), which causes cell cycle arrest, bcl-2-like protein 4 (BAX), p53 upregulated modulator of apoptosis(PUMA) and Phorbol-12-myristate-13-acetate-induced protein 1(NOXA), which induce apoptosis<sup>192,193</sup>. In addition p53 regulates the transcription of genes, which regulate metabolism, autophagy, the immune system and stem cell differentiation<sup>191</sup>.

Exercising the central role in the DDR, p53 is the target of many signalling pathways involved in DDR. Nevertheless, some pathways, although targeting p53, can act without the involvement of the DDR key player, like the mitogen-activated protein kinase (MAPK) pathway. This pathway is initiated by ATM, which activates the thousand and one amino acid (Tao) kinases<sup>194,195</sup>. Leading to the activation of p38, this pathway can cause cell cycle arrest in a p53 dependent manner as well as a p53 independent, via the activation of MAPK-activated protein kinase 2 (MK2), which inhibits the members of the cdc25 family

195-197

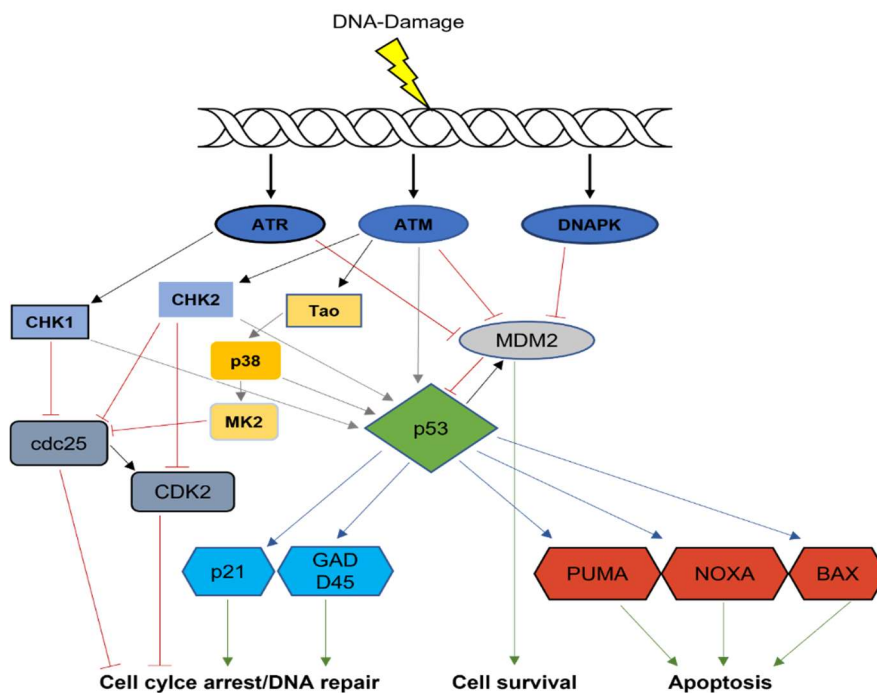


**Figure 3 Extract of the DNA damage response pathway (designed according to 176,179-185,189,191-193,195-197)**

Through the induction of DNA damage, the PIKKs ATR, ATM and DNA-PK are activated. They stabilize p53 by phosphorylating and deactivating MDM2, which functions as an inhibitor of p53. ATR and ATM phosphorylate CHK1 and CHK2, which, through phosphorylation, stabilize p53 and regulate its activity. CHK2 phosphorylates and thus inactivates CDK2, which in turn will not be dephosphorylated by cdc25, because it is also inactivated via phosphorylation by CHK1 and CHK2, resulting in cell cycle arrest. Depending on its posttranslational modifications, p53 acts as a transcription factor for different proteins with diverse effects on the cell. Via the transcription of MDM2 a negative feedback loop is activated which leads to cell survival. Through the activation of p21 and GADD45 cell cycle arrest as well as DNA repair are initiated. Transcription of PUMA, NOXA and BAX lead to apoptosis. As another example of a p53 independent pathway leading to cell cycle arrest, the MAPK pathway via Tao, p38 and MK2 is depicted<sup>176,179-185,189,191-193,195-197</sup>.

The importance of the DDR is well illustrated by the fact that a disruption of the DDR is associated with different kinds of diseases, like heart failure, Xeroderma pigmentosum(XP), Cockayne syndrome(CS), Ataxia Telangiectasia(AT), Seckle Syndrome and Fanconi anemia<sup>198-203</sup>. Furthermore, malfunction in the DDR is associated with aging and is the cause for a hallmark of aging, genome instability<sup>204</sup>. Genome instability also causes different hallmarks of cancer and a dysfunctional DDR can result in reduced apoptosis and exaggerated proliferation, two hallmarks of cancer<sup>99</sup>. The deficient DDR in cancer cells can be used as a therapy target once the tumor is established. Throughout the use of chemotherapeutics DNA damage is induced, which causes the cancer cells to become apoptotic. Because of their dysregulated DDR, they are more susceptible to DNA damage<sup>172</sup>. DDR inhibitors are also being developed and approved in recent years like Olaparib, a PARP inhibitor<sup>205</sup>. These drugs try to exploit the fact that most cancers strongly rely on certain DDR pathways, because of dysfunctions in the other DDR pathways<sup>206</sup>. In an approach to sensitize tumor cells against radiotherapy DDR inhibitors are used as well<sup>207</sup>. Transferring this concept to chemotherapy is not very successful yet, because of similar side effect profiles<sup>205</sup>.

### 3.5 Immunological effects of chemotherapy

For a long time, efficacy of chemotherapeutics as anti-cancer therapy was solely associated with their cytotoxic effect on tissues with a high proliferation rate and they were used as immunosuppressive drugs in the therapy of autoimmune diseases, but in the last two decades many studies showed immunostimulatory effects of common chemotherapeutics, which seem to contribute to their anti-cancer potency<sup>208-210</sup>. A normal immune response in patients is possible while they are being treated with common anti-cancer doses of chemotherapeutics<sup>211</sup>. Moreover, different chemotherapeutics show diverse immunostimulatory effects, which can trigger an anti-cancer immune response. Anthracyclines, like Doxorubicin and Daunorubicin, change the composition of infiltrating immune cells in the TME and their therapeutic efficacy is undermined by the absence of certain T cell subsets, the inhibition of DCs tumor infiltration or of immunostimulatory cytokines, which highlights the importance of the immune system in regards to the therapeutic effect of these drugs<sup>212-216</sup>. The immune response is based on immunogenic cell death(ICD) of cancer cells caused by anthracyclines<sup>217</sup>. In addition, anthracyclines were shown to diminish MDSC counts which partially neutralizes the immunosuppressive milieu of the TME<sup>218</sup>. Via the induction of ICD, oxaliplatin, a platin-based chemotherapeutic, fosters a tumor focused CD8<sup>+</sup> T cell reaction<sup>219</sup>. Furthermore, it induces the expression of class I human leukocyte antigen (HLA I) in malignant cells as well as represses the programmed death ligand 2(PDL2) expression on cancer cells<sup>220,221</sup>. Another chemotherapeutic which can induce ICD is cyclophosphamide<sup>222</sup>. Through a mechanism based on the relocation of bacteria from the intestine to secondary lymphoid organs, cyclophosphamide as well as oxaliplatin can provoke an anti-cancer immune response<sup>223,224</sup>. Furthermore, Cyclophosphamide depletes T<sub>reg</sub> cells as well as MDSCs and inhibits the production of immunosuppressive cytokines, thus interfering with the immunosuppressive measures of cancer cells<sup>225-227</sup>. It was shown in a mouse model of a double-hit lymphoma that the application of cyclophosphamide and alemtuzumab, a monoclonal anti-CD52 antibody, was capable of inducing tumor cell clearance in refractory sites, like the bone marrow, by macrophages<sup>228</sup>. The main factor for the induced tumor cell clearance was the initiation of an acute

secretory activating phenotype (ASAP) in leukaemic cells through cyclophosphamide treatment, leading to the secretion of VEGF-A, TNF- $\alpha$ , IL8 and CCL4, which enhanced the tumoricidal activity of macrophages<sup>228</sup>. Like oxaliplatin, cyclophosphamide as well as gemcitabine stimulate the expression of HLA I on malignant cells<sup>221</sup>. Besides fostering cross-priming of CD8<sup>+</sup> T cells, gemcitabine also promotes reprogramming of TAMs towards an anti-tumor phenotype<sup>229,230</sup>. Taxanes and vinca alkaloids were also described to have immunomodulatory effects, which will not be discussed further here<sup>231-233</sup>.

### 3.6 Aim of Research

This study was performed to accept or deny the following hypotheses. In order to accomplish this, two new methods to evaluate the phagocytic capacity of macrophages were established.

Biological hypotheses:

- Chemotherapy treatment induces phenotypical changes in macrophages which suggests a more phagocytically active phenotype.
- Direct chemotherapy treatment increases opsonised and non-opsonised Fc-independent phagocytic capacity of macrophages.
- The effects of direct chemotherapy treatment can be conveyed by soluble factors which suggests the induction of a secretory phenotype in macrophages.

Method development:

- Non-opsonised phagocytosis assay based on *Mycobacterium bovis* strain Bacille Calmette-Guérin (BCG)
- Opsonised Fc-independent phagocytosis assay based on pH-sensitive beads

## 4 Materials and Methods

### 4.1 Materials

#### 4.1.1 Devices

-20°C and -80° Freezer	AEG, Stockholm, Sweden
4°C Fridge	AEG, Stockholm, Sweden
Eppendorf Xplorer 12-Channel Orange	Eppendorf, Hamburg, Germany
Analytic Balance	Satorius, Göttingen, Germany
Autoclave Systec VX-150	Systec, Bergheim, Germany
Centrifuge 5415 R	Eppendorf, Hamburg, Germany
Centrifuge 5810 R	Eppendorf, Hamburg, Germany
CO <sub>2</sub> Incubator for Cell Culture	Labotect, Göttingen, Germany
Easypet 3 Pipettboy	Eppendorf, Hamburg, Germany
FluoSTAR Optima	BGLabtech, Ortenberg, Germany
Flow Cytometer MACSQuant VYB	Milentyi Biotech, Bergisch Gladbach, Germany
Freezing Container “Mr. Frosty”	Nalgene, Neerijse, Belgium
Heater/Magnetic Shaker MR3001	Heidolph, Schwabach, Germany
Laminar Flow Hood	Labogene, Lygne, Denmark
Microscope Confocal Meta710	Zeiss, Oberkochen, Germany
Microscope Inverted Phase Telaval 31	Zeiss, Oberkochen, Germany
UV236B irradiation devic	Waldmann, Villingen-Schwenningen, Germany

Mini-Protean Tetra Vertical Electrophoresis Cell	BioRad, Hercules, CA, USA
Electrophoresis Power Supply EPS 3500	Pharmacia Biotech, Uppsala, Sweden
Neubauer Hemacytometer	Laboroptic, Lancing, UK
Odyssey CLX Imaging System	LI-COR Biotech., Bad Homburg, Germany
PowerPac HC Power Supply	BioRad, Hercules, CA, USA
pH-Meter	Mettler-Toledo, Schwerzenbach, Germany
Pipettes Eppendorf Research Plus (10µl-1000µl)	Eppendorf, Hamburg, Germany
Roller Mixer SRT9	Stuart, Bibby Scientific, Staffordshire, UK
Rotilabo®-Mini-Centrifuge	Carl Roth, Karlsruhe, Germany
Shaker IKA-VIBRAX-VXR	IKA, Staufen, Germany
Thermomixer Compact	Eppendorf, Hamburg, Germany
Vortex "Lab Dancer"	IKA, Staufen, Germany
Water Purification System Milli-Q	Millipore, Eschwege, Germany
Waterbath	Heidolph, Schwabach, Germany
Sonicator	Bandelin Electronics, Berlin, Germany
Eppisonne	Cole-Parmer, Wertheim, Germany
Photometer	GE Healthcare, Berlin, Germany
BCG Incubator	Infors, Eisenbach, Germany

Erlenmeyer Flask (100ml) Merck, Darmstadt, Germany

#### 4.1.2 Disposable Materials

Cell culture chamber for microscopy Ibidi, Martinsried, Germany

Cell Scraper 16cm Sarstedt, Nümbrecht, Germany

Cell Scarper 25cm Sarstedt, Nümbrecht, Germany

Cover glass VWR, Darmstadt, Germany

Microscope Slides VWR, Darmstadt, Germany

CryoPure Tube 1.8ml Sarstedt, Nümbrecht, Germany

Experimental Gloves Paul Hartmann, Heidenheim, Germany

Experimental Tubes 15, 50ml Sarsted, Nümbrecht, Germany

Filtropour BT500 0.45, 500ml Bottle Top Filter Sarsted, Nümbrecht, Germany

Flow Cytometry Tubes 5ml Sarstedt, Nümbrecht, Germany

Mini Trans-Blot Filter Paper BioRad, Hercules, CA, USA

Multiwell Plate 6-Well Falcon/VWR, Darmstadt, Germany

Multiwell Plate 12-Well Falcon/VWR, Darmstadt, Germany

Multiwell Plate 96-Well Falcon/VWR, Darmstadt, Germany

Nitocellulose Membran Hybond-C Extra Amersham Biosciences, Amersham, UK

Parafilm Echiney Plastic Packaging, Chicago, IL, USA

Pipet Tips 10, 100 and 1000µl	Sarstedt, Nümbrecht, Germany
Receiver Bottle 500ml	Sarsted, Nümbrecht, Germany
Reagent Reservoirs 60ml	Starlab, Hamburg, Germany
Safe-Lock Tubes "Eppi" 1.5 and 2ml	Eppendorf, Hamburg, Germany
Tissue Culture Dishes 10cm,	Falcon/VWR, Darmstadt, Germany

### 4.1.3 Chemicals and substances

#### 4.1.3.1 General

Dimethylsulphoxide (DMSO)	Sigma, St. Louis, MO, USA
Dulbecco's Balanced Salt Solution (DPBS)	Gibco/Thermo Fisher Scientific, MA, USA
Ethanol	Carl Roth, Karlsruhe, Germany
FACS Clean	BD, Franklin Lakes, NJ, USA
FACS Flow	BD, Franklin Lakes, NJ, USA
FcR blocking reagent anti-mouse/human	Miltenyi Biotech, Berg. Gladbach, Germany
Formaldehyde	Carl Roth, Karlsruhe, Germany
Glycerol	Carl Roth, Karlsruhe, Germany
Kanamycin	AppliChem, Darmstadt, Germany
MACSQuant Running Buffer	Miltenyi Biotech, Berg. Gladbach, Germany
Nuclease Free Water	Ambion, Austin, TX, USA
Sodium Chloride (NaCl)	Carl Roth, Karlsruhe, Germany

CypHer5E mono N-hydroxysuccinimide (NHS) ester	GE Healthcare, Little Chalfont, UK
Polybead Amino Microspheres 3µm	Polysciences Inc., PA, USA
Gentamycin	Merck, Darmstadt, Germany
4.1.3.2 Western Blot	
Acrylamid Rotiphorese Gel30	Carl Roth, Karlsruhe, Germany
Ammonium Persulfate (APS)	AppliChem, Darmstadt, Germany
Bromophenol Blue	Carl Roth, Karlsruhe, Germany
Bovine Serum Albumin (BSA)	PAA, Pasching, Austria
Complete Mini Protease Inhib. Tablets	Roche, Basel, Switzerland
1.4-Dithiothreit (DTT)	Carl Roth, Karlsruhe, Germany
DNase/RNase Free Water	Gibco/Thermo Fisher Scientific, MA, USA
Ethylendiamine Tetra Acetic Acid (EDTA)	Carl Roth, Karlsruhe, Germany
Glycine	Carl Roth, Karlsruhe, Germany
Hydrochlorid Acid 37%	Carl Roth, Karlsruhe, Germany
Isopropanol	Carl Roth, Karlsruhe, Germany
Methanol Absolute	Th. Geyer, Renningen, Germany
Milk Powder	Carl Roth, Karlsruhe, Germany
Nonidet P-40 (NP-40)	Roche, Basel, Switzerland
Odyssey Blocking Buffer	LI-COR Biotech., Bad Homburg, Germany
PageRuler Plus Prestained Protein Ladder	Thermo Fisher Scientific, Waltham, USA

PhosSTOP	Roche, Basel, Switzerland
Ponceau S	Carl Roth, Karlsruhe, Germany
RIPA Buffer (10x)	CST, Boston, MA, USA
Sodium Dodecyl Sulfate (SDS)	AppliChem, Darmstadt, Germany
TEMED 99%	Carl Roth, Karlsruhe, Germany
Tris HCL	Carl Roth, Karlsruhe, Germany
Tris	Promega, Madison, WI, USA
Tween-20	AppliChem, Darmstadt, Germany
<b>4.1.3.3 Confocal Microscopy</b>	
Vectashield mounting medium	Vector Laboratories, Burlingame, CA, USA
Phalloidin FITC Reagent (ab235137)	Abcam, Cambridge, UK
DAPI (D9542)	Sigma-Aldrich Chemie GmbH, Taufkirchen, Germany
<b>4.1.3.4 Cell culture</b>	
Dulbecco's Modified Eagle Medium (DMEM)	Gibco/Thermo Fisher Scientific, MA, USA
Fetal Bovine Serum (FBS)	Gibco/Thermo Fisher Scientific, MA, USA
Penicillin/Streptomycin (PS) (5000 U/ml)	Gibco/Thermo Fisher Scientific, MA, USA
Middlebrook OADC	BD, Franklin Lakes, NJ, USA
Difco Middlebrook 7H9 Broth	BD, Franklin Lakes, NJ, USA
20% Tyloxapol	Santa Cruz, Santa Cruz, CA, USA

#### 4.1.4 Buffer, Media and Solution composition

Bacteria 7H9 Medium	2.35g Difco Middlebrook 7H9 Broth, 450ml dH <sub>2</sub> O, 50ml BBLTM Middlebrook OADC Enrichment, 5ml 50% Glycerin, 1.25ml 20% Tyloxapol
Blocking Buffer	5% BSA or Milk in TBS-T
Macrophage Culture Medium	1% Penicillin/Streptomycin, 10% FBS in DMEM
Freezing Medium	90% FBS, 10% DMSO
MACS Buffer	2mM EDTA, 0.5% BSA fill up to 250ml with 1xPBS
10x TBS	0.2M Tris, 1.83M NaCl, HCl (pH 7.6), Add H <sub>2</sub> O to 1L
TBS-T Wash Buffer	100ml 10x TBS, 0.1% Tween-20, Add H <sub>2</sub> O to 1L
10x Towbin Buffer	0.25M Tris, 1.92 Glycine, Add H <sub>2</sub> O to 1L
Transfer Buffer	200ml Methanol, 100ml 10x Towbin Buffer, Add H <sub>2</sub> O to 1L
Ripa Buffer+Pi+PS	1ml RIPA Buffer (10x), 1 Tablet PhosSTOP, 1 Tablet Protease Inhibitor, Add H <sub>2</sub> O to 1L
Running Buffer	100ml 10x Towbin Buffer, 0.1% SDS, Add H <sub>2</sub> O to 1L

Separating Gel Buffer 1.5M Tris with HCL (pH 8.8),  
04% SDS, Add H<sub>2</sub>O to 1L

Stacking Gel Buffer 0.5M Tris with HCL (pH 6.8),  
0.4% SDS, Add H<sub>2</sub>O to 1L

#### 4.1.5 Kits

Pierce BCA Protein Assay Kit Thermo Fisher Scientific,  
Waltham, USA

CellTiter-Glo® Luminescent Cell Viability Assay Promega, Fitchburg, WI, USA

#### 4.1.6 Agents

##### 4.1.6.1 Chemotherapeutics

Doxorubicin Hydrochloride Tocris Bioscience, Bristol, UK

Mafosfamide Sodium Salt Santa Cruz, Santa Cruz, CA,  
USA

##### 4.1.6.2 MDM2 Inhibitor

Nutlin-3A Tocris Bioscience, Bristol, UK

#### 4.1.7 Antibodies

##### 4.1.7.1 Primary Antibodies

<b>Specificity</b>	<b>Host species</b>	<b>Order #</b>	<b>Company</b>
βActin	Mouse Monoclonal	MAB1501	Millipore, Eschwege, Germany
p53	Mouse monoclonal	2524	CST, Boston, MA, USA
pp53	Rabbit-monoclonal	12571S	CST, Boston, MA, USA

#### 4.1.7.2 Secondary Antibodies

IRDye 800CW Goat anti-Mouse

LI-COR Biotech., Bad Homburg,  
Germany

IRDye 680RD Goat anti-Mouse

LI-COR Biotech., Bad Homburg,  
Germany

#### 4.1.7.3 Fluochrome Conjugated Antibodies

<b>Specificity</b>	<b>Conjugation</b>	<b>Order #</b>	<b>Company</b>
--------------------	--------------------	----------------	----------------

CD11b	Vio Green	130-097-299	Miltenyi Biotec, Bergisch Gladbach, Germany
-------	-----------	-------------	--

#### 4.1.8 Cell Lines and Bacterial Strains

##### 4.1.8.1 Cell Lines

J774A.1

Murine ascites derived  
macrophages cell line, ATCC,  
Manassas, VA, USA

##### 4.1.8.2 Bacterial Strains

*Mycobacterium bovis*, Bacille Calmette-Guérin  
(BCG)

non-pathogenic vaccine,  
transfected with DsRed,  
Gift from Dr. Mario Fabri,  
University Hospital Cologne

#### 4.1.9 Software

Endnote

Thomson Reuters, Philadelphia,  
PA, USA

FlowJo

Treestar, Ashland, OR, USA

GraphPad PRISM	GraphPad Software Inc., La Jolla, CA, USA
ImageJ	W. Rasband, NIH, Bethesda, MD, USA
Image Studio Lite	LI-COR, Biotech., Bad Homburg, Germany
MACSQuantify Software	Miltenyi, Berg. Gladbach, Germany
Microsof Office	Microsoft, Redmond, WA, USA
Fijii	J. Schindelin, Madison, Wisconsin, USA

## 4.2 Methods

### 4.2.1 Cell culture

The murine macrophage cell line J774A.1 was cultured in macrophage culture medium (see 4.1.4) at 37°C and 5% CO<sub>2</sub> in a humidified incubator in 10 cm tissue culture dishes. Cells were split every second day at a confluence of 70-90%. They were scraped off the cell culture plate, 2ml of the cell suspension were transferred onto a new dish and 8ml of macrophage culture medium were added to the plate. Live cell number was determined using Trypan blue and a Neubauer chamber.

Mycobacterium bovis strain Bacille Calmette-Guérin (BCG), which was provided by Prof. Dr. Mario Fabri (University Hospital Cologne), was used as a phagocytic target. The BCG bacteria were cultured in 7H9 medium (see 4.1.4) with 20µg/ml Kanamycin at 37°C and a slow rotation of 80rpm in a 100ml Erlenmeyer flask. To initiate the bacterial culture 200µl of a roughly 3x10<sup>8</sup> bacteria/ml solution were added to 10ml 7H9 medium with 20µg/ml Kanamycin and cultivated for 5 days, before being used as a phagocytic target in the BCG-phagocytosis assay (4.2.5.1). 100-200µl of the previous bacterial culture, depending on the amount of bacteria, was added to a fresh Erlenmeyer flask with 10ml 7H9 medium and 20µg/ml Kanamycin.

### 4.2.2 CellTiter-Glo viability assay

To assess cell viability, the CellTiter-Glo kit from Promega was used. Cells were plated out on a 96-well plate with 100µl per well in a concentration of 1\*10<sup>5</sup> cells per ml. After cells attached to the plate, the medium was replaced with fresh medium and the chemotherapeutics of interest were added. Also, 3 wells without cells were filled with 100µl of medium to obtain a value for background luminescence. Triplets were used for every condition. After 24 h of incubation, the cells were washed twice with 100µl of phosphate buffered saline (PBS) and then resuspended in 100µl of medium. The plate was incubated for 16h at 37°C and then equilibrated to room temperature for 30min. 100µl CellTiter-Glo

reagent, which was prepared according to the manufacture's protocol, was added to each well and the plate was shaken for 2min on an orbital shaker<sup>234</sup>. Then the plate was incubated at room temperature for 10min. Afterwards, the luminescence was measured with the FluoSTAR Optima plate reader at a wavelength of 560nm. The obtained luminescence was blank-corrected, before the average of the triplet conditions was calculated and then normalised to the average of the untreated control, resulting in one data point per replication of the assay. The CellTiter-Glo reagent contains an Ultra-Glo recombinant luciferase, which produces a luminescent signal upon engagement with ATP. The luminescent signal represents the number of live and metabolically active cells.

### 4.2.3 Measurement of protein levels

#### 4.2.3.1 Generation of cell lysates

A fully confluent 10cm dish of cells was used to generate cell lysates. The medium was replaced by 5ml of ice cold PBS and the cells were scraped off the plate. This suspension was centrifuged for 5min at 300g and 4°C. After resuspending the cell pellet in 20-100µl, depending on the pellet size, of 1x RIPA buffer plus 1x phosphatase inhibitor and 1x protease inhibitor, cell lysis was achieved through 30min incubation on ice. The cell lysates were centrifuged at 16.000rpm for 5min at 4°C. The supernatant was collected and either used right away or stored at -80°C.

#### 4.2.3.2 Measuring protein amount by Pierce BCA protein assay kit

Protein amount was measured by the Pierce BCA protein assay kit following the manufacture's protocol. A 1:50 dilution of the cell lysates (see 4.2.3.1) with RIPA buffer was prepared and 12.5µl of this dilution was added, in duplicates, to a 96-well plate. 12.5µl of BCA standards, which were prepared according to the manufactures protocol, were added to the 96-well plate in duplicates. Then the BCA reagent was prepared following the protocol and 100µl were mixed with the cell lysates or BCA standards in each well<sup>235</sup>. After 30min of incubation at 37°C, the absorbance at 540nm was measured with the FluoSTAR Optima

plate reader. By using a standard curve, which was created with the BCA standards, and subtracting the absorbance of the blank, the protein concentration in  $\mu\text{g/ml}$  for each sample could be determined.

#### 4.2.3.3 SDS polyacrylamide gel electrophoresis (SDS-PAGE)

To evaluate the effects of different concentrations of chemotherapeutics on the level of DNA-damage response proteins, SDS-PAGE was used to separate proteins according to their molecular weight. The amount of cell lysate, which contained  $60\mu\text{g}$  of protein, was mixed with  $4\mu\text{l}$  of 5x sample buffer and filled up with distilled water to a total amount of  $20\mu\text{l}$ . This mixture was boiled for 10min at  $95^\circ\text{C}$  while shaking to denature the proteins. Self-casted 5% stacking gels and 12.5% separating gels were used (Table 1). The samples as well as  $5\mu\text{l}$  of page ruler plus, a prestained protein marker, were loaded onto the gel. A vertical Mini Protean Tetra Cell apparatus (BioRad), containing 1x running buffer, was used for the electrophoretic separation, first at 120V for 30min and then at 180V for 45min.

**Table 1: Recipe for separating and stacking gel**

Ingredients	12.5% separating Gel	5% stacking gel
ddH <sub>2</sub> O	1.4ml	1.75ml
Stacking gel buffer	-	0.31ml
Separating gel buffer	2.4ml	-
30% PAA	2.7ml	0.42ml
10% APS	$52.8\mu\text{l}$	$12.5\mu\text{l}$
TEMED	$5.28\mu\text{l}$	$2.5\mu\text{l}$

#### 4.2.3.4 Western blotting (WB)

To allow protein detection, a BioRad semi-dry blot system was used to blot the SDS-PAGE gel onto a nitrocellulose membrane. Throughout the blotting process, 360mA were used for 1h at  $4^\circ\text{C}$ , and the blotting chamber was filled

with 1x blotting buffer. The nitrocellulose membrane was blocked with 5% milk in tris-buffered saline (TBS) for 1h while rotating at room temperature. After being washed twice with TBS Tween-20 (TBS-T), the membrane was incubated with the primary antibodies against the protein of interest, diluted 1:1000 in 5% milk in TBS-T, at 4°C overnight. Before adding the secondary fluorescent dye labelled antibody, diluted 1:3000 in Odyssey blocking buffer, and incubating the membrane for 1h at room temperature while rotating and protected from light, the membrane was washed 3 times with TBS-T. To detect phosphorylated p53 (pp53), the membrane was scanned with the LI-COR Odyssey infrared imaging system and then incubated with the primary p53 antibody as described above. Following 3 washing steps with TBS-T, the membrane was incubated for 1h at room temperature while rotating with the primary antibody against the housekeeping protein,  $\beta$ -actin. The primary antibody was labelled as described above. After 3 washing steps with TBS-T, the LI-COR Odyssey infrared imaging system was used to detect protein bands. The images were analysed with Image Lite software (LI-COR) and intensities of the protein of interest were normalised to  $\beta$ -actin.

## 4.2.4 Confocal Microscopy

### 4.2.4.1 Preparation of conditions

In order to visualize morphological changes of macrophages through genotoxic stress, as well as a change in their phagocytic capacity, confocal microscopy was performed.

8 wells of a 12-well plate were equipped with coverslips. Afterwards, the 12-well plate was put into a UV-chamber for 20min to sterilize the plate and coverslips. Macrophages were plated out as described in 4.2.5.1. After letting them attach for 6h, the medium was replaced with fresh macrophage culture medium and chemotherapeutics were added in the concentration of interest to the different conditions. Macrophages were incubated at 37°C and 5% CO<sub>2</sub> in a humidified incubator for 24h. Then washed twice with 1ml PBS and resuspended in 1ml macrophage culture medium. Then pH-sensitive beads were added, which were

labelled with the pH-sensitive fluorescent CypHer5E according to the protocol of A. Beletskii and colleagues<sup>236</sup>. To one well of untreated macrophages, no beads were added; to another well of untreated macrophages,  $5 \times 10^5$  unlabelled beads were added and to the remaining wells,  $5 \times 10^5$  labelled beads were added per well. Before being cultured for 16h at 37°C and 5% CO<sub>2</sub> in a humidified incubator, the 12-well plate was centrifuged for 1min at 300g. The cells were washed two times with 1ml PBS. Then fixation was performed with 500µl 4% paraformaldehyde in PBS per well for 15min at 37°C. The macrophages were washed twice with 500µl PBS while gently shaking for 5min and once with 500µl PBS without shaking. The permeabilization was achieved through incubation with 500µl 0.1% Tween 20 in PBS per well while shaking for 5min, followed by a washing step with 500µl PBS while shaking for 5min. To prevent background staining, the cells were incubated for 1h, while shaking, with 500µl 2% bovine serum albumin (BSA) in PBS per well. After that, the actin cytoskeleton was stained, in every well where labelled beads had been added. Phalloidin conjugated with Fluorescein-5-isothiocyanat (FITC) was used for this purpose. It was diluted 1:1000 in 2% BSA in PBS. The cells were incubated for 30min in 500µl of this solution while shaking and then washed 3 times with 500µl PBS per well. In addition, a 4',6'-Diamidin-2-phenylindol (DAPI) staining was performed with DAPI diluted 1:500 in PBS and an incubation time of 10min. Again, the cells were washed 3 times with PBS. The whole staining process was performed protected from light, to keep the staining from bleaching out. A drop of mounting medium (Vectashield) was used to mount the coverslips onto object slides. These were dried for 15min at room temperature and then for a few hours at 4°C. The confocal microscopy was performed with a Zeiss Meta 710 microscope in the CECAD imaging core facility. Two pictures were taken of each object slide, resulting in two technical replicates per biological replicate.

#### 4.2.4.2 Analysis

After pictures were taken with the Zeiss Meta 710 microscope, they were merged and a scalebar was added with the open source softwares ImageJ and Fiji. CellProfiler was used to assess the nucleus and cell size, as well as perimeter. Phagocytically active macrophages as well as the number of beads

they phagocytosed were counted by manual identification of beads, which were located within a macrophage. The number of active phagocytic cells in one picture was divided by the number of cells on the same picture to obtain the phagocytosis rate, which then was normalised to the phagocytosis rate of the untreated control, resulting in the normalised phagocytosis (see 4.2.5.1, 4.2.6). The total number of phagocytosed beads in one picture was divided by the number of active phagocytic macrophages in the same picture, providing beads per cell.

## 4.2.5 Phagocytosis assays

### 4.2.5.1 Non-opsonised phagocytosis assay based on *Mycobacterium bovis* strain Bacille Calmette-Guérin (BCG)

To evaluate the effect of genotoxic stress on non-opsonised phagocytosis, BCGs were used as phagocytic targets. From a, 5 days in advance commenced, bacteria culture, 4ml of the bacteria suspension were withdrawn and centrifuged for 10min at 3000rpm, before being resuspended in 3ml 7H9 medium. This suspension was sonicated for 20 seconds and then the OD<sub>600</sub> was measured via a photometer. The concentration of bacteria was calculated through the OD<sub>600</sub> with the assumption that an OD<sub>600</sub> of 1 equals a concentration of  $3 \cdot 10^8$  bacteria/ml. The necessary number of bacteria was added, in 100µl 7H9 medium, to each well of macrophages.

The macrophages were plated out on 12-well plates in 1ml DMEM plus FBS, which constitutes 10% of the medium, at a concentration of  $1 \cdot 10^5$  macrophages/ml. According to previously performed viability assays, the number of macrophages, in wells which undergo treatment, was increased to compensate for cell death caused by the chemotherapeutic treatment. After letting the cells attach to the plate for 6h at 37°C and 5% CO<sub>2</sub> in a humidified incubator, the medium was replaced by fresh DMEM plus FBS. In addition, the chemotherapeutics of interest were added to the designated wells. Each condition was assigned two wells resulting in two biological replicates per experimental run. The cells were incubated for 24h, at 37°C and 5% CO<sub>2</sub> in a

humidified incubator, and then washed twice with 1ml PBS. Then, 900µl of DMEM plus FBS and  $5 \times 10^5$  bacteria, in 100µl 7H9 medium, were added. To the negative control, 100µl of 7H9 medium were added without any bacteria. The bacteria medium should not exceed 10% of the medium overall. After 16h of co-culture, at 37°C and 5% CO<sub>2</sub> in a humidified incubator, the macrophages were washed two times with 1ml PBS and then resuspended in DMEM plus FBS with 10µg Gentamycin/ml to eliminate any bacteria that was not engulfed. The macrophages were incubated for another hour, at 37°C and 5% CO<sub>2</sub> in a humidified incubator, before being scraped off the plate, washed with 1ml PBS and centrifuged at 300g for 5min. The cell pellet was resuspended in 100µl PBS and a fluorochrome conjugated antibody against CD11b was added. After an incubation of 20min at 4°C, the cells were washed with 1ml PBS and resuspended in 200µl PBS. Then, the macrophages were analysed by MACS Quant VYB. Macrophages which phagocytosed bacteria were identified by first gating on living cells in a plot of forward-scatter(FSC) against side scatter(SSC), then gating on single cells in a plot of FSC height (FSC-H) against FSC width (FSC-W) and finally gating on cells that were double positive for the fluorochrome of the conjugated antibody against CD11b and dsRed, which is expressed by the BCG strain. Analysis was performed with the FlowJo software. The percentage of double positive cells was divided by the mean percentage of double positive cells of the respective control conditions, resulting in mean fold changes of the double positive cells or rather phagocytically active cells, which will be referred to as normalised phagocytosis throughout this work. The total macrophage count was put into relation with the number of BCGs used for each condition, resulting in the bacteria to macrophage ratio.

#### 4.2.5.2 Opsonised Fc-independent phagocytosis assay based on pH-sensitive beads

To elucidate the impact of chemotherapy on opsonised Fc-independent phagocytosis the pH-sensitive beads, mentioned in 4.2.4.1, were utilized as phagocytic targets.

Macrophages were prepared according to the protocol of 4.2.5.1, except for the fact that full macrophage culture medium was used. After macrophages were treated and resuspended in 1ml macrophage culture medium, containing 10% FBS to assure opsonization,  $5 \times 10^5$  labelled beads were added to each well, except for the negative control, which was incubated with  $5 \times 10^5$  unlabelled beads. To improve interaction between macrophages and beads, the 12-well plates were centrifuged at 300g for 1min after beads were added. Then the plates were incubated at 37°C and 5% CO<sub>2</sub> in a humidified incubator for 16h. The macrophages were scraped off the plate and washed twice with 1ml of PBS to eliminate any beads which were not phagocytosed. 100µl of PBS were used to resuspend the macrophages before they were stained with a fluorochrome labelled anti-CD11b antibody for 20min at 4°C. Then they were washed twice with 1ml PBS, resuspended in 200µl PBS and analysed via flowcytometry. To identify macrophages which phagocytosed labelled beads, the same gating strategy as described in 4.2.5.1 was used identifying the cells positive for CypHer5E and the fluorochrome of the anti-CD11b-Antibody. Analysis was performed as depicted in 4.2.5.1.

#### 4.2.5.3 Evaluation of the bacteria to macrophage and bead to macrophage impact on the phagocytosis rate

1ml of a J774A.1 cell suspension, with a concentration of  $1 \times 10^5$  cells per milliliter, was plated out into each well of a 12-well plate. After 6h, the cells were reattached and increasing concentrations of BCG or pH-sensitive beads were added to the wells with at least two wells receiving the same amount of BCG or pH-sensitive beads, creating two biological replicates per condition.  $5 \times 10^5$  unlabelled beads were added to the negative control of the pH-sensitive bead assay. The plates were incubated for 16h at 37°C and 5% CO<sub>2</sub> in a humidified incubator. Cells were prepared for measurement by MACS Quant VYB according to 4.2.5.1 and 4.2.5.2, respectively. Gating and analysis were carried out as described in 4.2.5.1; the bacteria to macrophage or bead to macrophage ratio was not calculated. The different concentrations were normalised to the condition with the lowest number of BCG or pH-sensitive beads in the same experiment.

#### 4.2.5.4 Modification to the BCG and pH-sensitive bead phagocytosis assay

To cancel out the possible effect of the bacteria to macrophage and bead to macrophage ratio on the phagocytosis rate, the BCG and pH-sensitive bead phagocytosis assays were modified. For the BCG-phagocytosis assay, two modifications were tried; the discontinued modification is described in 8.1.4.

3ml J774A.1 were plated out onto 6 well plates in a concentration of  $1 \times 10^5$  cells per milliliter. After cells reattached for 6h, the medium was changed either to DMEM plus FBS in case of the BCG-phagocytosis assay or macrophage culture medium for the pH-sensitive bead assay, with the chemotherapeutic concentrations of interest or without chemotherapeutics for the untreated control. Cells were incubated for 24h, then washed twice with 2ml PBS, resuspended in DMEM plus FBS or macrophage culture medium, scrapped off the plate and counted with Trypan blue and the Neubauer chamber. By centrifuging at 300g for 5min and resuspending the cells in either DMEM plus FBS or macrophage culture medium, the cell suspension was concentrated to  $1 \times 10^5$  cells per milliliter. This cell suspension was plated out onto 12-well plates with 1ml per well. Each condition was designated at least two wells, resulting in at least two biological replicates. After the cells reattached for 6h,  $5 \times 10^5$  BCG or pH-sensitive beads were added to each well, except to the negative control, where either 100 $\mu$ l of 7H9 medium or  $5 \times 10^5$  unlabelled beads were added. Cells were incubated for 16h. Preparation for measurement, gating and analysis were performed as described in 4.2.5.1 and 4.2.5.2.

#### 4.2.5.5 Generation of conditioned medium

J774A.1 macrophages were plated out on a 12-well plate, at a concentration of  $1 \times 10^5$  cells per milliliter and 1 ml per well, 6h before the medium was replaced with fresh DMEM plus 10% FBS and the agents of interest were added. After an incubation of 24h at 37°C and 5% CO<sub>2</sub> in a humidified incubator, the cells were washed twice with 1 ml PBS. Then 1.5 ml of fresh DMEM plus 10% FBS were added to each well and the cells were incubated for another 24h at 37°C and 5% CO<sub>2</sub> in a humidified incubator. 1ml of the generated conditioned medium was transferred onto untreated J774A.1, which were plated out in a concentration of  $1 \times 10^5$  cells per milliliter and 1 ml per well 6h before on a 12-

well plate. Each condition was assigned two wells, resulting in two biological replicates. After incubating them for 24h at 37°C and 5% CO<sub>2</sub> in a humidified incubator, these macrophages were used for a phagocytosis assay with BCGs as engulfment targets (see 4.2.5.1).

#### 4.2.6 Statistical analysis and data illustration

GraphPad Prism software was used to generate diagrams and perform the statistical analysis. Results are shown as mean or mean fold changes of biological replicates, each represented by at least one data point, and error bars as standard deviation (SD). Mean fold changes were utilized to display the changes in the phagocytic capacity, because there were high deviations in the phagocytosis rates in between different experiments for the control as well as the treated conditions, but the increase in the phagocytosis rate for the treated conditions, compared to the untreated control, was consistent in every experiment. They were calculated by dividing the percentage of macrophages, which phagocytosed targets, after treatment by the mean percentage of phagocytically active macrophages of the respective control conditions. This will be referred to as normalised phagocytosis in this work. For the phagocytosis assays, the number of biological replicates was used as sample size (N), to show the data as unchanged as possible and avoid further averaging; for further details, please see description of each figure. Statistical significance was calculated by an unpaired t-test, if the treated conditions were only compared to the untreated control, or an one-way ANOVA with Bonferroni post-test, if treated conditions were compared to the untreated control as well as other treated conditions. Significance was displayed as \*=p<0.05, \*\*=p<0.01, \*\*\*=p<0.001 and \*\*\*\*=p<0.0001.

## 5 Results

### 5.1 Murine macrophage viability decreases dose-dependently when treated with Mafosfamide or Doxorubicin

Chemotherapeutics induce apoptosis in highly proliferating cells, like cancer cells, but also healthy immune cells or epithelia<sup>172</sup>. Bearing this in mind, the effect of the alkylating agent Mafosfamide, the active form of Cyclophosphamide *in vitro*, and the intercalating topoisomerase II inhibitor Doxorubicin on the viability of the murine macrophage cell line J774A.1 was evaluated<sup>174,237</sup>. The viability was assessed with the ATP-dependent CellTiter-Glo kit and the chemotherapeutics were used in serial dilutions ranging in concentration from 1 $\mu$ M to 10 $\mu$ M. Each concentration was used in three wells, resulting in three biological replicates per experiment, which were averaged for each experiment to follow the manufacture's protocol<sup>234</sup>. The J774A.1 macrophages exhibited a dose-dependent reduction of viability between the chemotherapeutic concentrations of 1 $\mu$ M to 10 $\mu$ M (Figure 4). Mafosfamide showed a greater mean reduction in viability for 1 $\mu$ M, 5 $\mu$ M and 10 $\mu$ M agent concentration compared to Doxorubicin, with means of 72%(1 $\mu$ M), 47%(5 $\mu$ M) and 29%(10 $\mu$ M) viability for Mafosfamide and means of 85%(1 $\mu$ M), 55%(5 $\mu$ M) and 40%(10 $\mu$ M) viability for Doxorubicin. Although the statistical significance was greater for the changes induced by Doxorubicin, because of the lower standard deviation within the different conditions. 2.5 $\mu$ M Mafosfamide and Doxorubicin had nearly the same effect on the mean viability of J774A.1 macrophages, with 60% viability for 2.5 $\mu$ M Mafosfamide and 59% viability for 2.5 $\mu$ M Doxorubicin. Beside the control, also the 1 $\mu$ M concentration for both chemotherapeutics showed significant differences, which were not shown in Figure 4, to other concentrations. In the case of 1 $\mu$ M Mafosfamide, a significant difference could be seen when compared to 10 $\mu$ M Mafosfamide( $p < 0.05$ ). 1 $\mu$ M Doxorubicin was significantly different from 2.5 $\mu$ M( $p < 0.05$ ), 5 $\mu$ M( $p < 0.01$ ) and 10 $\mu$ M Doxorubicin( $p < 0.0001$ ). For following experiments, 5 $\mu$ M of the respective

chemotherapeutic should not be exceeded, because of the great reduction in viability by concentrations beyond 5µM.

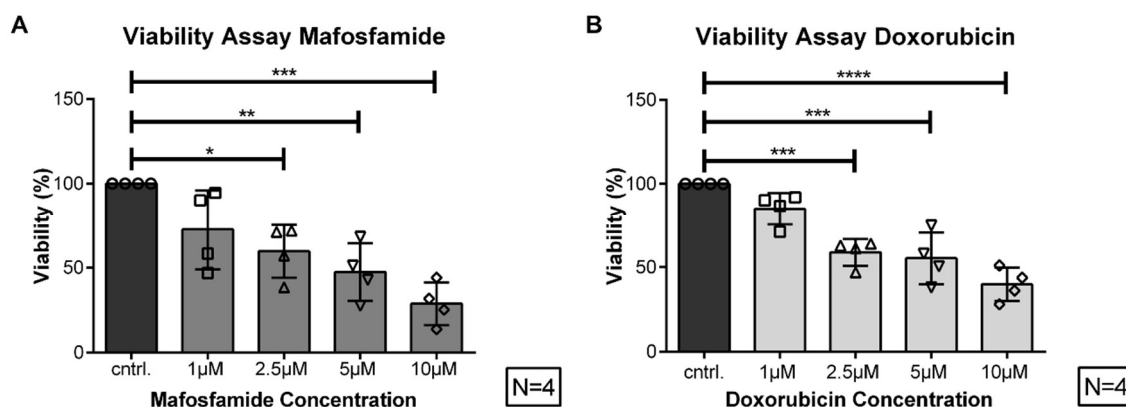


**Figure 4 Viability Assay of J774A.1 treated with different concentrations of Mafosfamide and Doxorubicin.**

J774A.1 macrophages were treated with increasing concentrations of Mafosfamide(A) and Doxorubicin(B) for 24h and then incubated for another 16h in macrophage culture medium. Through the measurement of the ATP amount with the CellTiter-Glo kit in each sample and the normalization to an untreated control, the viability of the macrophages was assessed. Data are expressed as mean +/- SD. The experiment was performed on four separate days with three biological replicates per condition, which were averaged for each experiment to follow the manufacturer's protocol, resulting in a sample size of N=4. (\*=p<0.05; \*\*=p<0.01; \*\*\*=p<0.001; \*\*\*\*=p<0.0001)

## 5.2 Mafosfamide and Doxorubicin induced p53 expression and phosphorylation

In order to evaluate the impact of different Mafosfamide and Doxorubicin concentrations on the DDR pathway of macrophages, J774A.1 cells were incubated for 24h with different concentrations of Mafosfamide or Doxorubicin, ranging from 10nM up to 5µM, before being lysed for protein analysis. The protein lysates were separated according to molecular weight by SDS-PAGE and then blotted onto a nitrocellulose membrane via WB. The nitrocellulose membranes were stained with antibodies against p53, phosphorylated p53(pp53) and β-actin, used as housekeeping protein (Figure 5 A, C; Figure 6 A, C and see 4.1.7.1 for antibodies). Mafosfamide showed an induction of p53 in murine macrophages with a very clear increase in protein levels at 2.5µM, with 153% of the normalised protein amount measured in the untreated control,

and even higher normalised protein levels at 5 $\mu$ M, with 183% compared to the control protein amount (Figure 5 B). Furthermore, Mafosfamide fostered p53 phosphorylation, which suggests its activation. The fluorescence levels of pp53, which were obtained by utilizing fluorescent-tagged secondary antibodies, were normalised to the p53 fluorescent levels of the same condition, showing a general increase in pp53 levels up to 100% of the p53 fluorescence for 5 $\mu$ M Mafosfamide (see 4.2.3.4 for protocol). In addition, 2.5 $\mu$ M and 1 $\mu$ M Mafosfamide showed a clear rise in pp53 levels up to 57% and 35%, respectively, compared to the untreated control, with pp53 levels of 12% (Figure 5 D). Similar results were acquired for Doxorubicin. An increase in p53 levels was generated through the incubation with 2.5 $\mu$ M and 5 $\mu$ M Doxorubicin, with percentages of 136% and 129%, respectively (Figure 6 B). The induction of pp53 was even more impressive, demonstrated by pp53 levels of 63% for 1 $\mu$ M Doxorubicin compared to 34% of the untreated control. Furthermore, 2.5 $\mu$ M and 5 $\mu$ M Doxorubicin displayed very high levels of pp53 of 106% and 136%, respectively; these suggest phosphorylation of every p53 protein in the respective condition, like shown for the case of 5 $\mu$ M Mafosfamide (Figure 6 D). Further experiments were first performed with a concentration of 5 $\mu$ M Mafosfamide or Doxorubicin, because of the clear effect on p53 as well as pp53 levels seen for these conditions, suggesting an effect on protein levels within the macrophages as well as the induction of a distinct DDR. The results shown for the induction of p53 were validated by replication of the same experiment (see 8.1.1).

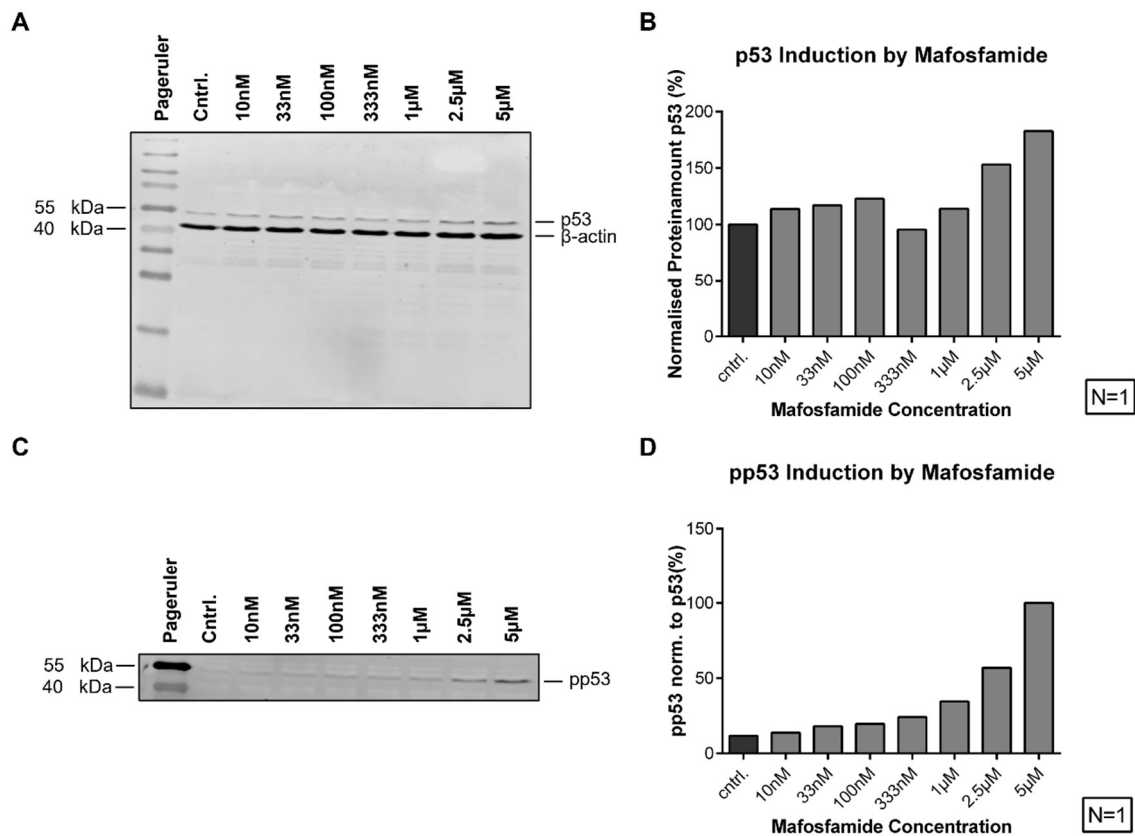


**Figure 5: Induction of p53 and pp53 by Mafosfamide**

J774A.1 cells were treated with different concentrations of Mafosfamide, lysed, separated according to molecular weight by SDS-PAGE and blotted onto a nitrocellulose membrane via WB. The blot with p53 and  $\beta$ -actin staining(**A**) as well as with pp53 staining(**C**) is shown. p53 fluorescence was normalised to  $\beta$ -actin and compared to the normalised p53 levels of the untreated control(**B**). The fluorescent signal of pp53 was normalised to the respective p53 fluorescence(**D**). The results of one WB are shown here.

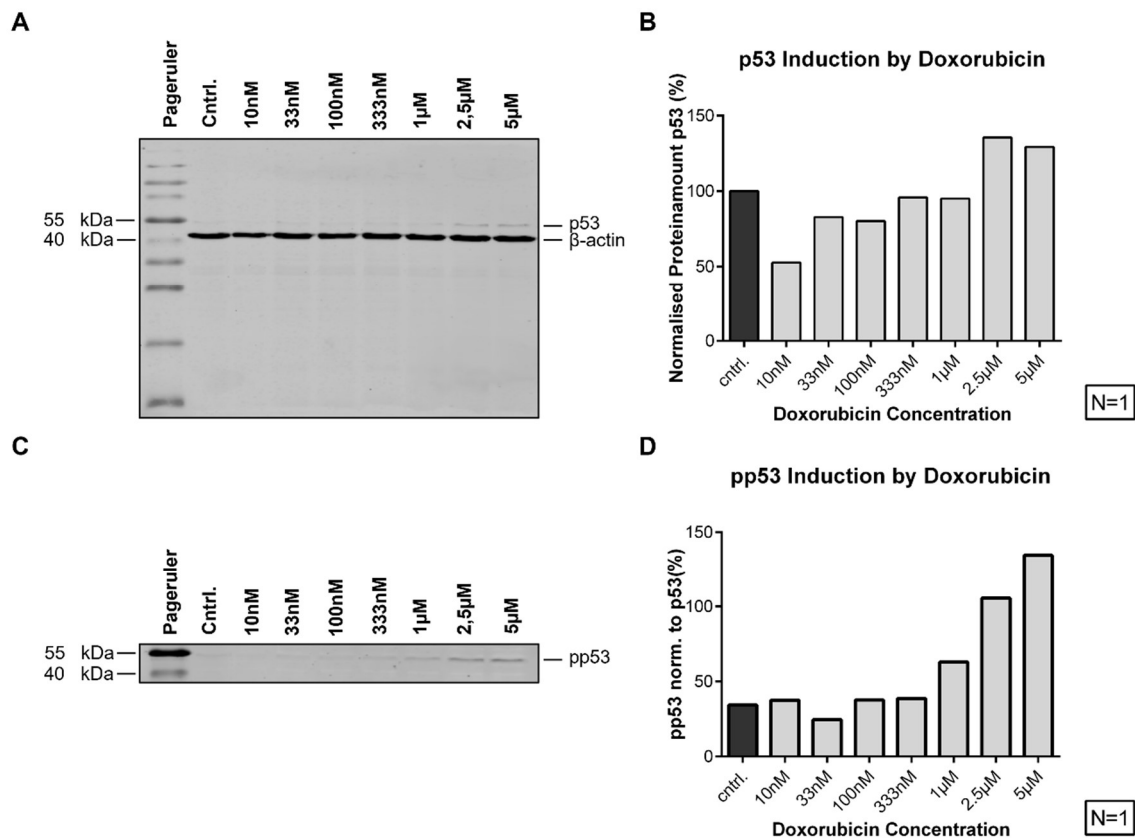


**Figure 6: Induction of p53 and pp53 by Doxorubicin**

J774A.1 cells were treated with different concentrations of Doxorubicin, lysed, separated according to molecular weight by SDS-PAGE and blotted onto a nitrocellulose membrane via WB. The blot with p53 and  $\beta$ -actin staining (A) as well as with pp53 staining (C) is shown. p53 fluorescence was normalised to  $\beta$ -actin and compared to the normalised p53 levels of the untreated control (B). The fluorescent signal of pp53 was normalised to the respective p53 fluorescence (D). The results of one WB are shown here.

### 5.3 Mafosfamide and Doxorubicin induce phenotypical and phagocytic changes in murine macrophages

To evaluate if chemotherapy induces phenotypical and phagocytic changes in macrophages, J774A.1 macrophages were either treated with 5 $\mu$ M Mafosfamide, 5 $\mu$ M Doxorubicin or incubated in macrophage culture medium, after being plated out onto coverslips in a 12-well plate. Two wells per condition were used, resulting in two biological replicates per condition. According to 5.1, more macrophages were plated out in wells of treated conditions to compensate for cell death. After cells were incubated for 24h and washed twice, pH-sensitive

beads were added to each condition and cells were incubated for 16h. Then staining was conducted, after washing away potential non-phagocytosed beads. Two pictures of each biological replicate were acquired with the Zeiss Meta 710 microscope, resulting in four technical replicates per condition. A selection of pictures with scale bars can be seen in Figure 7. In Mafosfamide- and Doxorubicin-treated conditions the rate of active phagocytic cells and the number of beads they phagocytosed increased (Figure 8 E,F). Furthermore, the nuclei of the untreated control appeared to have a denser structure than the nuclei of the treated conditions and the actin staining appeared to be more intense for the treated conditions (see Figure 7). Besides an increase in cell and nucleus size, a general morphology change was apparent with only round cell morphology for the control condition and a more spread out, spindle-like cell morphology for the treated conditions (Figure 8 A-D, see Figure 7).

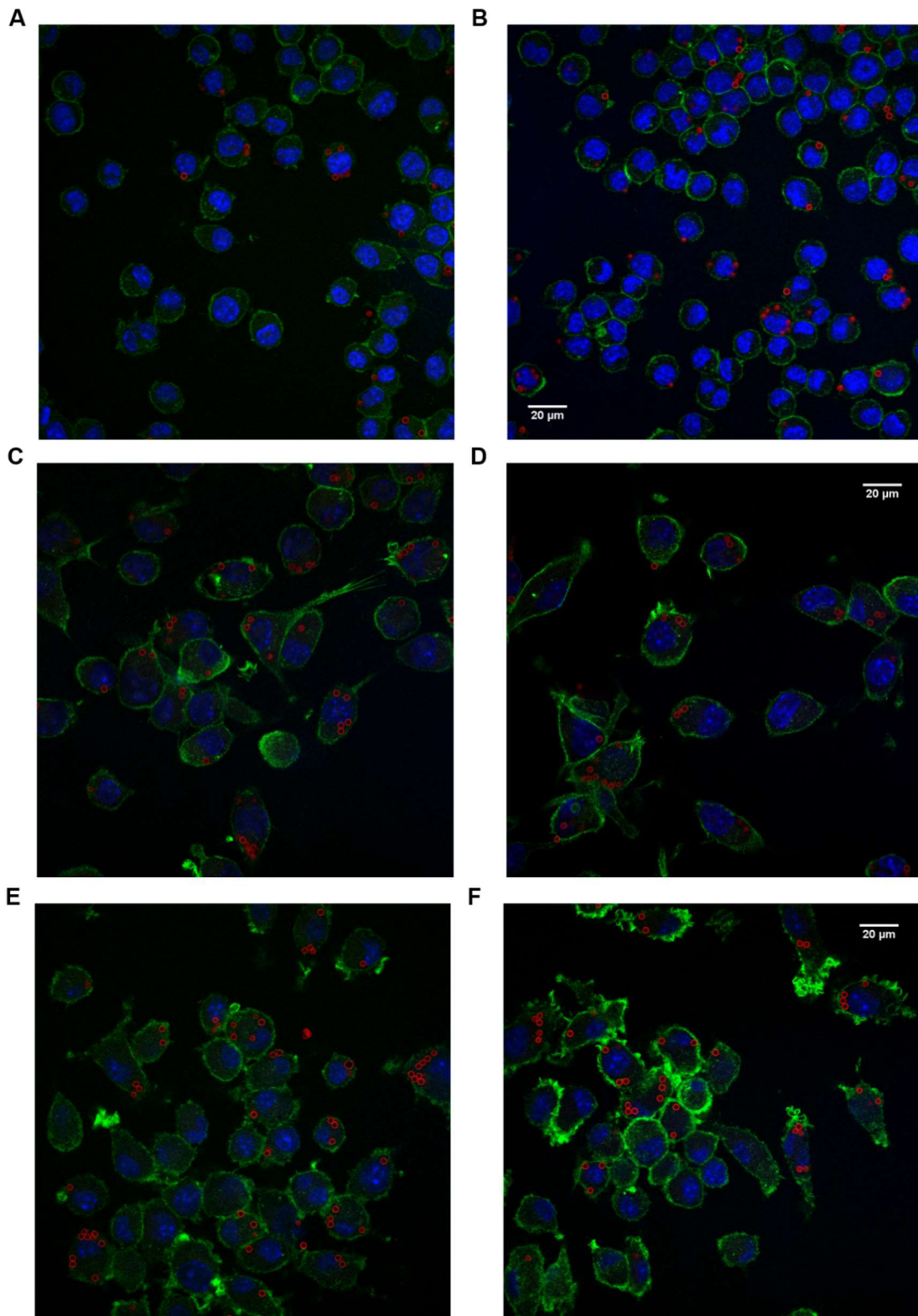


**Figure 7: Microscopy pictures of untreated and treated J774A.1 macrophages with pH-sensitive beads**

Untreated and treated, with 5µM Mafosfamide or Doxorubicin, J774A.1 macrophages were incubated with beads, conjugated with the pH-sensitive fluorochrome CypHer5E, for 16h. Then they were washed, fixed and stained with Phalloidin, conjugated with FITC, and DAPI. Two pictures of the untreated control (**A**, **B**), 5µM Mafosfamide (**C**, **D**) and 5µM Doxorubicin (**E**, **F**), are displayed.

To quantify changes induced by treatment, the microscopy pictures were analysed with the open-source software CellProfiler, which identified the nuclei and respective cells and then measured the size and perimeter of both. Furthermore, cells that phagocytosed beads and the number of beads they phagocytosed were counted by hand (see 4.2.4.2). Based on these data, and for phagocytosis and beads per cell further calculations, the plots seen in Figure 8 were obtained (see 4.2.4.2). To test for significance, the unpaired t-test was utilized, comparing treated conditions to the untreated control to get a preliminary idea of the changes which were induced. The treated conditions were not compared to each other. Nucleus size was significantly increased by Doxorubicin treatment in comparison to the control, resulting in a mean size of 3972.7 pixels compared to 2567.4 pixels for the untreated control. Although the mean increase in nucleus size was greater by Mafosfamide treatment than by Doxorubicin treatment, to a level of 4880.6 pixels, it was not significant compared to the untreated control, because of the higher standard deviation observed for the Mafosfamide conditions (Figure 8 A). Both treatments induced a significant increase in nucleus perimeter with a mean value of 265.2 pixels for Mafosfamide and 235.6 pixels for Doxorubicin compared to 190.5 pixels for the untreated control (Figure 8 B). Furthermore, size and perimeter of the cells were enhanced significantly by the chemotherapeutics compared to the control. Mafosfamide-treated conditions showed a mean cell size of 12545.9 pixels and a mean perimeter of 687.3 pixels. Doxorubicin increased the cell size to a mean of 9952.9 and the mean cell perimeter to 597.6 pixels. The untreated control displayed a mean cell size of 5151.5 pixels and a cell perimeter of 399.3 pixels (Figure 8 C, D). The calculated normalised phagocytosis and beads per cell were also significantly elevated by Mafosfamide and Doxorubicin, with normalised phagocytosis of 1.9 for Mafosfamide-treated conditions and 1.7 for Doxorubicin-treated conditions as well as 2.8 beads per cell for Mafosfamide treatment and 3 beads per cell for Doxorubicin treatment. The control showed a mean of 1.6 beads per phagocytically active cell (Figure 8 E, F). This data showed that macrophages undergo phenotypical changes when treated with chemotherapeutics, like Mafosfamide and Doxorubicin. Furthermore, it suggested that the phagocytic capacity of the macrophage population as well as

each individual macrophage was increased through the treatment with the respective chemotherapeutics.

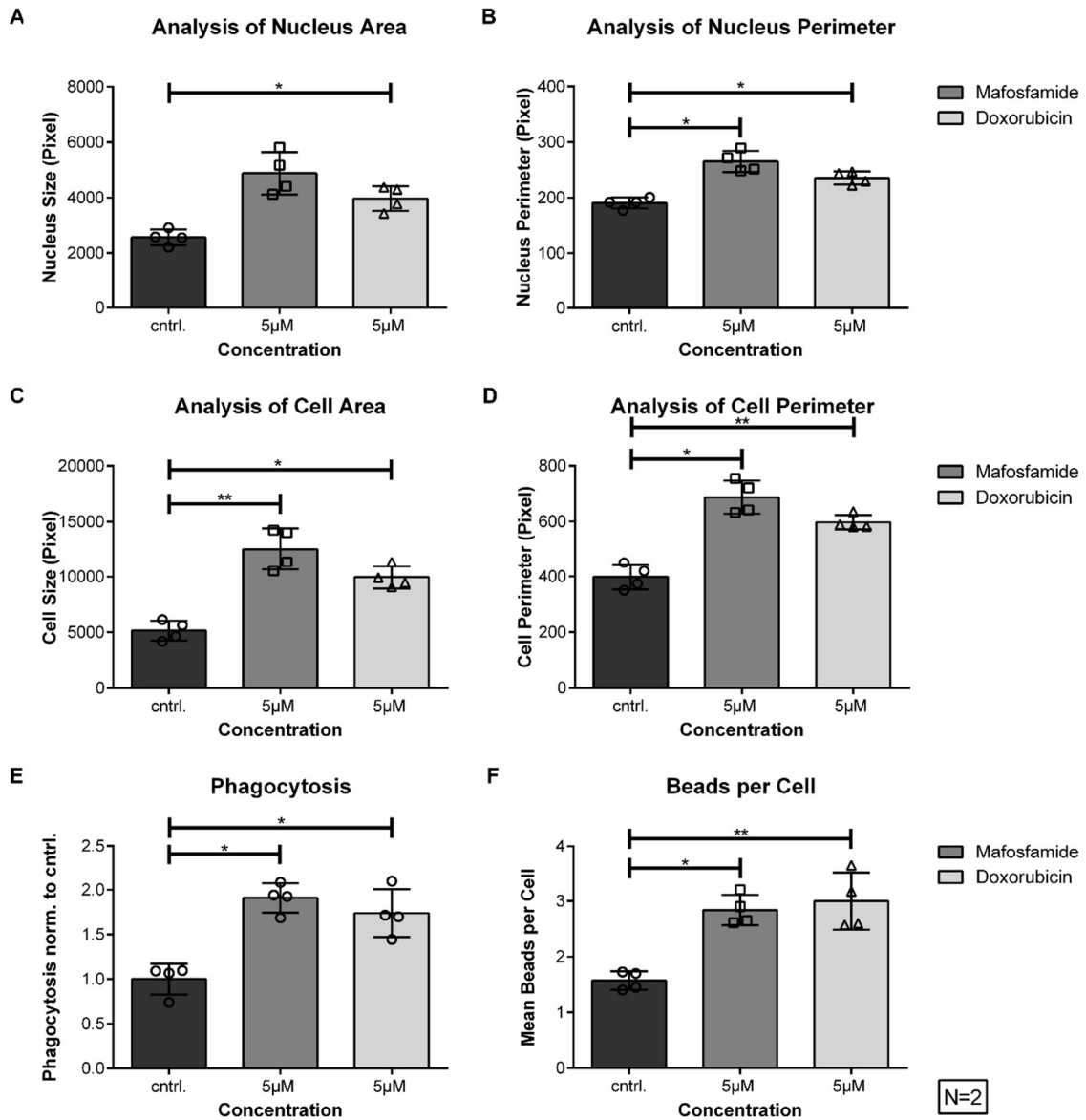


**Figure 8: Analysis of microscopy pictures**

Analysis was carried out by CellProfiler for nucleus and cell size as well as perimeter (A, B, C, D) and by hand for phagocytosis and beads per cell (E, F). The phagocytosis rates were normalised to the phagocytosis rate of the untreated control, resulting in the normalised phagocytosis. Data are expressed as mean +/- SD. The experiment was performed once with two biological replicates, resulting in a sample size of N=2. Each biological replicate is represented by two technical replicates. (\*=p<0.05; \*\*=p<0.01; \*\*\*=p<0.001; \*\*\*\*=p<0.0001)

## 5.4 High concentrations of Mafosfamide and Doxorubicin increase the non-opsonised phagocytic capacity of murine macrophages

To further evaluate the effect of genotoxic stress by Mafosfamide and Doxorubicin on the non-opsonised phagocytosis of macrophages a phagocytosis assay with dsRED-marked BCG bacteria as phagocytic targets was established. First, this assay was performed with 5 $\mu$ M of each chemotherapeutic and an untreated control. Both agents had a clear impact on non-opsonised phagocytosis, increasing it significantly (Figure 9 A). The differences in phagocytic capacity were displayed as mean fold changes, which were calculated by dividing the phagocytosis rate of the particular condition by the mean phagocytosis rate of the respective control conditions, which will be referred to as normalised phagocytosis (see 4.2.5.1, 4.2.6). Each displayed data point represents a biological replicate, with two of them being acquired in the same experiment. This was applied for every phagocytosis assay shown in this work. For 5 $\mu$ M Mafosfamide treatment the mean increase of the normalised phagocytosis was 2 and for Doxorubicin treatment, it was 1.7 (Figure 9 A). Although, according to the viability assay from 5.1, more cells were plated out for the treated conditions, to compensate for cell death, the total cell count and along with this, the bacteria to macrophage ratios differed between the untreated and treated conditions. The untreated control displayed only a ratio of 6.6 bacteria per macrophage, but the treated conditions had a ratio of 36.7 for Mafosfamide, and 44.4 for Doxorubicin, bacteria per macrophage. Especially two biological replicates of the same experimental run, for each treated condition, increase the bacteria to macrophage ratio, as they displayed a much higher ratio than the mean (Figure 9 B). This data suggested an increase in non-opsonised phagocytosis of macrophages by chemotherapy with the respective chemotherapeutics.

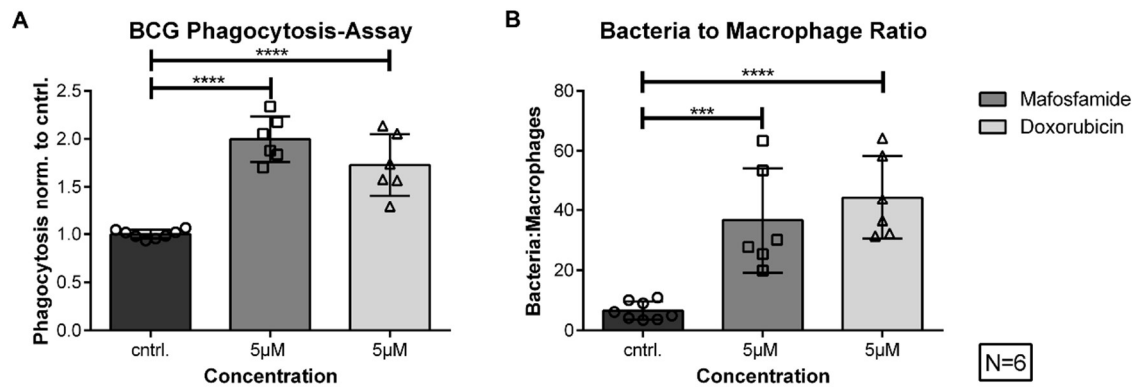


**Figure 9: Mafosfamide and Doxorubicin increased the non-opsonised phagocytosis of J774A.1 macrophages**

J774A.1 were used for a BCG-phagocytosis assay, after being treated with 5 $\mu$ M Mafosfamide or Doxorubicin for 24h or not being treated at all (cntrl.). The rate of double positive cells, for dsRED and the VioGreen anti-CD11b antibody, was identified and then normalised to the double positive cell rate of the respective control(A). The total macrophage cell count and the number of bacteria per condition were put into relation, resulting in the bacteria to macrophage ratio(B). Data are expressed as mean +/- SD. The experiment was performed three times with two biological replicates per run, resulting in a sample size of N=6. (\*=p<0.05; \*\*=p<0.01; \*\*\*=p<0.001; \*\*\*\*=p<0.0001)

## 5.5 The phagocytosis rate was dependent on the bacteria to macrophage ratio

The cause for the increase in phagocytosis in 5.4 was not certain, either being the effect of the chemotherapeutic treatment or just the result of the reduced macrophage number along with the altered bacteria to macrophage ratio. To clarify the impact of the bacteria to macrophage ratio on the phagocytosis rate macrophages were plated out and incubated for 24h, before being co-cultured with increasing amounts of bacteria for 16h. A gain in phagocytic capacity was seen up to a ratio of 1 macrophage per 50 bacteria with a mean increase of 1.9 compared to a ratio of 1 macrophage per 5 bacteria (Figure 10). Significant increases were also shown for ratios of 1:10, 1:20 and 1:40, with mean increases of 1.3, 1.6 and 1.7 (Figure 10 A). A significant decrease in phagocytosis was apparent from a ratio of 1:500 upwards, with a normalised phagocytosis rate of 0.3 (Figure 10 B). This led to the conclusion that in order to acquire reliable results in regard to the impact of chemotherapy on non-

opsonised phagocytosis of macrophages, further experiments had to be performed to equate the differences in the bacteria to macrophage ratios seen in 5.4.

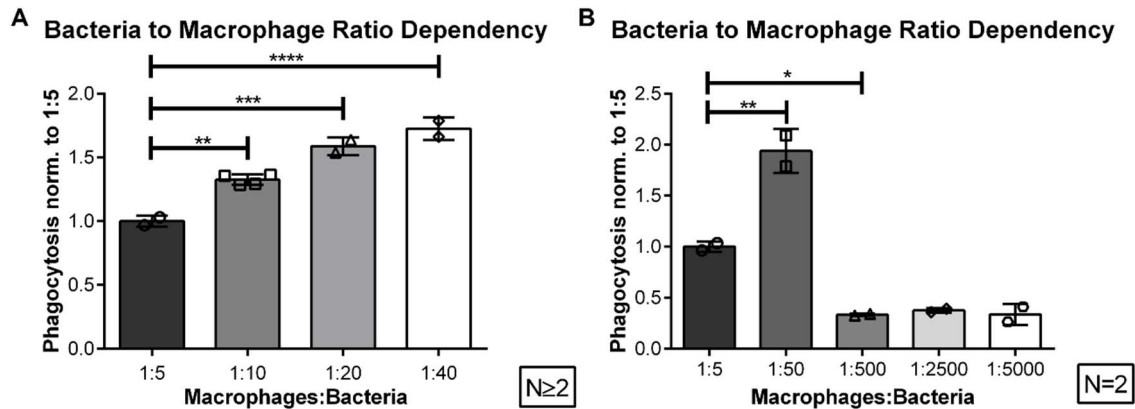


**Figure 10: Dependency of the phagocytic capacity on the bacteria to macrophage ratio**

J774A.1, plated out in the same concentration, were incubated with different amounts of bacteria, resulting in macrophage to bacteria ratios as labelled. The double positive cell rate, for dsRED and the VioGreen anti-CD11b antibody, was measured and then normalised to the double positive cell rate of the 1:5 ratio. Ratios varied from 1:5 to 1:5000 (A, B). Data are expressed as mean +/- SD. The experiment was performed once with at least 2 biological replicates per condition, leading to a sample size of N≥2 or N=2. Only important significances are shown in this figure for clarity reasons. For all significances see 8.1.2. (\*=p<0.05; \*\*=p<0.01; \*\*\*=p<0.001; \*\*\*\*=p<0.0001)

## 5.6 Lower concentrations of Mafosfamide and Doxorubicin seem to have a positive effect on non-opsonised phagocytosis of murine macrophages

The first approach to clarify the results from 5.4 was to reduce the dosage of chemotherapeutic treatment used before macrophages were co-cultured with bacteria. With regards to the results shown in 5.1 and 5.2, concentrations of 2.5µM and 1µM were utilized as they had less impact on viability, but clearly triggered a DDR. Both chemotherapeutics in either concentration increased non-opsonised phagocytosis of the J774A.1 cell line compared to an untreated control. Furthermore, a significant difference in the normalised phagocytosis

could be seen for 1 $\mu$ M Doxorubicin compared to 1 $\mu$ M Mafosfamide treatment. Concentrations of 2.5  $\mu$ M raised the phagocytosis to means of 1.5 for Mafosfamide and 1.7 for Doxorubicin (Figure 11 A). In the case of 1 $\mu$ M concentrations the normalised phagocytosis was increased to levels of 1.2, Mafosfamide, and 1.3, Doxorubicin (Figure 11 C). Different concentrations of the same chemotherapeutic were not compared here, because they were measured in separate experimental runs. The differences in the bacteria to macrophage ratios were reduced, but still could not be cancelled out of influencing the phagocytosis rate with absolute certainty (Figure 11 B, D). The mean bacteria to macrophage ratio for 2.5 $\mu$ M Mafosfamide was 24.5 bacteria per macrophage and for Doxorubicin 28.5 in comparison to 7.1 for the untreated control, although for both treated conditions there were two outliers, which were located well above the remaining values (Figure 11 B). Conditions treated with 1 $\mu$ M Mafosfamide displayed a mean ratio of 13.9 bacteria per macrophage, 1 $\mu$ M Doxorubicin treatment showed a mean ratio of 21.6 bacteria per macrophage and respective control conditions demonstrated a mean ratio of 7.6 (Figure 11 D). This data further indicated a positive effect of chemotherapy on the non-opsonised phagocytosis of macrophages.

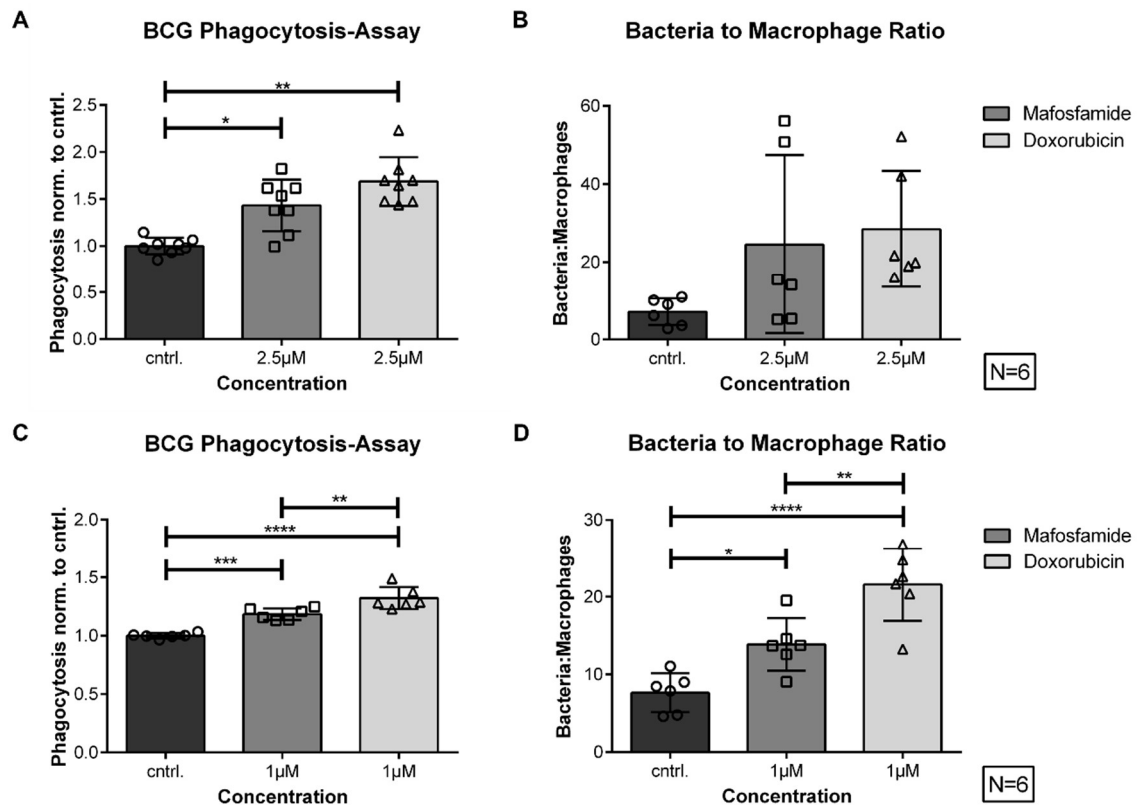


**Figure 11: Lower Mafosfamide and Doxorubicin concentrations increased the non-opsonised phagocytosis of murine macrophages**

J774A.1 were treated with 2.5µM or 1µM of Mafosfamide or Doxorubicin and then used for a BCG-phagocytosis assay. The rate of double positive cells, for dsRED and the VioGreen anti-CD11b antibody, was measured and then normalised to the double positive cell rate of the respective control (A, C). Total macrophage cell count and number of bacteria per condition were put into relation, resulting in the bacteria to macrophage ratio (B, D). Data are expressed as mean +/- SD. The experiments were performed three times with two biological replicates per run, resulting in a sample size of N=6. (\*=p<0.05; \*\*=p<0.01; \*\*\*=p<0.001; \*\*\*\*=p<0.0001)

## 5.7 Modification of the BCG-phagocytosis assay resolves bacteria to macrophage differences

Two modifications of the BCG-phagocytosis assay were tested to eliminate the different bacteria to macrophage ratios, which possibly affected the phagocytosis rate of each condition. After first results, one modification method, in which the bacteria amount, added to each condition, was adapted to cell counts from respective conditions in previous experiments, was discarded, because of impracticability caused by diverging cell counts in between different

repeats (see Appendices). The second modification, in which J774A.1 macrophages were pretreated with the agents of interest and then plated out in the desired concentration, before being incubated with equal amounts of bacteria, was established (see 4.2.5.4). This experiment was performed with a concentration of 5µM Mafosfamide and 5µM Doxorubicin, both conditions still showed significantly higher non-opsonised phagocytosis than the control, as well as 10µM Nutlin-3A, which is a p53 stabilizer and was shown to not have a significant impact on opsonised FcR-dependent phagocytosis (pers comms. Dr. Daniela Vorholt). Normalised phagocytosis was increased to a mean of 1.3 for Mafosfamide conditions, 1.4 for Doxorubicin-treated conditions and 1.2 by Nutlin-3A treatment, compared to untreated control (Figure 12 A). Mean bacteria to macrophage ratios were nearly the same for Mafosfamide, 22 bacteria per macrophage, Nutlin-3A conditions, 20.8 bacteria per macrophage, and the control, 21.9 bacteria per macrophage. Doxorubicin displayed a mean bacteria to macrophage ratio of 39.8. Outliers were present for Doxorubicin, Nutlin-3A as well as for control condition in the bacteria to macrophage ratio (Figure 12 B). This data validated the positive effects of chemotherapy on the non-opsonised phagocytic capacity of macrophages displayed in 5.4 and 5.6.

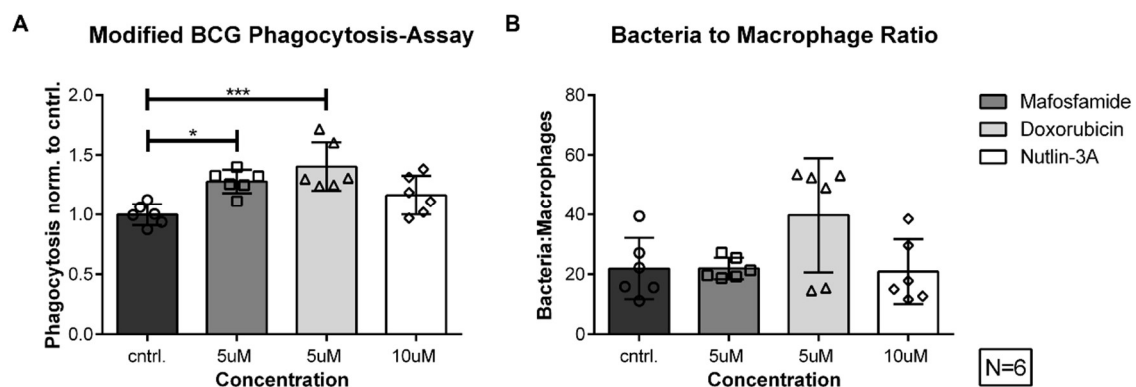


**Figure 12: Mafosfamide and Doxorubicin increased the phagocytic capacity of murine macrophages independent from the bacteria to macrophage ratio.**

J774A.1 were preincubated with Mafosfamide, Doxorubicin and Nutlin-3A, then counted and plated out in the desired concentration, before being co-cultured with bacteria. Double positive cell rate, for dsRED and the VioGreen anti-CD11b antibody, was identified and then normalised to the double positive cell rate of the respective control (A). Macrophage cell count and number of used bacteria per condition were put into relation, resulting in the bacteria to macrophage ratio (B). Data are expressed as mean +/- SD. The experiment was performed three times with 2 biological replicates in each run, resulting in a sample size of N=6. (\*=p<0.05; \*\*=p<0.01; \*\*\*=p<0.001; \*\*\*\*=p<0.0001)

## 5.8 Positive effect on non-opsonised phagocytic capacity of Doxorubicin was conveyed by soluble factors

After the direct effect of Mafosfamide and Doxorubicin on non-opsonised phagocytosis was confirmed, the question arose if this effect could be transferred by the supernatant of treated cells, suggesting the induction of cytokine secretion, like it was observed for leukaemic cells, which transitioned into an ASAP through cyclophosphamide treatment (see 3.5). Pretreated J774A.1, with 5 $\mu$ M Mafosfamide or 5 $\mu$ M Doxorubicin, and untreated J774A.1 were used to generate conditioned medium (see 4.2.5.5). Untreated J774A.1 were incubated with the conditioned medium for 24h, before being used in a phagocytosis assay with BCGs as phagocytic targets (see 4.2.5.1). The conditioned media, generated by Doxorubicin-pretreated J774A.1, did increase the phagocytic capacity of murine macrophages significantly in comparison to the conditioned media of an untreated control as well as conditioned medium generated by Mafosfamide pretreated macrophages, with a mean increase in normalised phagocytosis of 1.3. No difference in the phagocytic capacity was apparent between conditioned medium of untreated cells compared to Mafosfamide pretreated conditions (Figure 13 A). The bacteria to macrophage ratios were equal for the conditioned media of the untreated control and the Mafosfamide-pretreated media, with 3.3 and 3.2 bacteria per macrophage, respectively. The bacteria to macrophage ratio for Doxorubicin-pretreated media was slightly higher, especially caused by two outliers, which were two biological replicates of one experimental run, leading to a mean of 3.9 bacteria per macrophage. These two outliers in ratio also displayed the highest increase in normalised phagocytosis of 1.6 and 1.5 compared to the respective control (Figure 13 A and B). The results of this experiment showed that the effect of Doxorubicin treatment could be conveyed to untreated macrophages through conditioned medium.

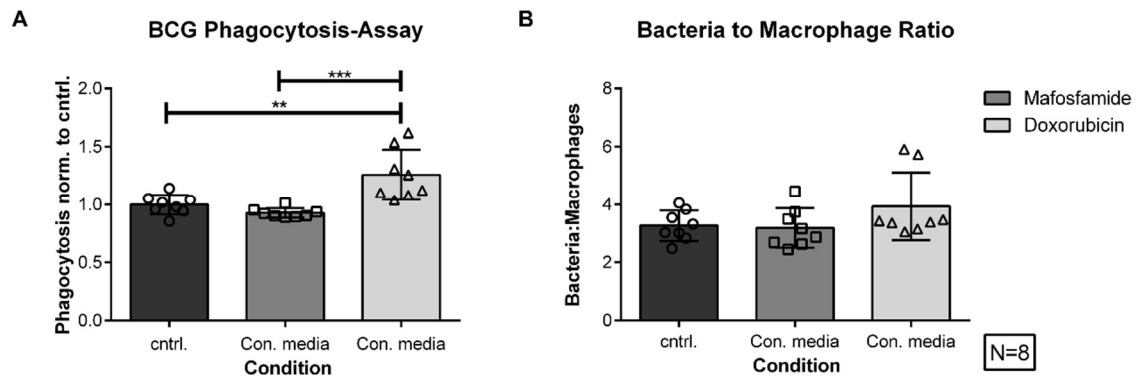


**Figure 13: Effect of conditioned media on the phagocytic capacity of J774A.1.**

J774A.1 were incubated in conditioned media, generated by pretreated J774A.1, and then used for a BCG-phagocytosis assay. Identification of double positive cell rate, for dsRED and VioGreen, was carried out and then normalised to the double positive cell rate of the control (A). Total macrophage cell count and number of bacteria per condition were put into relation, resulting in the bacteria to macrophage ratio (B). Data are expressed as mean +/- SD. The experiment was performed four times with two biological replicates per run, resulting in a sample size of N=8. (\*=p<0.05; \*\*=p<0.01; \*\*\*=p<0.001; \*\*\*\*=p<0.0001)

## 5.9 Phagocytosis rate was dependent on pH-sensitive bead to macrophage ratio

A second phagocytosis assay was established to explore the effects of Mafosfamide and Doxorubicin on opsonised FcR-independent phagocytosis. The phagocytic targets were pH-sensitive beads, which were also used for the microscopy images in 5.3. The dependency on the bead to macrophage ratio was evaluated first. The same amount of J774A.1 were co-cultured with different numbers of beads and then the double positive cell rate was identified. It became apparent that the phagocytosis rate was influenced by the bead to macrophage ratio. It increased up to a ratio of one macrophage per 20 beads, with a mean increase in normalised phagocytosis of 1.5 compared to a ratio of 1:5. Then it hit a plateau till a ratio of 1:80, in which no difference in phagocytosis was seen. And decreased significantly, compared to the plateau, at a ratio of 1:160 with a phagocytosis rate of 1.3, normalised to a ratio of 1:5 (Figure 14 A, B). This dependency of the phagocytosis rate on the bead to

macrophage ratio demonstrated the need to monitor the bead to macrophage ratio in the following experiments.

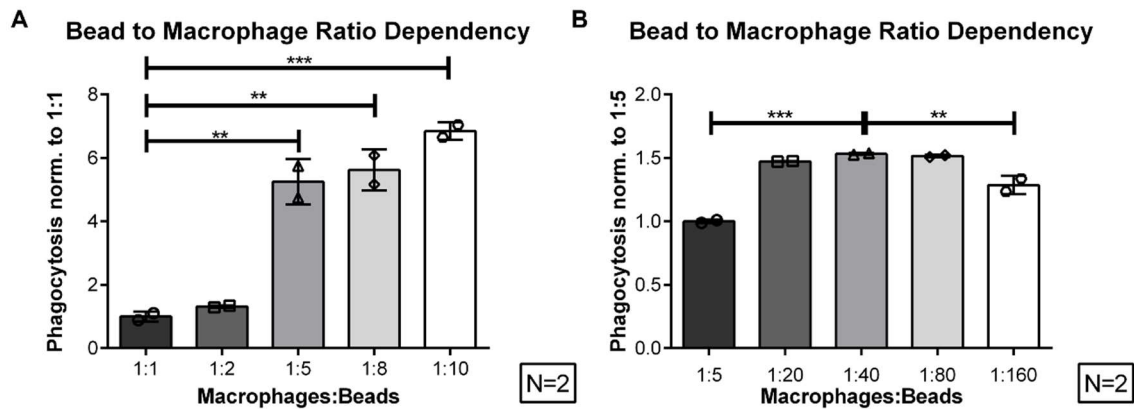


**Figure 14: Impact of the bead to macrophage ratio on the phagocytosis of J774A.1**

J774A.1 were plated out in the same concentrations, before being incubated with different amounts of pH-sensitive beads. The double positive cells, for CypHer5E and the VioGreen anti-CD11b antibody, were measured and then normalised to the bead to macrophage ratio of 1:1 (**A**) or 1:5 (**B**). Data are expressed as mean +/- SD. The experiment was performed once with two biological replicates, resulting in a sample size of N=2. Only important significances are shown in this figure for clarity reasons. For every calculated significance see 8.1.3. (\*=p<0.05; \*\*=p<0.01; \*\*\*=p<0.001; \*\*\*\*=p<0.0001)

## 5.10 Phagocytosis of pH-sensitive beads was enhanced by Mafosfamide and Doxorubicin

Following the protocol of the BCG-phagocytosis assay, a phagocytosis assay based on pH-sensitive beads was established. First J774A.1 were pretreated with 5µM Mafosfamide or Doxorubicin, before being incubated with pH-sensitive beads. A significant increase in phagocytosis became apparent, 5µM Mafosfamide and 5µM Doxorubicin showed a mean increase of 2.7 in normalised phagocytosis in comparison to an untreated condition (Figure 15 A). But the bead to macrophage ratios differed a lot between untreated, 6.4 beads per macrophage, and treated conditions, 44.6 beads per macrophage for

Mafosfamide and 44.4 beads per macrophage in the case of Doxorubicin treatment (Figure 15 B).

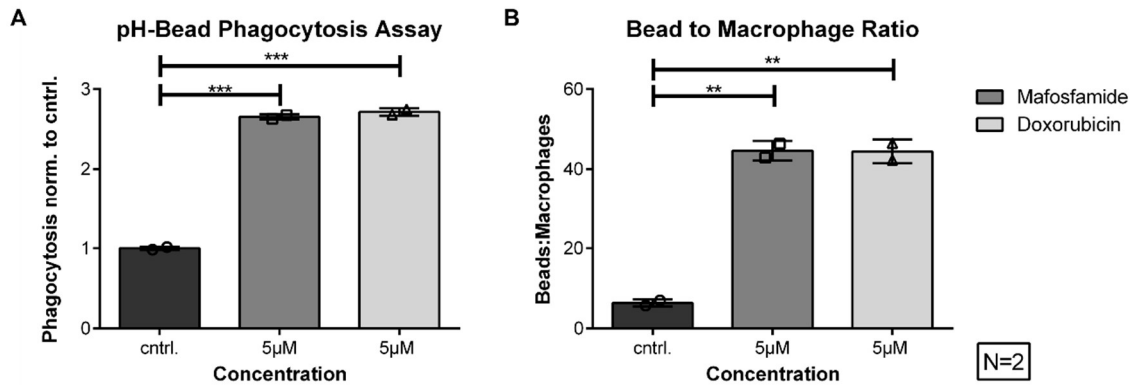


**Figure 15: 5µM Mafosfamide and Doxorubicin increased pH-sensitive bead phagocytosis by murine macrophages**

J774A.1 were treated with 5µM Mafosfamide or Doxorubicin and then incubated with pH-sensitive beads. Double positive cells, for CypHer5E and the VioGreen anti-CD11b antibody, were identified by flowcytometry and the double positive cell rate was normalised to the double positive cell rate of the control (A). The bead to macrophage ratio was calculated by dividing the used bead number by the total macrophage count obtained by flowcytometry (B). Data are expressed as mean +/- SD. The experiment was performed once with two biological replicates, resulting in a sample size of N=2. (\*=p<0.05; \*\*=p<0.01; \*\*\*=p<0.001; \*\*\*\*=p<0.0001)

This experiment was only performed once with 5µM concentrations of the respective chemotherapeutics, because of the high difference in bead to macrophage ratios. Again, the first approach to eliminate these differences was a reduction in chemotherapeutic concentration to levels of 2.5µM and 1µM. Significantly elevating the phagocytic capacity, 2.5µM Mafosfamide displayed a mean increase in normalised phagocytosis of 1.7 and 1µM Mafosfamide of 1.3 compared to the untreated control. Furthermore, a significant difference between the phagocytosis capacity of 2.5µM and 1µM Mafosfamide can be seen (Figure 16 A). Doxorubicin significantly increased the normalised phagocytosis at concentrations of 2.5µM, with means of 1.6, and 1µM, means of 1.3, compared to the untreated control as well as displaying a significant increase between the two concentrations of the chemotherapeutic (Figure 16 C). Still the bead to macrophage ratios differed between treated conditions and

respective control (Figure 16 B, D). The differences were not as great as seen for the concentration of 5 $\mu$ M, but 2.5 $\mu$ M Mafosfamide demonstrated a mean ratio of 11.8 beads per macrophage and 1 $\mu$ M Mafosfamide of 7.2 with the control showing a mean ratio of 3.3 (Figure 16 B). Doxorubicin-treated conditions showed a mean bacteria to macrophages ratio of 18.4 for 2.5 $\mu$ M and 9.2 for 1 $\mu$ M and the respective control had a mean ratio of 3.3 (Figure 16 D). Outliers for the treated conditions must be considered regarding the bead to macrophage ratio and the comparison to respective control conditions. This data suggested a positive impact of chemotherapy, in different doses, on opsonised Fc-independent phagocytosis by macrophages.

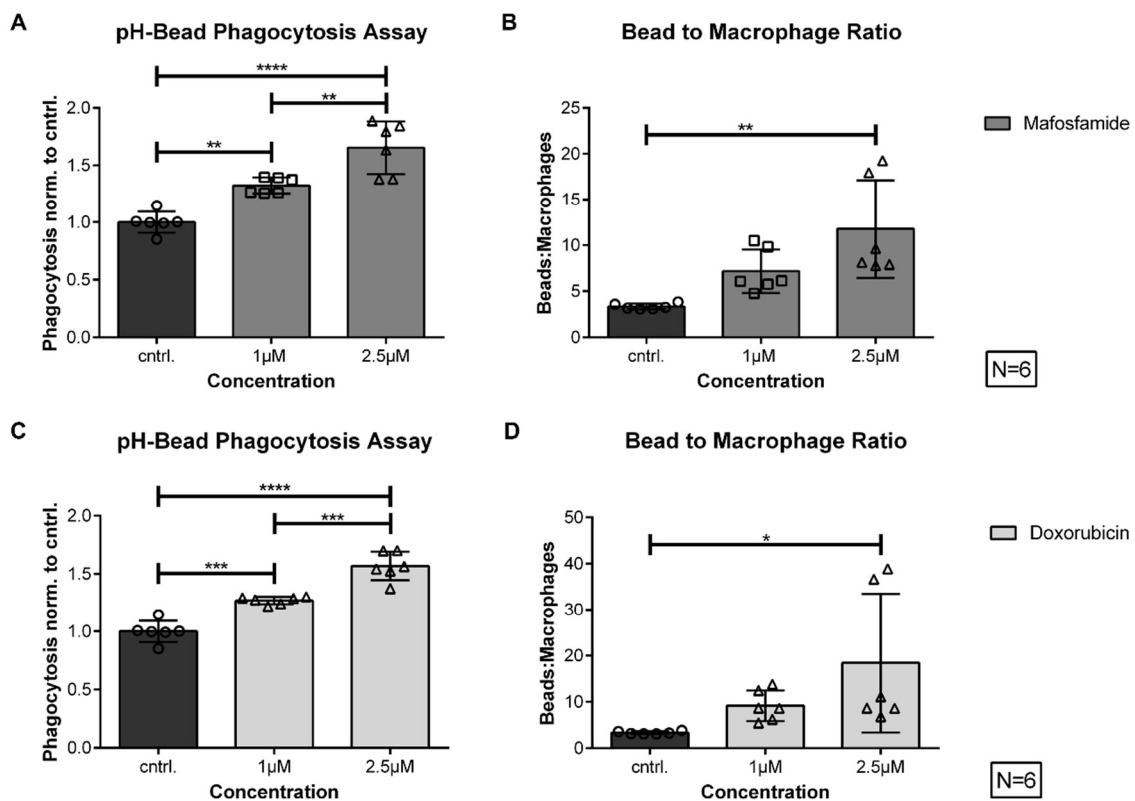


**Figure 16: Lower concentrations of Mafosfamide and Doxorubicin increase phagocytosis of pH-sensitive beads by murine macrophages**

J774A.1 were pretreated with 2.5 $\mu$ M or 1 $\mu$ M Mafosfamide or Doxorubicin, before being incubated with pH-sensitive beads. Double positive cells, for CypHer5E and the VioGreen anti-CD11b antibody, were identified by flowcytometry and the double positive cell rate was normalised to the double positive cell rate of the respective control (A, C). The bead to macrophage ratio was calculated by dividing the used bead number by the total macrophage count obtained by flowcytometry (B, D). Data are expressed as mean +/- SD. Three separate experimental runs were performed with 2

biological replicates for each condition, resulting in a sample size of N=6. (\*= $p < 0.05$ ; \*\*= $p < 0.01$ ; \*\*\*= $p < 0.001$ ; \*\*\*\*= $p < 0.0001$ )

## 5.11 In a modified pH-sensitive bead phagocytosis assay, Mafosfamide and Doxorubicin have a positive effect on phagocytic capacity

Because of the differences in the bead to macrophage ratios seen in 5.10, the pH-sensitive bead phagocytosis assay was modified based on the adjustments made to the BCG-phagocytosis assay (4.2.5.4). Pretreated J774A.1 were plated out in equal concentrations and then incubated with the same number of pH-sensitive beads. Each condition was assigned at least two wells, resulting in at least two biological replicates per experiment. Both chemotherapeutics, Mafosfamide and Doxorubicin, induced a significant increase in normalised phagocytosis in murine macrophages, regardless of their concentration, compared to respective control conditions (Figure 17 A, C). For 5 $\mu$ M Mafosfamide the mean increase in normalised phagocytosis was 1.7 and 2.5 $\mu$ M Mafosfamide displayed a mean increase of 1.4. The different concentrations of Mafosfamide displayed a significant difference in normalised phagocytosis with 5 $\mu$ M displaying a significantly higher phagocytic capacity (Figure 17 A). Doxorubicin demonstrated an increase of 1.5, for 5 $\mu$ M, and 1.4, for 2.5 $\mu$ M, on average, also showing a general increase for higher doses (Figure 17 C). The differences in the bead to macrophage ratio were reduced, but not fully eliminated through the modifications (Figure 17 B, D). The Mafosfamide-treated conditions displayed a ratio of 37.7 beads per macrophage for 5 $\mu$ M and 25.4 for 2.5 $\mu$ M, demonstrating a significant difference between the different conditions as well as to the untreated control with 11.9 beads per macrophage (Figure 17 B). For Doxorubicin the bead to macrophage ratio was raised to a mean of 31.3 for 5 $\mu$ M and 38 for 2.5 $\mu$ M, but with one extreme outlier at 101 beads per macrophage, also showing a significant increase compared to the respective control, displaying a ratio of 11.9 beads per macrophage (Figure 17 D). The data obtained by this experiment demonstrated the positive impact of

Mafosfamide and Doxorubicin on the opsonised Fc-independent phagocytosis capacity of macrophages.

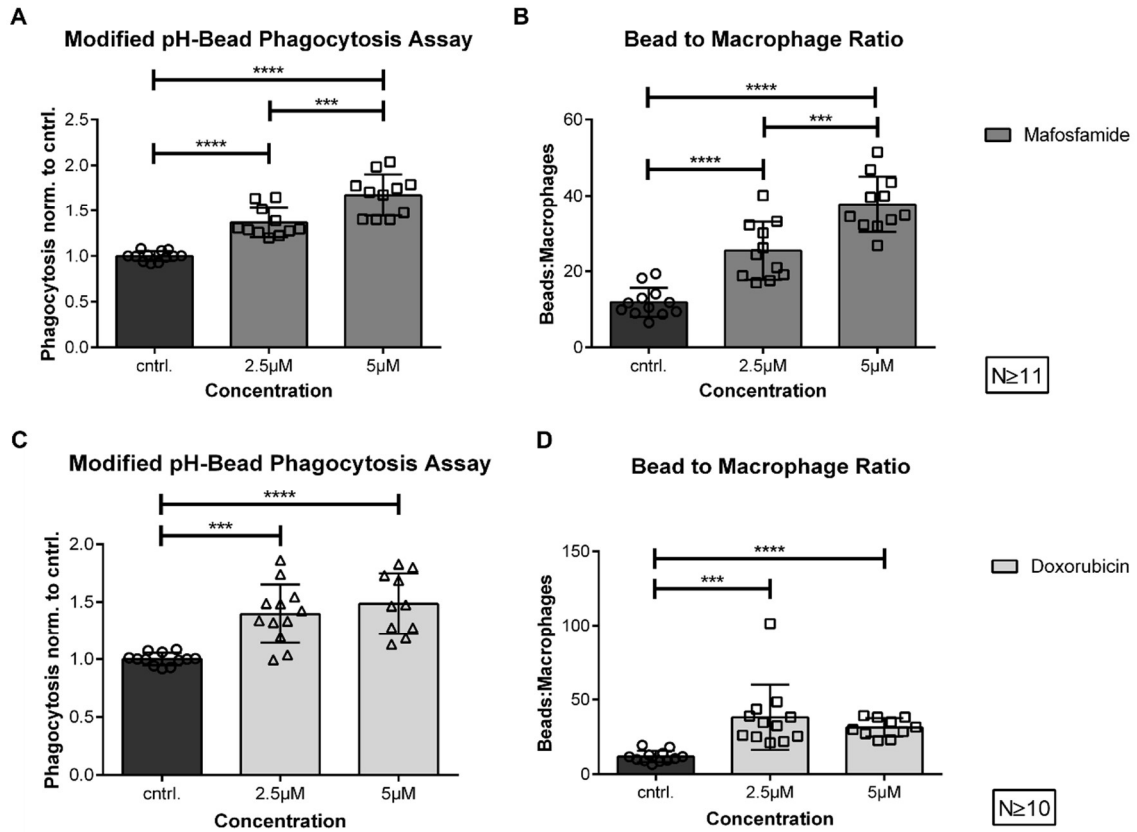


**Figure 17: Mafosfamide and Doxorubicin increased the phagocytic capacity of murine macrophages in a modified pH-sensitive bead phagocytosis assay**

Pretreated J774A.1 were counted and plated out in equal concentrations, before being incubated with the same number of pH-sensitive beads. Double positive cells, for CypHer5E and the VioGreen anti-CD11b antibody, were measured by flowcytometry and the double positive cell rate was normalised to the double positive cell rate of the respective control (**A**, **C**). The bead to macrophage ratio was calculated by dividing the used number of beads by the total macrophage count obtained by flowcytometry (**B**, **D**). Data are expressed as mean +/- SD. The experiment was performed three times with at least two biological replicates per experimental run, resulting in a sample size of N≥11 for Mafosfamide-treated conditions and N≥10 for Doxorubicin-treated conditions. (\*=p<0.05; \*\*=p<0.01; \*\*\*=p<0.001; \*\*\*\*=p<0.0001)

## 6 Discussion

In the beginning of cancer therapy, chemotherapeutics were identified as anti-cancer agents, because of their cytotoxic effect on highly proliferating tissues, which also causes many side effects seen for chemotherapy<sup>208</sup>. Within the last decades more evidence has arisen, proving the immunological effect of chemotherapeutics, e.g. Cyclophosphamide and Doxorubicin, and showing its positive impact on anti-cancer therapy, like the depletion of certain immunosuppressive cells, e.g. Treg cells and MDSCs, as well as ICD (see 3.5). Furthermore, the introduction of monoclonal antibodies, like the CD20 antibody rituximab, and their addition to established chemotherapeutic regimens, e.g. CHOP scheme (Cyclophosphamide, Doxorubicin, Vincristine and Prednisolone) for the treatment of DLBCL or FC scheme (Fludarabine and Cyclophosphamide) for CLL treatment, showed an improved overall survival compared to standard therapy, which in the case of Rituximab plus CHOP scheme (R-CHOP) was associated with high TAM levels<sup>133,238,239</sup>. This further highlighted the impact of interactions between chemotherapeutics and the immune system, especially TAMs, on the efficacy of cancer therapy. Cancer infiltrating macrophages were believed to be a negative prognostic factor for therapy response and overall survival, because of their ability to directly suppress immune responses after chemotherapy, protect cancer cells from chemotherapeutic induced cell death and even protect cancer stem cells (CSCs) from the cytotoxic effect of chemotherapeutics<sup>240-242</sup>. But also, it was shown that Doxorubicin and Cyclophosphamide are dependent on the support of the immune system, notably macrophages, to reach their full anti-tumor efficiency<sup>243-245</sup>. Moreover, the working group of Prof. Dr. Pallasch could show the importance of macrophages in cancer cell clearance in a humanized MYC/Bcl2 (hMB) mouse model, treated with Cyclophosphamide and the CD52 antibody Alemtuzumab<sup>228,240,246</sup>. Leukaemic cells were shown to transition into an acute secretory activating phenotype (ASAP), under the influence of Cyclophosphamide, secreting VEGF-A, TNF- $\alpha$ , IL8 and CCL4, which led to an increased phagocytic capacity of macrophages and in combination with Alemtuzumab to more effective tumor cell clearance<sup>228</sup>. In addition, a direct positive effect by Mafosfamide and Doxorubicin on macrophages, in terms of

opsonised FcR-dependent phagocytosis, was shown<sup>247(Preprint)</sup>. This study was performed to further elucidate the direct effects of chemotherapeutics on phenotype and phagocytic capacity of macrophages.

## 6.1 Chemotherapy treatment induced phenotypical changes in macrophages which suggested a more phagocytically active phenotype.

In this study, it was demonstrated that throughout the incubation of J774A.1 murine macrophages with Mafosfamide or Doxorubicin phenotypical changes could be induced in macrophages. In general, treated macrophages exhibited a more spread-out morphology with more cells having a spindle-like form (Figure 7 C-F). This shift in morphology to an elongated, more spindle-like cell form was demonstrated for M1 polarisation of human macrophages, suggesting a repolarisation of the treated macrophages towards the M1 pole of the macrophage polarisation spectrum<sup>248</sup>. A significant increase in nucleus size and perimeter was apparent for macrophages which were treated with Doxorubicin. Mafosfamide treatment displayed a significant increase in nucleus perimeter and the greatest mean nucleus size, which did not display significance compared to the control condition, because of the standard deviation in the small sample size, used in this study (5.3). Furthermore, a looser chromatin structure was observed for Mafosfamide- and Doxorubicin-treated macrophages (Figure 7). A larger nucleus with looser chromatin has been usually associated with euchromatin, which is transcriptionally active<sup>13</sup>. Going hand in hand with the elevated protein amounts seen in the WBs, this indicated more gene activity within the treated cells, which represented the induction of a DDR, but also had further impacts on macrophages (5.2). The significant increase in cell size and perimeter indicated an effect on the actin cytoskeleton by the induced gene activity (5.3). This was also underlined by a more intense actin staining, which can be seen in the microscopy pictures (see Figure 7). The actin cytoskeleton plays a crucial role in the process of phagocytosis by contributing to the formation of pseudopodia and the engulfment of phagocytic targets (see 3.2.2).

Furthermore, a greater macrophage cell size and perimeter, as seen for the treated macrophages, was associated with an increased phagocytic capacity<sup>249,250</sup>. This could be due to a larger cell surface with more potential for interaction with surrounding particles.

The data presented throughout this thesis, especially in 5.3, allowed for the acceptance of the biological hypothesis that chemotherapy induces phenotypical changes in macrophages, which suggest a more phagocytically active phenotype.

To further elucidate the impact of chemotherapy on macrophage polarisation and phenotype, a characterization of treated cells in comparison to untreated cells by surface and intracellular markers could be of great use. Different macrophage polarisations were associated with certain intracellular and extracellular markers. CD80, CD86, CD68 and inducible Nitric oxide synthase (iNOS) could be employed as M1 surface markers<sup>63</sup>. To identify M2a-polarisation CD200 receptor (CD200R), Arginase 1 (Arg1) and found in inflammatory zone protein (Fizz1) could be utilized<sup>251</sup>. M2b macrophages express high levels of CD86<sup>252</sup>. M2c-polarisation could be distinguished by CD206 and CD164 expression<sup>253</sup>. By the simultaneous expression of iNOS and TGF- $\beta$  M2d macrophages could be identified<sup>252</sup>. Characterization by surface and intracellular markers of Mafosfamide and Doxorubicin-treated J774A.1 was performed by the working group of Prof. Dr. Pallasch. Treated macrophages, with either chemotherapeutic, displayed high levels of M1-markers CD68, CD80 and CD86 as well as M2c-polarisation marker CD206. Furthermore, J774A.1 expressed high levels of the immune checkpoint ligand PD-L1 after chemotherapy treatment<sup>247(Preprint)</sup>. The high expression of CD206 and PD-L1 suggested an immunoregulatory function for chemotherapy treated macrophages, with CD206 being a marker for M2c-polarisation and PD-L1 being the ligand of PD-1, which upon binding inhibit the proliferation and activation of T cells<sup>253,254</sup>. The increased levels of PD-L1 could provide a mechanistic explanation for the efficacy of combining PD-1 or PD-L1 inhibitors with standard chemotherapy<sup>255,256</sup>. The clear expression of M1-polarisation markers questioned the classification into the known M2-polarisation subtypes, leading to the conclusion that a new macrophage polarisation was observed

here. To further characterize this activation status, it would be helpful to identify the cytokine profile of treated macrophages via enzyme-linked immunosorbent assay (ELISA) or real-time quantitative PCR. Cytokines of interest would be IL-1, -6, -10, -12, TNF and TGF- $\beta$  as they would allow for classification into the defined macrophage polarisations<sup>252,257</sup>. Further defining the observed macrophage activation status after chemotherapy treatment, could provide further insight into their role and function in the TME as well as their tumoricidal capabilities.

## 6.2 Direct chemotherapy treatment increased opsonised and non-opsonised Fc-independent phagocytic capacity of macrophages.

Phagocytosis has been identified as a key function of macrophages to eliminate pathogens, apoptotic cells, debris and mutated cells<sup>258</sup>. Prof. Dr. Pallaschs working group could already show an increase in opsonised FcR-dependent phagocytosis by Mafosfamide- and Doxorubicin-treated macrophages, therefore this study focused on the opsonised FcR-independent phagocytosis as well as the non-opsonic phagocytic capacity of macrophages<sup>247(Preprint)</sup>.

Besides displaying a significant increase in nucleus and cell perimeter as well as cell size for both chemotherapeutics and a significant increase in nucleus size after Doxorubicin treatment, the analysis of the microscopy pictures also revealed a significant increase in phagocytosis rate as well as phagocytosed beads per cell (5.3). The higher rate of engulfment could be linked to the increased cell size and perimeter, as depicted in 6.1. In addition, it indicated a different activation state or polarisation of treated macrophages, which was induced by Mafosfamide and Doxorubicin. To further elucidate the effect of these chemotherapeutics on phagocytosis, a pH-sensitive bead and a BCG based phagocytosis assay were established.

The impact on opsonised FcR-independent phagocytosis was evaluated utilizing latex beads, labelled with a pH-sensitive fluorochrome, as phagocytic

targets, which do not depend on recognition by Igs, but require FBS for opsonization and phagocytosis<sup>236</sup>. The effect of the bead to macrophage ratio on the phagocytosis rate became apparent, showing an increase up to a ratio of 20 beads per macrophage, reaching a plateau till a ratio of 80 beads per macrophage before declining again for higher ratios (5.9). A significant increase in phagocytosis was seen for Mafosfamide and Doxorubicin at a concentration of 5 $\mu$ M, but also different bead to macrophage ratios for the control and the treated conditions, which could have caused the observed increase in phagocytosis. This issue could be resolved partly by reducing the concentrations of the chemotherapeutics to 2.5 $\mu$ M or 1 $\mu$ M. A significant elevation in the phagocytosis rate was still seen with these concentrations and the differences in the bead to macrophage ratio were reduced, but not completely abolished. Still an influence of the bead to macrophage ratio on the phagocytosis rate could not be ruled out, but the degree of difference was mainly caused by two outliers for every treated condition. Interestingly these outliers, in ratio, were obtained in the same experimental run. In addition, these outliers did not correlate with a divergently higher phagocytosis rate, compared to the other biological replicates. Either the phagocytosis rate did not show a great deviation or, in the case of 2.5 $\mu$ M Mafosfamide, the outliers in ratio displayed the lowest phagocytosis rate of all the replicates (5.10). Questioning the real impact of the measured bead to macrophage ratio on the phagocytosis rate within the assay, this further underlined the positive effect of Mafosfamide and Doxorubicin treatment on the phagocytic capacity of macrophages. Furthermore, a significant difference in phagocytic capacity was seen for the different concentrations of the same chemotherapeutic. Diverging bead to macrophage ratios were observed for 1 $\mu$ M and 2.5 $\mu$ M Mafosfamide. But for two experimental runs the differences in the phagocytic capacity were higher than expected, when taking the diverging bead to macrophage ratios into account. For 1 $\mu$ M and 2.5 $\mu$ M Doxorubicin only in one experimental run different bead to macrophage ratios were observed, which could also not explain the increase in phagocytic capacity between the concentrations. Two experimental runs did not show any difference in the bead to macrophage ratio between 1 $\mu$ M and 2.5 $\mu$ M Doxorubicin, but still the higher concentration displayed a greater phagocytic capacity (5.10). This further highlighted the positive impact of Mafosfamide and

Doxorubicin on the opsonised FcR-independent phagocytic capacity of macrophages and even hinted towards a dose dependent effect. Nevertheless, the protocol of the pH-sensitive bead phagocytosis assay was modified to abolish the differences in the bead to macrophage ratio. In the modified pH-sensitive bead phagocytosis assay Mafosfamide- and Doxorubicin-treated macrophages displayed a significant increase in phagocytosis at concentrations of 5 $\mu$ M as well as 2.5 $\mu$ M. The bead to macrophage ratios were not equalized completely by the modification, but again it became obvious that outliers in the bead to macrophage ratio did not show a higher phagocytosis rate than their respective replicates. The outliers were biological replicates of different experimental runs (5.11). But in between the different concentrations of one chemotherapeutic the bead to macrophage ratios could not have impacted the phagocytosis rate, because they were located in the described plateau between a ratio of 1:20 and 1:80, but still the phagocytosis rate was significantly higher for 5 $\mu$ M Mafosfamide than 2.5 $\mu$ M Mafosfamide and higher for 5 $\mu$ M Doxorubicin than 2.5 $\mu$ M Doxorubicin. Also, this hinted at a dose dependent effect of the chemotherapy on opsonised FcR-independent phagocytosis. Furthermore, the displayed increase in phagocytosis was greater as anticipated based of the differences in the bead to macrophage ratio. An increase of 1.1 to 1.2 could have been caused by the different ratios, but the mean increases in phagocytic capacity, for treated conditions, were up to levels of 1.7 for 5 $\mu$ M Mafosfamide, 1.5 for 5 $\mu$ M Doxorubicin and 1.4 for 2.5 $\mu$ M Mafosfamide as well as 2.5 $\mu$ M Doxorubicin compared to the untreated control (5.9 and 5.11). This led to the conclusion, that Mafosfamide- and Doxorubicin-treated J774A.1 macrophages displayed a significantly higher opsonised Fc-independent phagocytic capacity than untreated J774A.1 macrophages.

To evaluate the effect of Mafosfamide and Doxorubicin treatment on non-opsonised phagocytic capacity of macrophages a BCG based phagocytosis assay was established. BCG-phagocytosis assays, performed with different amounts of bacteria for the diverse conditions, showed that the phagocytosis rate was depending on the bacteria to macrophage ratio. An increase in phagocytosis was seen up to a ratio of 50 bacteria per macrophage and a decrease could be seen from 500 bacteria per macrophage onwards (5.5). The

bacteria to macrophage ratio was monitored in the performed BCG-phagocytosis assays. A significant increase in phagocytosis was achieved through the incubation of J774A.1 macrophages with 5 $\mu$ M Mafosfamide or 5 $\mu$ M Doxorubicin, but also a great difference in bacteria to macrophage ratios was observed between the treated conditions and untreated control. Again, the change in mean bacteria to macrophage ratio was especially caused by outliers, which were two biological replicates of the same experimental run and did not display a higher phagocytosis rate than their respective replicates (5.4). Nevertheless, the assay was performed with lower concentrations of the same chemotherapeutics. At concentrations of 2.5 $\mu$ M and 1 $\mu$ M both chemotherapeutics showed a significant increase in phagocytosis, accompanied by a change in bacteria to macrophage ratios. An influence of the different bacteria to macrophage ratios on the resulting phagocytosis rates could not be ruled out completely, although especially for the 2.5 $\mu$ M concentrations two outliers were responsible for the degree of divergence, which were two biological replicates obtained in the same experimental run and did not correlate with a higher phagocytosis rate, except for 2.5 $\mu$ M Mafosfamide (5.6). Modifications to the BCG-phagocytosis assay were implemented to reduce the divergence of the bacteria to macrophage ratios. The modified BCG-phagocytosis assay was performed with 5 $\mu$ M Mafosfamide, 5 $\mu$ M Doxorubicin and 10 $\mu$ M Nutlin-3A. Mafosfamide as well as Doxorubicin still induced a significant increase in the phagocytosis rate compared to the untreated control. The bacteria to macrophage ratios of the untreated control and Mafosfamide-treated conditions did not show a great divergence, canceling out a possible impact on the phagocytosis rate. A difference was still apparent between the bacteria to macrophage ratios of the untreated control and Doxorubicin, but two outliers for Doxorubicin, which were two biological replicates of one experimental run, showed the same bacteria to macrophage ratio as the respective control conditions and still displayed an increase in phagocytosis. Furthermore, one outlier of the control had a similar bacteria to macrophage ratio than the Doxorubicin-treated conditions without displaying an increased phagocytosis rate (5.7). Taking the impact of different bacteria to macrophage ratios, which was described in 5.5, in account, it became apparent that the great increase in phagocytic capacity, caused by Doxorubicin, could not be explained

by the diverging bacteria to macrophage ratios. A shift of the mean bacteria to macrophage ratio as seen in the modified BCG-phagocytosis assay, between control and Doxorubicin-treated conditions, should have led to an increase in normalised phagocytosis of 1.1 to 1.2, but a substantially higher increase of 1.4 was seen for the Doxorubicin-treated conditions (5.5 and 5.7). Nutlin-3A treated macrophages displayed a slight increase in phagocytosis, which was not significant (5.7). These results lead to the conclusion that Mafosfamide as well as Doxorubicin have a positive effect on the non-opsonised phagocytic capacity of macrophages. Surprisingly, p53, as the main player of the DDR, was seemingly not playing a vital role in the signalling pathway leading to the positive effect on macrophages' phagocytic capacity, demonstrated by the not significantly increased phagocytosis rate of Nutlin-3A treated macrophages.

The data presented in this thesis lead to the approval of the biological hypothesis that direct chemotherapy induced an increase in opsonised and non-opsonised Fc-independent phagocytic capacity of macrophages, which was not depending on the target to macrophage ratio.

M1 macrophages were linked to greater phagocytic capacity, specially opsonised Fc-dependent phagocytosis, although also M2 macrophages displayed effective phagocytic capacity in regard to debris and apoptotic cells (see 3.2.1). Some studies even showed higher phagocytic capabilities for M2-like macrophages regarding bacterial particles<sup>259</sup>. Here it was demonstrated that through treatment with Mafosfamide and Doxorubicin the non-opsonised and opsonised Fc-independent phagocytic capacity of macrophages was increased (5.7 and 5.11). Furthermore, in previous work of Prof. Dr. Pallaschs working group it was shown that opsonised Fc-dependent phagocytic capacity was heightened by chemotherapy<sup>247(Preprint)</sup>. No macrophage polarisation was associated to a higher phagocytic capacity in every different type of phagocytosis, which was mentioned here. Suggesting that a new macrophage activation state was observed. Just considering the increase in phagocytic capacity, especially in opsonised Fc-dependent phagocytosis, it could be assumed that the observed polarisation is located closer to the M1 pole of the macrophage polarisation spectrum, because M1 macrophages were generally associated with higher phagocytic capacity, particularly opsonised Fc-

dependent phagocytosis (see 3.2.1). But keeping the polarisation described in 6.1 in mind with high CD206 and PD-L1 levels, an activation state close to M1 macrophages is unlikely as the observed polarisation also seems to perform immunoregulatory functions. Interestingly the high expression of CD206 gives notion to a mechanistic explanation on why the non-opsonised phagocytic capacity of treated macrophages was increased, because CD206 is a PRR which is involved in the binding of bacteria<sup>260</sup>. The macrophage polarisation which was induced by chemotherapy has immunoregulatory functions, but also seems to hold great tumoricidal potential with a generally increased phagocytic capacity. This gave insight into the efficacy of already utilized combination therapies, as mentioned in 6.1, but also elucidated the complex relationship of chemotherapy and the immune system, especially macrophages.

It is described in the literature that Doxorubicin as well as Cyclophosphamide and its activated *in vivo* form, Mafosfamide, depend on a working immune system to reach their full anti-tumor potential<sup>243-245</sup>. For Doxorubicin it was shown that macrophages are able to release Doxorubicin, after being exposed to it beforehand, which enhanced the anti-tumor efficacy<sup>261</sup>. Cyclophosphamide was associated with an increased level of anti-tumor antibodies and the induction of cytotoxicity in leukocytes<sup>245</sup>. Furthermore, both chemotherapeutics are able to evoke ICD in tumor cells, which promotes an anti-tumor response by the immune system (see 3.5). Nevertheless, the relation between Doxorubicin or Cyclophosphamide and the immune system was never elucidated completely. Giving new insight into the direct effect of Doxorubicin and Cyclophosphamide on macrophages, this study shed more light on this intricate relationship. Proving an increase in non-opsonised, opsonised Fc-independent and Fc-dependent phagocytosis by the chemotherapeutics hinted towards an impact on a general effector of phagocytosis, because different kinds of phagocytosis were proven to be regulated separately<sup>262</sup>. A general effect chemotherapy was described to have on cells, is the induction of genotoxic stress, which causes a DDR. Although being a key player of the DDR and the induction of the ASAP in leukaemic cells, p53 stabilization did not display a positive effect on the phagocytic capacity of murine macrophages and p53-deficient macrophages still displayed increased phagocytosis rates after

chemotherapeutic treatment (5.7 and <sup>247(Preprint)</sup>). But another player of the DDR signalling pathway was shown to influence the increase in phagocytic capacity of macrophages, p38<sup>263,264</sup>. Furthermore, a p38 dependent signalling was shown to not only increase the rate of phagocytes engulfing targets, but also the phagocytosed targets per macrophage, which was also demonstrated in 5.3<sup>82</sup>. In addition, the working group of Prof. Dr. Pallasch showed that p38 deficient murine macrophages displayed a significantly diminished increase in opsonised Fc-dependent phagocytosis after chemotherapeutic treatment<sup>247(Preprint)</sup>. Activation of p38, in response to genotoxic stress, can be carried out by Ras-related C3 botulinum toxin substrate 1 (Rac1) or via the MAPK pathway (see 3.4), which separate the regulation of p38 from p53 activity<sup>265</sup>. The activation of p38 and its downstream targets promotes actin polymerization<sup>266</sup>. The promotion of actin polymerization could explain the displayed increases in the diverse forms of phagocytosis and the greater cell size as well as actin staining in treated macrophages (5.3, 5.7, 5.11 and <sup>247(Preprint)</sup>).

For future experiments it would be of interest to repeat the BCG and pH-sensitive bead phagocytosis assay with p38 deficient macrophages to see if the effect of the chemotherapeutics on non-opsonised and opsonised Fc-independent phagocytosis is also conveyed via p38. This could elucidate if the positive effect on the different kinds of phagocytosis is conveyed via the same mechanism or if diverse pathways are involved. Moreover the effect of direct p38 activation, via e.g. Neferine, on phagocytosis as well as polarisation-marker expression could be tested, as the working group of Prof. Dr. Pallasch could show that a knock down of p38 did not affect PD-L1 expression in treated macrophages <sup>(Preprint)</sup><sup>247,267</sup>. A direct p38 activation could yield the possibility of increasing the phagocytic capacity of macrophages without initiating immunoregulatory effects. In addition the upstream signalling pathway leading to p38 activation after DNA damage via chemotherapy could be investigated. Here ATM is a very promising target, as it was already shown to play a central role in p38 activation after UV-light induced DNA damage, which is very likely to activate the same signalling pathway as chemotherapy induced DNA damage<sup>247(Preprint)</sup>. The generation of knock down cell lines, via the viral transduction of small hairpin RNA (shRNA), or even knock out cell lines, by

performing the Clustered Regularly Interspaced Short Palindromic Repeats/CRISPR-associated method (CRISPR/Cas method), would be helpful to further elucidate the signalling pathway. If these methods are not feasible, ATM inhibitors, like KU 55933, could also be utilized to examine if the effects of chemotherapy on macrophages can be diminished or even abolished. It could also be useful to perform a phosphoproteom analysis of chemotherapy treated macrophages. To further dissect the underlying intracellular signalling, resulting in the effects of Mafosfamide and Doxorubicin on macrophages, could give further mechanistic insight into the efficacy of already utilized combination therapies, as mentioned in 6.1, and also yield new targets to activate the tumoricidal potential of TAMs within the TME, e.g. increased phagocytic capacity.

### 6.3 Soluble factors conveyed the positive effect of Doxorubicin, suggesting the induction of a secretory phenotype in macrophages

Prof. Dr. Pallaschs working group could already show, that through the application of cyclophosphamide in a humanized mouse leukaemia model, an ASAP was induced in leukaemic cells. This phenotype of leukaemic cells led to an increased phagocytosis and tumor cell clearance by macrophages in an opsonised Fc-dependent manner, which was mediated by soluble factors like TNF- $\alpha$ , VEGF-A, IL8 and CCL4<sup>228</sup>.

To evaluate if chemotherapeutics can also directly promote a secretory phenotype in macrophages, which then stimulates further macrophages via soluble factors, the BCG-phagocytosis assay was performed with conditioned medium, generated by untreated, Mafosfamide- and Doxorubicin-treated J774A.1 macrophages. Conditioned medium of Mafosfamide-pretreated macrophages did not increase the phagocytosis rate of J774A.1 macrophages compared to conditioned medium of an untreated control, suggesting that Mafosfamide did not induce a secretory phenotype in macrophages upon treatment (5.8). This differed from the findings made with conditioned medium

of pretreated leukaemic cells (see above). Leading to the conclusion that, in the case of Mafosfamide, a direct treatment was necessary to have a positive effect on macrophages' phagocytic capacity. Doxorubicin-pretreated macrophages generated a medium, which promoted an increase in phagocytic capacity of previously untreated macrophages compared to conditioned medium of untreated as well as Mafosfamide-pretreated macrophages (5.8). A minimal deviation was seen in the bacteria to macrophage ratios, but only for two biological replicates of the same experimental run. This deviation could not account for the drastic increase in phagocytic capacity seen for these two replicates, especially if compared to the data shown in Figure 10 A. An increase of the bacteria to macrophage ratio as seen for the two biological replicates compared to their respective control conditions could increase normalised phagocytosis to levels of 1.2 to 1.3, but not up to 1.5 or 1.6 as observed for these replicates (5.5 and 5.8). Furthermore, replicates with the same bacteria to macrophage ratio as their respective control also demonstrated a positive effect on the phagocytic capacity of macrophages (5.8). The positive effect of Doxorubicin on non-opsonized phagocytosis was, to some extent, conveyed by soluble factors, suggesting the induction of a secretory phenotype in macrophages.

It was also described in the literature that Doxorubicin can induce secretion of cytokines, like IL-1 and PGE2, in macrophages<sup>268</sup>. PGE2, as a co-stimulus, together with a TLR agonist has been known to induce a M2b polarisation in macrophages, which are known to be immunoregulatory, but also secrete proinflammatory cytokines, like IL-1 (see 3.2.1). But as depicted above, the general increase in phagocytosis as well as the marker expression did not indicate a M2b-polarisation of the treated macrophages. This again suggested that a potentially novel polarisation was observed in this study, which also could differ for Doxorubicin- and Mafosfamide-treated macrophages, given the lack of an effect by conditioned medium generated by Mafosfamide in contrast to the significant increase in phagocytosis induced by conditioned medium generated by Doxorubicin-pretreated macrophages, indicating cytokine secretion by these macrophages. Certain macrophage polarisations were associated with different cytokine profiles, hinting to potentially different polarisations of Mafosfamide-

and Doxorubicin-treated macrophages (see 3.2.1). Keeping the marker characterization of Mafosfamide- and Doxorubicin-treated macrophages in mind, which did not show great differences, cytokine release induced by an off-target effect of Doxorubicin is also a likely explanation (see 6.1).

The potential induction of pro-phagocytic cytokine secretion by Doxorubicin treatment could have great implications for the effect on macrophages in an *in vivo* setting. It could lead to the potentiation of the effect Doxorubicin has on macrophages, because macrophages, which received Doxorubicin treatment, could repolarize further macrophages, which did not interact with the chemotherapeutic, through cytokine secretion. This implies that not every macrophage would have to undergo treatment to demonstrate an increased phagocytic capacity. Furthermore, the necessary dose of Doxorubicin, to effect a significant number of TAMs, could be reduced by this effect, which would lead to a better effect-side effect profile.

To further enlighten the impact pretreated macrophages have on untreated macrophages, more experiments have to be performed. It would be interesting to pretreat wild type macrophages with Mafosfamide and Doxorubicin, co-culture them one to one with untreated macrophages, expressing a fluorescent protein (like GFP or mCherry) and use this co-culture in the BCG or pH-sensitive bead based as well as the antibody dependent phagocytosis assay. Double positive macrophages, for the fluorescent protein and the fluorochrome used to label the phagocytic targets, could be identified. The rate of double positive cells could be compared to the double positive rate of an one to one co-culture of untreated macrophages and untreated fluorescent macrophages. Furthermore, the phagocytic capacity of directly treated macrophages and untreated macrophages, which are co-cultured with pretreated macrophages, could be compared by also identifying the rate of cells, which are positive for the fluorochrome. This would allow an insight into the activation efficacy of pretreated macrophages towards untreated macrophages compared to the effect of a direct chemotherapy. Also, the experiment would better represent an *in vivo* setting with the influence of secreted cytokines as well as direct cell to cell interactions. In addition, the pH-sensitive bead phagocytosis and the Antibody-dependent cellular phagocytosis (ADCP) assay could be performed

with macrophages which were incubated in conditioned medium from Mafosfamide- and Doxorubicin-treated macrophages, to examine if the positive effect on opsonised Fc-independent and opsonised Fc-dependent phagocytosis can also be conveyed by soluble factors. Performing a characterization of surface and intracellular markers for macrophages incubated in conditioned medium would be beneficial to explore the induced activation status, which could be compared to the one of directly treated macrophages. An analysis of the cytokine profile, secreted by Doxorubicin-pretreated macrophages, could also yield interesting insight into the effect of the chemotherapeutic on macrophages. It could allow a better characterization of the polarisation of Doxorubicin-treated macrophages, because certain macrophage polarisations are associated with different cytokine profiles, or could hint towards a potential off target effect (see Figure 1 and <sup>251</sup>). Furthermore, pro-phagocytic cytokines or cytokine profiles could be identified, like already shown for the ASAP of chemotherapy treated leukaemic cells<sup>228</sup>. This could yield new therapeutic approaches to activate macrophages phagocytosis in order to harness their tumoricidal potential.

## 6.4 Outlook

Throughout this study it was shown that Mafosfamide as well as Doxorubicin alter the phagocytic capacity of J774A.1 murine macrophages, leading to a higher phagocytosis rate. In addition, basic changes to macrophage morphology and phenotype, regarding cell perimeter and size as well as nucleus perimeter, were shown. These findings lead to the assumption that a new macrophage polarisation was observed here. Furthermore, it was demonstrated that Doxorubicin could trigger the production of soluble factors, which stimulate untreated macrophages by an unknown pathway.

To further elucidate the macrophage polarisation induced by Mafosfamide and Doxorubicin an analysis of cytokine profiles could be performed, comparing secretion by untreated and treated cells as well as correlating them with already defined cytokine profiles of macrophage polarisations. Especially the cytokine profile of Doxorubicin-treated macrophages could hold potential pro-phagocytic cytokines. Furthermore, transcriptomic, proteomic and phosphor-proteomic analysis could be performed to further define the induced polarisation and identify underlying signalling pathways.

Future studies should be performed with other macrophage cell lines, like THP-1, isolated murine macrophages, human macrophages as well as in an *in-vivo* setting to replicate the observed effects of Mafosfamide and Doxorubicin on J774A.1 murine macrophages and underline the validity of the presented results. The generation of knock-out or knock-down cell lines for signalling pathway key players upstream of p38, like ATM, could elucidate how the effect of Mafosfamide and Doxorubicin is conveyed on an intracellular level. Furthermore, through the dissection of the intracellular signalling new treatment targets could be uncovered, which would allow for an activation of the anti-tumor potential of macrophages, e.g. higher phagocytic capacity, while circumventing the immunoregulatory effects induced by chemotherapy.

Co-culturing of pretreated and untreated macrophages for phagocytosis assays, could enlighten the effect of direct cell-to-cell interactions, which would allow for a better idea of the effects in an *in-vivo* setting.

The elucidation of the mechanisms behind the observed effects of Mafosfamide and Doxorubicin yield new insights into the interactions between chemotherapy, the immune system, specifically macrophages, and cancer cells. These insights can result in a better mechanistic understanding of current therapy regimens, new therapy adjustments, strategies and targets.

## 7 References

1. Travers P, Walport MJ, Janeway C, Murphy KP. Janeway's immunobiology: Garland Science; 2008.
2. Riera Romo M, Pérez-Martínez D, Castillo Ferrer C. Innate immunity in vertebrates: an overview. *Immunology* 2016; **148**(2): 125-39.
3. Iwasaki A, Medzhitov R. Control of adaptive immunity by the innate immune system. *Nature immunology* 2015; **16**(4): 343.
4. Matsui T, Amagai M. Dissecting the formation, structure and barrier function of the stratum corneum. *International Immunology* 2015; **27**(6): 269-80.
5. DE VEER MJ, KEMP JM, MEEUSEN ENT. The innate host defence against nematode parasites. *Parasite Immunology* 2007; **29**(1): 1-9.
6. Bowdish DM, Davidson DJ, Hancock R. A re-evaluation of the role of host defence peptides in mammalian immunity. *Current Protein and Peptide Science* 2005; **6**(1): 35-51.
7. Cray C, Zaias J, Altman NH. Acute phase response in animals: a review. *Comparative medicine* 2009; **59**(6): 517-26.
8. O'Shea JJ, Ma A, Lipsky P. Cytokines and autoimmunity. *Nature Reviews Immunology* 2002; **2**(1): 37.
9. Dunkelberger JR, Song W-C. Complement and its role in innate and adaptive immune responses. *Cell research* 2010; **20**(1): 34.
10. Kleinnijenhuis J, Quintin J, Preijers F, et al. Bacille Calmette-Guérin induces NOD2-dependent nonspecific protection from reinfection via epigenetic reprogramming of monocytes. *Proceedings of the National Academy of Sciences of the United States of America* 2012; **109**(43): 17537-42.
11. Quintin J, Saeed S, Martens JHA, et al. *Candida albicans* infection affords protection against reinfection via functional reprogramming of monocytes. *Cell Host and Microbe* 2012; **12**(2): 223-32.

12. Beutler B. Innate immunity: an overview. *Molecular immunology* 2004; **40**(12): 845-59.
13. Lüllmann-Rauch R, Asan E. Taschenlehrbuch Histologie. Stuttgart, New York: Thieme 2015.
14. Brinkmann V, Zychlinsky A. Neutrophil extracellular traps: Is immunity the second function of chromatin? *The Journal of Cell Biology* 2012; **198**(5): 773-83.
15. Häger M, Cowland J, Borregaard N. Neutrophil granules in health and disease. *Journal of internal medicine* 2010; **268**(1): 25-34.
16. Kessenbrock K, Krumbholz M, Schönemarker U, et al. Netting neutrophils in autoimmune small-vessel vasculitis. *Nature Medicine* 2009; **15**: 623.
17. Yipp BG, Petri B, Salina D, et al. Infection-induced NETosis is a dynamic process involving neutrophil multitasking in vivo. *Nature Medicine* 2012; **18**: 1386.
18. Elkabets M, Ribeiro VS, Dinarello CA, et al. IL-1 $\beta$  regulates a novel myeloid-derived suppressor cell subset that impairs NK cell development and function. *European journal of immunology* 2010; **40**(12): 3347-57.
19. Li Y, Tu Z, Qian S, et al. Myeloid-Derived Suppressor Cells as a Potential Therapy for Experimental Autoimmune Myasthenia Gravis. *The Journal of Immunology* 2014.
20. Gabrilovich DI, Ostrand-Rosenberg S, Bronte V. Coordinated regulation of myeloid cells by tumours. *Nature Reviews Immunology* 2012; **12**: 253.
21. Diefenbach A, Colonna M, Koyasu S. Development, Differentiation, and Diversity of Innate Lymphoid Cells. *Immunity* 2014; **41**(3): 354-65.
22. Martinez-Gonzalez I, Mathä L, Steer Catherine A, Ghaedi M, Poon Grace FT, Takei F. Allergen-Experienced Group 2 Innate Lymphoid Cells

Acquire Memory-like Properties and Enhance Allergic Lung Inflammation. *Immunity* 2016; **45**(1): 198-208.

23. O'Leary JG, Goodarzi M, Drayton DL, von Andrian UH. T cell- and B cell-independent adaptive immunity mediated by natural killer cells. *Nature Immunology* 2006; **7**: 507.

24. Suerbaum S, Burchard G-D, Kaufmann SH, Schulz TF. *Medizinische Mikrobiologie und Infektiologie*: Springer-Verlag; 2016.

25. Bonilla FA, Oettgen HC. Adaptive immunity. *Journal of Allergy and Clinical Immunology* 2010; **125**(2): S33-S40.

26. Bettelli E, Carrier Y, Gao W, et al. Reciprocal developmental pathways for the generation of pathogenic effector TH17 and regulatory T cells. *Nature* 2006; **441**: 235.

27. Chatila TA. Role of regulatory T cells in human diseases. *Journal of Allergy and Clinical Immunology* 2005; **116**(5): 949-59.

28. Veldhoen M, Uyttenhove C, van Snick J, et al. Transforming growth factor- $\beta$  reprograms the differentiation of T helper 2 cells and promotes an interleukin 9-producing subset. *Nature Immunology* 2008; **9**: 1341.

29. Vos Q, Lees A, Wu ZQ, Snapper CM, Mond JJ. B-cell activation by T-cell-independent type 2 antigens as an integral part of the humoral immune response to pathogenic microorganisms. *Immunological reviews* 2000; **176**: 154-70.

30. Liu YJ, Malisan F, De Bouteiller O, et al. Within germinal centers, isotype switching of immunoglobulin genes occurs after the onset of somatic mutation. *Immunity* 1996; **4**(3): 241-50.

31. Wagner SD, Neuberger MS. Somatic hypermutation of immunoglobulin genes. *Annual Review of Immunology*; 1996. p. 441-57.

32. Haniffa M, Bigley V, Collin M. Human mononuclear phagocyte system reunited. *Semin Cell Dev Biol* 2015; **41**: 59-69.

33. Ginhoux F, Greter M, Leboeuf M, et al. Fate mapping analysis reveals that adult microglia derive from primitive macrophages. *Science* 2010; **330**(6005): 841-5.
34. Guilliams M, De Kleer I, Henri S, et al. Alveolar macrophages develop from fetal monocytes that differentiate into long-lived cells in the first week of life via GM-CSF. *J Exp Med* 2013; **210**(10): 1977-92.
35. Hashimoto D, Chow A, Noizat C, et al. Tissue-resident macrophages self-maintain locally throughout adult life with minimal contribution from circulating monocytes. *Immunity* 2013; **38**(4): 792-804.
36. Yona S, Kim KW, Wolf Y, et al. Fate mapping reveals origins and dynamics of monocytes and tissue macrophages under homeostasis. *Immunity* 2013; **38**(1): 79-91.
37. Epelman S, Lavine KJ, Beaudin AE, et al. Embryonic and adult-derived resident cardiac macrophages are maintained through distinct mechanisms at steady state and during inflammation. *Immunity* 2014; **40**(1): 91-104.
38. Peranzoni E, Zilio S, Marigo I, et al. Myeloid-derived suppressor cell heterogeneity and subset definition. *Curr Opin Immunol* 2010; **22**(2): 238-44.
39. Serbina NV, Jia T, Hohl TM, Pamer EG. Monocyte-mediated defense against microbial pathogens. *Annu Rev Immunol* 2008; **26**: 421-52.
40. Gautier EL, Shay T, Miller J, et al. Gene-expression profiles and transcriptional regulatory pathways that underlie the identity and diversity of mouse tissue macrophages. *Nat Immunol* 2012; **13**(11): 1118-28.
41. Helming L, Gordon S. The molecular basis of macrophage fusion. *Immunobiology* 2007; **212**(9-10): 785-93.
42. Hume DA, Robinson AP, MacPherson GG, Gordon S. The mononuclear phagocyte system of the mouse defined by immunohistochemical localization of antigen F4/80. Relationship between macrophages, Langerhans cells, reticular cells, and dendritic cells in lymphoid and hematopoietic organs. *J Exp Med* 1983; **158**(5): 1522-36.

43. Perry VH, Hume DA, Gordon S. Immunohistochemical localization of macrophages and microglia in the adult and developing mouse brain. *Neuroscience* 1985; **15**(2): 313-26.
44. Wisse E, Knook DL. The investigation of sinusoidal cells: a new approach to the study of liver function. *Progress in liver diseases* 1979; **6**: 153-71.
45. Mebius RE, Kraal G. Structure and function of the spleen. *Nature Reviews Immunology* 2005; **5**: 606.
46. Gordon S, Pluddemann A, Martinez Estrada F. Macrophage heterogeneity in tissues: phenotypic diversity and functions. *Immunol Rev* 2014; **262**(1): 36-55.
47. Lavin Y, Winter D, Blecher-Gonen R, et al. Tissue-resident macrophage enhancer landscapes are shaped by the local microenvironment. *Cell* 2014; **159**(6): 1312-26.
48. Mantovani A, Sozzani S, Locati M, Allavena P, Sica A. Macrophage polarization: tumor-associated macrophages as a paradigm for polarized M2 mononuclear phagocytes. *Trends in Immunology* 2002; **23**(11): 549-55.
49. Hamilton T. Molecular basis of macrophage activation: from gene expression to phenotypic diversity. *The macrophage* 2002; **2**: 73-102.
50. Biswas SK, Mantovani A. Macrophage plasticity and interaction with lymphocyte subsets: cancer as a paradigm. *Nat Immunol* 2010; **11**(10): 889-96.
51. Bonizzi G, Karin M. The two NF-kappaB activation pathways and their role in innate and adaptive immunity. *Trends Immunol* 2004; **25**(6): 280-8.
52. Sica A, Bronte V. Altered macrophage differentiation and immune dysfunction in tumor development. *J Clin Invest* 2007; **117**(5): 1155-66.
53. Wang YC, He F, Feng F, et al. Notch signalling determines the M1 versus M2 polarization of macrophages in antitumor immune responses. *Cancer Res* 2010; **70**(12): 4840-9.

54. Dale DC, Boxer L, Liles WC. The phagocytes: neutrophils and monocytes. *Blood* 2008; **112**(4): 935-45.
55. Sica A, Mantovani A. Macrophage plasticity and polarization: in vivo veritas. *J Clin Invest* 2012; **122**(3): 787-95.
56. Rhee I. Diverse macrophages polarization in tumor microenvironment. *Arch Pharm Res* 2016; **39**(11): 1588-96.
57. Martinez FO, Sica A, Mantovani A, Locati M. Macrophage activation and polarization. *Front Biosci* 2008; **13**: 453-61.
58. Canton J. Phagosome maturation in polarized macrophages. *J Leukoc Biol* 2014; **96**(5): 729-38.
59. Mantovani A, Sica A, Sozzani S, Allavena P, Vecchi A, Locati M. The chemokine system in diverse forms of macrophage activation and polarization. *Trends Immunol* 2004; **25**(12): 677-86.
60. Yunna C, Mengru H, Lei W, Weidong C. Macrophage M1/M2 polarization. *Eur J Pharmacol* 2020; **877**: 173090.
61. Zhang M, Hutter G, Kahn SA, et al. Anti-CD47 Treatment Stimulates Phagocytosis of Glioblastoma by M1 and M2 Polarized Macrophages and Promotes M1 Polarized Macrophages In Vivo. *PLoS One* 2016; **11**(4): e0153550.
62. Fleming BD, Mosser DM. Regulatory macrophages: setting the threshold for therapy. *Eur J Immunol* 2011; **41**(9): 2498-502.
63. Shapouri-Moghaddam A, Mohammadian S, Vazini H, et al. Macrophage plasticity, polarization, and function in health and disease. *J Cell Physiol* 2018; **233**(9): 6425-40.
64. Gordon S, Martinez FO. Alternative activation of macrophages: mechanism and functions. *Immunity* 2010; **32**(5): 593-604.

65. Odegaard JI, Ricardo-Gonzalez RR, Goforth MH, et al. Macrophage-specific PPAR $\gamma$  controls alternative activation and improves insulin resistance. *Nature* 2007; **447**: 1116.
66. Odegaard JI, Ricardo-Gonzalez RR, Red Eagle A, et al. Alternative M2 Activation of Kupffer Cells by PPAR $\delta$  Ameliorates Obesity-Induced Insulin Resistance. *Cell Metabolism* 2008; **7**(6): 496-507.
67. Edwards J, Zhang X, Frauwirth K, Mosser D, Edwards JP, Zhang X, Frauwirth KA, Mosser DM. Biochemical and functional characterization of three activated macrophage populations. *J Leukoc Biol* 80: 1298-1307; 2007.
68. Mosser DM, Edwards JP. Exploring the full spectrum of macrophage activation. *Nat Rev Immunol* 2008; **8**(12): 958-69.
69. Mosser DM. The many faces of macrophage activation. *J Leukoc Biol* 2003; **73**(2): 209-12.
70. Lucas M, Zhang X, Prasanna V, Mosser DM. ERK activation following macrophage Fc $\gamma$ R ligation leads to chromatin modifications at the IL-10 locus. *J Immunol* 2005; **175**(1): 469-77.
71. Lang R, Patel D, Morris JJ, Rutschman RL, Murray PJ. Shaping gene expression in activated and resting primary macrophages by IL-10. *J Immunol* 2002; **169**(5): 2253-63.
72. Zizzo G, Hilliard BA, Monestier M, Cohen PL. Efficient clearance of early apoptotic cells by human macrophages requires M2c polarization and MerTK induction. *J Immunol* 2012; **189**(7): 3508-20.
73. Barron L, Wynn TA. Fibrosis is regulated by Th2 and Th17 responses and by dynamic interactions between fibroblasts and macrophages. *American Journal of Physiology-Gastrointestinal and Liver Physiology* 2011; **300**(5): G723-G8.
74. Rojas J, Salazar J, Martinez MS, et al. Macrophage Heterogeneity and Plasticity: Impact of Macrophage Biomarkers on Atherosclerosis. *Scientifica (Cairo)* 2015; **2015**: 851252.

75. Ernst JD. Bacterial inhibition of phagocytosis. *Cellular Microbiology* 2001; **2**(5): 379-86.
76. Flannagan RS, Jaumouille V, Grinstein S. The cell biology of phagocytosis. *Annu Rev Pathol* 2012; **7**: 61-98.
77. Rabinovitch M. Professional and non-professional phagocytes: an introduction. *Trends in cell biology* 1995; **5**(3): 85-7.
78. Canton J, Neculai D, Grinstein S. Scavenger receptors in homeostasis and immunity. *Nature Reviews Immunology* 2013; **13**: 621.
79. Ezekowitz R, Sastry K, Bailly P, Warner A. Molecular characterization of the human macrophage mannose receptor: demonstration of multiple carbohydrate recognition-like domains and phagocytosis of yeasts in Cos-1 cells. *Journal of Experimental Medicine* 1990; **172**(6): 1785-94.
80. Herre J, Marshall AS, Caron E, et al. Dectin-1 uses novel mechanisms for yeast phagocytosis in macrophages. *Blood* 2004; **104**(13): 4038-45.
81. Krieger M. The other side of scavenger receptors: pattern recognition for host defense. *Curr Opin Lipidol* 1997; **8**(5): 275-80.
82. Doyle SE, O'Connell RM, Miranda GA, et al. Toll-like Receptors Induce a Phagocytic Gene Program through p38. *The Journal of Experimental Medicine* 2004; **199**(1): 81-90.
83. Anderson CL, Shen L, Eicher DM, Wewers MD, Gill JK. Phagocytosis mediated by three distinct Fc gamma receptor classes on human leukocytes. *The Journal of Experimental Medicine* 1990; **171**(4): 1333-45.
84. Ross GD, Reed W, Dalzell JG, Becker SE, Hogg N. Macrophage cytoskeleton association with CR3 and CR4 regulates receptor mobility and phagocytosis of iC3b-opsonized erythrocytes. *Journal of Leukocyte Biology* 1992; **51**(2): 109-17.

85. Bakema JE, van Egmond M. The human immunoglobulin A Fc receptor FcαRI: a multifaceted regulator of mucosal immunity. *Mucosal Immunology* 2011; **4**: 612.
86. Rosales C, Uribe-Querol E. Antibody - Fc Receptor Interactions in Antimicrobial Functions. *Current Immunology Reviews* 2013; **9**(1): 44-55.
87. Van Lookeren Campagne M, Wiesmann C, Brown EJ. Macrophage complement receptors and pathogen clearance. *Cellular Microbiology* 2007; **9**(9): 2095-102.
88. Le Cabec V, Cols C, Maridonneau-Parini I. Nonopsonic phagocytosis of zymosan and *Mycobacterium kansasii* by CR3 (CD11b/CD18) involves distinct molecular determinants and is or is not coupled with NADPH oxidase activation. *Infection and immunity* 2000; **68**(8): 4736-45.
89. Rosales C. Fc receptor and integrin signalling in phagocytes. *Signal Transduction* 2007; **7**(5-6): 386-401.
90. Sánchez-Mejorada G, Rosales C. Signal transduction by immunoglobulin Fc receptors. *Journal of Leukocyte Biology* 1998; **63**(5): 521-33.
91. Rosales C, Uribe-Querol E. Phagocytosis: A Fundamental Process in Immunity. *BioMed research international* 2017; **2017**: 9042851-.
92. Kiefer F, Brumell J, Al-Alawi N, et al. The Syk protein tyrosine kinase is essential for Fcγ receptor signalling in macrophages and neutrophils. *Molecular and cellular biology* 1998; **18**(7): 4209-20.
93. Newman S, Mikus L, Tucci M. Differential requirements for cellular cytoskeleton in human macrophage complement receptor-and Fc receptor-mediated phagocytosis. *The Journal of immunology* 1991; **146**(3): 967-74.
94. Weinberg RA. The biology of cancer. New York, NY: Garland Science; 2007.
95. Lee EY, Muller WJ. Oncogenes and tumor suppressor genes. *Cold Spring Harb Perspect Biol* 2010; **2**(10): a003236.

96. Kinzler KW, Vogelstein B. Cancer-susceptibility genes. Gatekeepers and caretakers. *Nature* 1997; **386**(6627): 761, 3.
97. A clinical evaluation of the International Lymphoma Study Group classification of non-Hodgkin's lymphoma. The Non-Hodgkin's Lymphoma Classification Project. *Blood* 1997; **89**(11): 3909-18.
98. Kuppers R, Hansmann ML. The Hodgkin and Reed/Sternberg cell. *Int J Biochem Cell Biol* 2005; **37**(3): 511-7.
99. Hanahan D, Weinberg RA. Hallmarks of cancer: the next generation. *Cell* 2011; **144**(5): 646-74.
100. Hanahan D, Coussens LM. Accessories to the crime: functions of cells recruited to the tumor microenvironment. *Cancer Cell* 2012; **21**(3): 309-22.
101. Panayiotidis P, Jones D, Ganeshaguru K, Foroni L, Hoffbrand AV. Human bone marrow stromal cells prevent apoptosis and support the survival of chronic lymphocytic leukaemia cells in vitro. *Br J Haematol* 1996; **92**(1): 97-103.
102. Quail DF, Joyce JA. Microenvironmental regulation of tumor progression and metastasis. *Nat Med* 2013; **19**(11): 1423-37.
103. Armulik A, Abramsson A, Betsholtz C. Endothelial/pericyte interactions. *Circ Res* 2005; **97**(6): 512-23.
104. Folkman J, Watson K, Ingber D, Hanahan D. Induction of angiogenesis during the transition from hyperplasia to neoplasia. *Nature* 1989; **339**(6219): 58-61.
105. Bergers G, Javaherian K, Lo KM, Folkman J, Hanahan D. Effects of angiogenesis inhibitors on multistage carcinogenesis in mice. *Science* 1999; **284**(5415): 808-12.
106. Butler JM, Kobayashi H, Rafii S. Instructive role of the vascular niche in promoting tumour growth and tissue repair by angiocrine factors. *Nat Rev Cancer* 2010; **10**(2): 138-46.

107. Yang J, Weinberg RA. Epithelial-mesenchymal transition: at the crossroads of development and tumor metastasis. *Dev Cell* 2008; **14**(6): 818-29.
108. Celis JE, Moreira JM, Cabezon T, et al. Identification of extracellular and intracellular signalling components of the mammary adipose tissue and its interstitial fluid in high risk breast cancer patients: toward dissecting the molecular circuitry of epithelial-adipocyte stromal cell interactions. *Molecular & cellular proteomics : MCP* 2005; **4**(4): 492-522.
109. Erez N, Truitt M, Olson P, Arron ST, Hanahan D. Cancer-Associated Fibroblasts Are Activated in Incipient Neoplasia to Orchestrate Tumor-Promoting Inflammation in an NF-kappaB-Dependent Manner. *Cancer Cell* 2010; **17**(2): 135-47.
110. Scherz-Shouval R, Santagata S, Mendillo Marc L, et al. The Reprogramming of Tumor Stroma by HSF1 Is a Potent Enabler of Malignancy. *Cell* 2014; **158**(3): 564-78.
111. Chaffer CL, Weinberg RA. A perspective on cancer cell metastasis. *Science* 2011; **331**(6024): 1559-64.
112. Balliet RM, Capparelli C, Guido C, et al. Mitochondrial oxidative stress in cancer-associated fibroblasts drives lactate production, promoting breast cancer tumor growth: understanding the aging and cancer connection. *Cell cycle (Georgetown, Tex)* 2011; **10**(23): 4065-73.
113. Rattigan YI, Patel BB, Ackerstaff E, et al. Lactate is a mediator of metabolic cooperation between stromal carcinoma associated fibroblasts and glycolytic tumor cells in the tumor microenvironment. *Experimental cell research* 2012; **318**(4): 326-35.
114. Burnet FM. The concept of immunological surveillance. *Progress in experimental tumor research* 1970; **13**: 1-27.

115. Shankaran V, Ikeda H, Bruce AT, et al. IFN $\gamma$  and lymphocytes prevent primary tumour development and shape tumour immunogenicity. *Nature* 2001; **410**(6832): 1107-11.
116. Wang T, Niu G, Kortylewski M, et al. Regulation of the innate and adaptive immune responses by Stat-3 signalling in tumor cells. *Nat Med* 2004; **10**(1): 48-54.
117. Caligiuri MA. Human natural killer cells. *Blood* 2008; **112**(3): 461-9.
118. Laurent C, Muller S, Do C, et al. Distribution, function, and prognostic value of cytotoxic T lymphocytes in follicular lymphoma: a 3-D tissue-imaging study. *Blood* 2011; **118**(20): 5371-9.
119. Larsen SK, Gao Y, Basse PH. NK cells in the tumor microenvironment. *Crit Rev Oncog* 2014; **19**(1-2): 91-105.
120. Hui L, Chen Y. Tumor microenvironment: Sanctuary of the devil. *Cancer Lett* 2015; **368**(1): 7-13.
121. Jones EA, Pringle JH, Angel CA, Rees RC. Th1/Th2 cytokine expression and its relationship with tumor growth in B cell non-Hodgkin's lymphoma (NHL). *Leukaemia & lymphoma* 2002; **43**(6): 1313-21.
122. Yang ZZ, Grote DM, Ziesmer SC, et al. IL-12 upregulates TIM-3 expression and induces T cell exhaustion in patients with follicular B cell non-Hodgkin lymphoma. *J Clin Invest* 2012; **122**(4): 1271-82.
123. Talmadge JE, Gabrilovich DI. History of myeloid-derived suppressor cells. *Nat Rev Cancer* 2013; **13**(10): 739-52.
124. Gabrilovich DI, Ostrand-Rosenberg S, Bronte V. Coordinated regulation of myeloid cells by tumours. *Nat Rev Immunol* 2012; **12**(4): 253-68.
125. Liu C, Yu S, Kappes J, et al. Expansion of spleen myeloid suppressor cells represses NK cell cytotoxicity in tumor-bearing host. *Blood* 2007; **109**(10): 4336-42.

126. Mazzone A, Bronte V, Visintin A, et al. Myeloid suppressor lines inhibit T cell responses by an NO-dependent mechanism. *J Immunol* 2002; **168**(2): 689-95.
127. Sinha P, Clements VK, Ostrand-Rosenberg S. Reduction of myeloid-derived suppressor cells and induction of M1 macrophages facilitate the rejection of established metastatic disease. *J Immunol* 2005; **174**(2): 636-45.
128. von Boehmer H, Daniel C. Therapeutic opportunities for manipulating T(Reg) cells in autoimmunity and cancer. *Nat Rev Drug Discov* 2013; **12**(1): 51-63.
129. Yang ZZ, Novak AJ, Stenson MJ, Witzig TE, Ansell SM. Intratumoral CD4+CD25+ regulatory T-cell-mediated suppression of infiltrating CD4+ T cells in B-cell non-Hodgkin lymphoma. *Blood* 2006; **107**(9): 3639-46.
130. Frey DM, Droeser RA, Viehl CT, et al. High frequency of tumor-infiltrating FOXP3(+) regulatory T cells predicts improved survival in mismatch repair-proficient colorectal cancer patients. *International journal of cancer* 2010; **126**(11): 2635-43.
131. Fu J, Xu D, Liu Z, et al. Increased regulatory T cells correlate with CD8 T-cell impairment and poor survival in hepatocellular carcinoma patients. *Gastroenterology* 2007; **132**(7): 2328-39.
132. Biswas SK, Allavena P, Mantovani A. Tumor-associated macrophages: functional diversity, clinical significance, and open questions. *Semin Immunopathol* 2013; **35**(5): 585-600.
133. Riihijarvi S, Fiskvik I, Taskinen M, et al. Prognostic influence of macrophages in patients with diffuse large B-cell lymphoma: a correlative study from a Nordic phase II trial. *Haematologica* 2015; **100**(2): 238-45.
134. Franklin RA, Liao W, Sarkar A, et al. The cellular and molecular origin of tumor-associated macrophages. *Science* 2014; **344**(6186): 921-5.

135. Movahedi K, Laoui D, Gysemans C, et al. Different tumor microenvironments contain functionally distinct subsets of macrophages derived from Ly6C(high) monocytes. *Cancer Res* 2010; **70**(14): 5728-39.
136. Qian BZ, Li J, Zhang H, et al. CCL2 recruits inflammatory monocytes to facilitate breast-tumour metastasis. *Nature* 2011; **475**(7355): 222-5.
137. Shand FH, Ueha S, Otsuji M, et al. Tracking of intertissue migration reveals the origins of tumor-infiltrating monocytes. *Proc Natl Acad Sci U S A* 2014; **111**(21): 7771-6.
138. Friedman DR, Sibley AB, Owzar K, et al. Relationship of blood monocytes with chronic lymphocytic leukaemia aggressiveness and outcomes: a multi-institutional study. *Am J Hematol* 2016; **91**(7): 687-91.
139. Tadmor T, Bari A, Sacchi S, et al. Monocyte count at diagnosis is a prognostic parameter in diffuse large B-cell lymphoma: results from a large multicenter study involving 1191 patients in the pre- and post-rituximab era. *Haematologica* 2014; **99**(1): 125-30.
140. DeNardo DG, Brennan DJ, Rexhepaj E, et al. Leukocyte complexity predicts breast cancer survival and functionally regulates response to chemotherapy. *Cancer discovery* 2011; **1**(1): 54-67.
141. Lin EY, Li JF, Gnatovskiy L, et al. Macrophages regulate the angiogenic switch in a mouse model of breast cancer. *Cancer Res* 2006; **66**(23): 11238-46.
142. Linde N, Lederle W, Depner S, van Rooijen N, Gutschalk CM, Mueller MM. Vascular endothelial growth factor-induced skin carcinogenesis depends on recruitment and alternative activation of macrophages. *J Pathol* 2012; **227**(1): 17-28.
143. Mantovani A, Ming WJ, Balotta C, Abdeljalil B, Bottazzi B. Origin and regulation of tumor-associated macrophages: the role of tumor-derived chemotactic factor. *Biochim Biophys Acta* 1986; **865**(1): 59-67.

144. Duluc D, Delneste Y, Tan F, et al. Tumor-associated leukaemia inhibitory factor and IL-6 skew monocyte differentiation into tumor-associated macrophage-like cells. *Blood* 2007; **110**(13): 4319-30.
145. Pinhal-Enfield G, Ramanathan M, Hasko G, et al. An angiogenic switch in macrophages involving synergy between Toll-like receptors 2, 4, 7, and 9 and adenosine A(2A) receptors. *Am J Pathol* 2003; **163**(2): 711-21.
146. Wang Q, Ni H, Lan L, Wei X, Xiang R, Wang Y. Fra-1 protooncogene regulates IL-6 expression in macrophages and promotes the generation of M2d macrophages. *Cell Res* 2010; **20**(6): 701-12.
147. Karin M, Lawrence T, Nizet V. Innate immunity gone awry: linking microbial infections to chronic inflammation and cancer. *Cell* 2006; **124**(4): 823-35.
148. Mantovani A, Allavena P, Sica A, Balkwill F. Cancer-related inflammation. *Nature* 2008; **454**(7203): 436-44.
149. Maeda S, Kamata H, Luo JL, Leffert H, Karin M. IKKbeta couples hepatocyte death to cytokine-driven compensatory proliferation that promotes chemical hepatocarcinogenesis. *Cell* 2005; **121**(7): 977-90.
150. Greten FR, Eckmann L, Greten TF, et al. IKKbeta links inflammation and tumorigenesis in a mouse model of colitis-associated cancer. *Cell* 2004; **118**(3): 285-96.
151. Pollard JW. Tumour-educated macrophages promote tumour progression and metastasis. *Nat Rev Cancer* 2004; **4**(1): 71-8.
152. Ruffell B, Chang-Strachan D, Chan V, et al. Macrophage IL-10 Blocks CD8+ T Cell-Dependent Responses to Chemotherapy by Suppressing IL-12 Expression in Intratumoral Dendritic Cells. *Cancer Cell* 2014; **26**(5): 623-37.
153. Curiel TJ, Coukos G, Zou L, et al. Specific recruitment of regulatory T cells in ovarian carcinoma fosters immune privilege and predicts reduced survival. *Nat Med* 2004; **10**(9): 942-9.

154. Liu J, Zhang N, Li Q, et al. Tumor-associated macrophages recruit CCR6<sup>+</sup> regulatory T cells and promote the development of colorectal cancer via enhancing CCL20 production in mice. *PLoS One* 2011; **6**(4): e19495.
155. Rodriguez PC, Zea AH, DeSalvo J, et al. L-arginine consumption by macrophages modulates the expression of CD3 zeta chain in T lymphocytes. *J Immunol* 2003; **171**(3): 1232-9.
156. Sharda DR, Yu S, Ray M, et al. Regulation of macrophage arginase expression and tumor growth by the Ron receptor tyrosine kinase. *J Immunol* 2011; **187**(5): 2181-92.
157. Kryczek I, Banerjee M, Cheng P, et al. Phenotype, distribution, generation, and functional and clinical relevance of Th17 cells in the human tumor environments. *Blood* 2009; **114**(6): 1141-9.
158. Kuang DM, Zhao Q, Peng C, et al. Activated monocytes in peritumoral stroma of hepatocellular carcinoma foster immune privilege and disease progression through PD-L1. *J Exp Med* 2009; **206**(6): 1327-37.
159. Noman MZ, Desantis G, Janji B, et al. PD-L1 is a novel direct target of HIF-1alpha, and its blockade under hypoxia enhanced MDSC-mediated T cell activation. *J Exp Med* 2014; **211**(5): 781-90.
160. De Palma M, Venneri MA, Galli R, et al. Tie2 identifies a hematopoietic lineage of proangiogenic monocytes required for tumor vessel formation and a mesenchymal population of pericyte progenitors. *Cancer Cell* 2005; **8**(3): 211-26.
161. Mazziere R, Pucci F, Moi D, et al. Targeting the ANG2/TIE2 axis inhibits tumor growth and metastasis by impairing angiogenesis and disabling rebounds of proangiogenic myeloid cells. *Cancer Cell* 2011; **19**(4): 512-26.
162. Wyckoff JB, Wang Y, Lin EY, et al. Direct visualization of macrophage-assisted tumor cell intravasation in mammary tumors. *Cancer Res* 2007; **67**(6): 2649-56.

163. Condeelis J, Pollard JW. Macrophages: obligate partners for tumor cell migration, invasion, and metastasis. *Cell* 2006; **124**(2): 263-6.
164. Bonde AK, Tischler V, Kumar S, Soltermann A, Schwendener RA. Intratumoral macrophages contribute to epithelial-mesenchymal transition in solid tumors. *BMC cancer* 2012; **12**: 35.
165. Kessenbrock K, Plaks V, Werb Z. Matrix metalloproteinases: regulators of the tumor microenvironment. *Cell* 2010; **141**(1): 52-67.
166. Rohan TE, Xue X, Lin HM, et al. Tumor microenvironment of metastasis and risk of distant metastasis of breast cancer. *Journal of the National Cancer Institute* 2014; **106**(8).
167. Kioi M, Vogel H, Schultz G, Hoffman RM, Harsh GR, Brown JM. Inhibition of vasculogenesis, but not angiogenesis, prevents the recurrence of glioblastoma after irradiation in mice. *J Clin Invest* 2010; **120**(3): 694-705.
168. Rolny C, Mazzone M, Tugues S, et al. HRG inhibits tumor growth and metastasis by inducing macrophage polarization and vessel normalization through downregulation of PlGF. *Cancer Cell* 2011; **19**(1): 31-44.
169. Shree T, Olson OC, Elie BT, et al. Macrophages and cathepsin proteases blunt chemotherapeutic response in breast cancer. *Genes Dev* 2011; **25**(23): 2465-79.
170. Welford AF, Biziato D, Coffelt SB, et al. TIE2-expressing macrophages limit the therapeutic efficacy of the vascular-disrupting agent combretastatin A4 phosphate in mice. *J Clin Invest* 2011; **121**(5): 1969-73.
171. Ciccia A, Elledge SJ. The DNA damage response: making it safe to play with knives. *Molecular cell* 2010; **40**(2): 179-204.
172. Torgovnick A, Schumacher B. DNA repair mechanisms in cancer development and therapy. *Front Genet* 2015; **6**: 157.
173. Hoeijmakers JH. DNA damage, aging, and cancer. *N Engl J Med* 2009; **361**(15): 1475-85.

174. Tacar O, Sriamornsak P, Dass CR. Doxorubicin: an update on anticancer molecular action, toxicity and novel drug delivery systems. *Journal of Pharmacy and Pharmacology* 2013; **65**(2): 157-70.
175. Lawley PD. Effects of some chemical mutagens and carcinogens on nucleic acids. *Progress in nucleic acid research and molecular biology* 1966; **5**: 89-131.
176. Giglia-Mari G, Zotter A, Vermeulen W. DNA damage response. *Cold Spring Harb Perspect Biol* 2011; **3**(1): a000745.
177. Deans AJ, West SC. DNA interstrand crosslink repair and cancer. *Nat Rev Cancer* 2011; **11**(7): 467-80.
178. Nikolova T, Kiweler N, Krämer OH. Interstrand Crosslink Repair as a Target for HDAC Inhibition. *Trends in Pharmacological Sciences* 2017; **38**(9): 822-36.
179. Harper JW, Elledge SJ. The DNA damage response: ten years after. *Mol Cell* 2007; **28**(5): 739-45.
180. Cann KL, Hicks GG. Regulation of the cellular DNA double-strand break response. *Biochem Cell Biol* 2007; **85**(6): 663-74.
181. Davis AJ, Chen BP, Chen DJ. DNA-PK: a dynamic enzyme in a versatile DSB repair pathway. *DNA Repair (Amst)* 2014; **17**: 21-9.
182. Gannon HS, Woda BA, Jones SN. ATM phosphorylation of Mdm2 Ser394 regulates the amplitude and duration of the DNA damage response in mice. *Cancer Cell* 2012; **21**(5): 668-79.
183. Shinozaki T, Nota A, Taya Y, Okamoto K. Functional role of Mdm2 phosphorylation by ATR in attenuation of p53 nuclear export. *Oncogene* 2003; **22**(55): 8870-80.
184. Bozulic L, Surucu B, Hynx D, Hemmings BA. PKBalpha/Akt1 acts downstream of DNA-PK in the DNA double-strand break response and promotes survival. *Mol Cell* 2008; **30**(2): 203-13.

185. Caspari T. Checkpoints: How to activate p53. *Current Biology* 2000; **10**(8): R315-R7.
186. Brooks CL, Gu W. p53 ubiquitination: Mdm2 and beyond. *Mol Cell* 2006; **21**(3): 307-15.
187. Lu X, Ma O, Nguyen TA, Jones SN, Oren M, Donehower LA. The Wip1 Phosphatase acts as a gatekeeper in the p53-Mdm2 autoregulatory loop. *Cancer Cell* 2007; **12**(4): 342-54.
188. Wang X, Taplick J, Geva N, Oren M. Inhibition of p53 degradation by Mdm2 acetylation. *FEBS Lett* 2004; **561**(1-3): 195-201.
189. Kruse JP, Gu W. Modes of p53 regulation. *Cell* 2009; **137**(4): 609-22.
190. Tang Y, Zhao W, Chen Y, Zhao Y, Gu W. Acetylation is indispensable for p53 activation. *Cell* 2008; **133**(4): 612-26.
191. Meek DW. Regulation of the p53 response and its relationship to cancer. *Biochem J* 2015; **469**(3): 325-46.
192. Riley T, Sontag E, Chen P, Levine A. Transcriptional control of human p53-regulated genes. *Nat Rev Mol Cell Biol* 2008; **9**(5): 402-12.
193. Mirza A, Wu Q, Wang L, et al. Global transcriptional program of p53 target genes during the process of apoptosis and cell cycle progression. *Oncogene* 2003; **22**(23): 3645-54.
194. Raman M, Earnest S, Zhang K, Zhao Y, Cobb MH. TAO kinases mediate activation of p38 in response to DNA damage. *EMBO J* 2007; **26**(8): 2005-14.
195. Reinhardt HC, Aslanian AS, Lees JA, Yaffe MB. p53-deficient cells rely on ATM- and ATR-mediated checkpoint signalling through the p38MAPK/MK2 pathway for survival after DNA damage. *Cancer Cell* 2007; **11**(2): 175-89.
196. Thornton TM, Rincon M. Non-classical p38 map kinase functions: cell cycle checkpoints and survival. *Int J Biol Sci* 2009; **5**(1): 44-51.

197. Phong MS, Van Horn RD, Li S, Tucker-Kellogg G, Surana U, Ye XS. p38 mitogen-activated protein kinase promotes cell survival in response to DNA damage but is not required for the G(2) DNA damage checkpoint in human cancer cells. *Mol Cell Biol* 2010; **30**(15): 3816-26.
198. Giordano FJ. Oxygen, oxidative stress, hypoxia, and heart failure. *J Clin Invest* 2005; **115**(3): 500-8.
199. Tsutsui H, Kinugawa S, Matsushima S. Oxidative stress and heart failure. *Am J Physiol Heart Circ Physiol* 2011; **301**(6): H2181-90.
200. Iyama T, Wilson DM, 3rd. DNA repair mechanisms in dividing and non-dividing cells. *DNA Repair (Amst)* 2013; **12**(8): 620-36.
201. Teive HA, Moro A, Moscovich M, et al. Ataxia-telangiectasia - A historical review and a proposal for a new designation: ATM syndrome. *Journal of the neurological sciences* 2015; **355**(1-2): 3-6.
202. O'Driscoll M, Ruiz-Perez VL, Woods CG, Jeggo PA, Goodship JA. A splicing mutation affecting expression of ataxia-telangiectasia and Rad3-related protein (ATR) results in Seckel syndrome. *Nat Genet* 2003; **33**(4): 497-501.
203. Kennedy RD, D'Andrea AD. The Fanconi Anemia/BRCA pathway: new faces in the crowd. *Genes Dev* 2005; **19**(24): 2925-40.
204. Pan MR, Li K, Lin SY, Hung WC. Connecting the Dots: From DNA Damage and Repair to Aging. *Int J Mol Sci* 2016; **17**(5).
205. O'Connor MJ. Targeting the DNA Damage Response in Cancer. *Mol Cell* 2015; **60**(4): 547-60.
206. Jackson SP, Bartek J. The DNA-damage response in human biology and disease. *Nature* 2009; **461**(7267): 1071-8.
207. Begg AC, Stewart FA, Vens C. Strategies to improve radiotherapy with targeted drugs. *Nat Rev Cancer* 2011; **11**(4): 239-53.
208. Chabner BA, Roberts TG, Jr. Timeline: Chemotherapy and the war on cancer. *Nat Rev Cancer* 2005; **5**(1): 65-72.

209. Zack E. Chemotherapy and biotherapeutic agents for autoimmune diseases. *Clin J Oncol Nurs* 2012; **16**(4): E125-32.
210. Zitvogel L, Apetoh L, Ghiringhelli F, Kroemer G. Immunological aspects of cancer chemotherapy. *Nat Rev Immunol* 2008; **8**(1): 59-73.
211. Wumkes ML, van der Velden AMT, Los M, et al. Serum antibody response to influenza virus vaccination during chemotherapy treatment in adult patients with solid tumours. *Vaccine* 2013; **31**(52): 6177-84.
212. Ma Y, Adjemian S, Mattarollo SR, et al. Anticancer chemotherapy-induced intratumoral recruitment and differentiation of antigen-presenting cells. *Immunity* 2013; **38**(4): 729-41.
213. Ma Y, Aymeric L, Locher C, et al. Contribution of IL-17-producing gamma delta T cells to the efficacy of anticancer chemotherapy. *J Exp Med* 2011; **208**(3): 491-503.
214. Ruffell B, Au A, Rugo HS, Esserman LJ, Hwang ES, Coussens LM. Leukocyte composition of human breast cancer. *Proc Natl Acad Sci U S A* 2012; **109**(8): 2796-801.
215. Sistigu A, Yamazaki T, Vacchelli E, et al. Cancer cell-autonomous contribution of type I interferon signalling to the efficacy of chemotherapy. *Nat Med* 2014; **20**(11): 1301-9.
216. Yamazaki T, Hannani D, Poirier-Colame V, et al. Defective immunogenic cell death of HMGB1-deficient tumors: compensatory therapy with TLR4 agonists. *Cell death and differentiation* 2014; **21**(1): 69-78.
217. Kroemer G, Galluzzi L, Kepp O, Zitvogel L. Immunogenic Cell Death in Cancer Therapy. *Annual Review of Immunology* 2013; **31**(1): 51-72.
218. Alizadeh D, Trad M, Hanke NT, et al. Doxorubicin eliminates myeloid-derived suppressor cells and enhances the efficacy of adoptive T-cell transfer in breast cancer. *Cancer Res* 2014; **74**(1): 104-18.

219. Shalapour S, Font-Burgada J, Di Caro G, et al. Immunosuppressive plasma cells impede T-cell-dependent immunogenic chemotherapy. *Nature* 2015; **521**: 94.
220. Lesterhuis WJ, Punt CJ, Hato SV, et al. Platinum-based drugs disrupt STAT6-mediated suppression of immune responses against cancer in humans and mice. *J Clin Invest* 2011; **121**(8): 3100-8.
221. Liu WM, Fowler DW, Smith P, Dalglish AG. Pre-treatment with chemotherapy can enhance the antigenicity and immunogenicity of tumours by promoting adaptive immune responses. *Br J Cancer* 2010; **102**(1): 115-23.
222. Schiavoni G, Sistigu A, Valentini M, et al. Cyclophosphamide Synergizes with Type I Interferons through Systemic Dendritic Cell Reactivation and Induction of Immunogenic Tumor Apoptosis. *Cancer Research* 2011; **71**(3): 768-78.
223. Iida N, Dzutsev A, Stewart CA, et al. Commensal bacteria control cancer response to therapy by modulating the tumor microenvironment. *Science* 2013; **342**(6161): 967-70.
224. Viaud S, Saccheri F, Mignot G, et al. The intestinal microbiota modulates the anticancer immune effects of cyclophosphamide. *Science* 2013; **342**(6161): 971-6.
225. Ghiringhelli F, Menard C, Puig PE, et al. Metronomic cyclophosphamide regimen selectively depletes CD4+CD25+ regulatory T cells and restores T and NK effector functions in end stage cancer patients. *Cancer Immunology, Immunotherapy* 2007; **56**(5): 641-8.
226. Guerriero JL, Ditsworth D, Catanzaro JM, et al. DNA alkylating therapy induces tumor regression through an HMGB1-mediated activation of innate immunity. *J Immunol* 2011; **186**(6): 3517-26.
227. Medina-Echeverz J, Fioravanti J, Zabala M, Ardaiz N, Prieto J, Berraondo P. Successful colon cancer eradication after chemoimmunotherapy

is associated with profound phenotypic change of intratumoral myeloid cells. *J Immunol* 2011; **186**(2): 807-15.

228. Pallasch CP, Leskov I, Braun CJ, et al. Sensitizing protective tumor microenvironments to antibody-mediated therapy. *Cell* 2014; **156**(3): 590-602.

229. Di Caro G, Cortese N, Castino GF, et al. Dual prognostic significance of tumour-associated macrophages in human pancreatic adenocarcinoma treated or untreated with chemotherapy. *Gut* 2016; **65**(10): 1710-20.

230. Nowak AK, Lake RA, Marzo AL, et al. Induction of Tumor Cell Apoptosis In Vivo Increases Tumor Antigen Cross-Presentation, Cross-Priming Rather than Cross-Tolerizing Host Tumor-Specific CD8 T Cells. *The Journal of Immunology* 2003; **170**(10): 4905-13.

231. Liechtenstein T, Perez-Janices N, Gato M, et al. A highly efficient tumor-infiltrating MDSC differentiation system for discovery of anti-neoplastic targets, which circumvents the need for tumor establishment in mice. *Oncotarget* 2014; **5**(17): 7843-57.

232. Roselli M, Cereda V, di Bari MG, et al. Effects of conventional therapeutic interventions on the number and function of regulatory T cells. *Oncolimmunology* 2013; **2**(10): e27025.

233. Senovilla L, Vitale I, Martins I, et al. An Immunosurveillance Mechanism Controls Cancer Cell Ploidy. *Science* 2012; **337**(6102): 1678-84.

234. unknown. CellTiter-Glo® Luminescent Cell Viability Assay Instructions for Use of Products G7570, G7571, G7572 and G7573. 03.2015 2015. [https://www.promega.de/-/media/files/resources/protocols/technical-bulletins/0/celltiter-glo-luminescent-cell-viability-assay-protocol.pdf?rev=0d95c232094b41daa06d0c110d1d916f&sc\\_lang=en](https://www.promega.de/-/media/files/resources/protocols/technical-bulletins/0/celltiter-glo-luminescent-cell-viability-assay-protocol.pdf?rev=0d95c232094b41daa06d0c110d1d916f&sc_lang=en) (accessed 08.03.2022 2022).

235. unknown. User Guide Pierce™ BCA Protein Assay Kit. 30.01.2020 2020. <https://assets.thermofisher.com/TFS->

Assets/LSG/manuals/MAN0011430\_Pierce\_BCA\_Protein\_Asy\_UG.pdf  
(accessed 08.03.2022 2022).

236. Beletskii A, Cooper M, Sriraman P, et al. High-throughput phagocytosis assay utilizing a pH-sensitive fluorescent dye. *Biotechniques* 2005; **39**(6): 894-7.

237. Liang J, Huang M, Duan W, Yu X-Q, Zhou S. Design of new oxazaphosphorine anticancer drugs. *Current pharmaceutical design* 2007; **13**(9): 963-78.

238. Coiffier B, Thieblemont C, Van Den Neste E, et al. Long-term outcome of patients in the LNH-98.5 trial, the first randomized study comparing rituximab-CHOP to standard CHOP chemotherapy in DLBCL patients: a study by the Groupe d'Etudes des Lymphomes de l'Adulte. *Blood* 2010: blood-2010-03-276246.

239. Hallek M, Fischer K, Fingerle-Rowson G, et al. Addition of rituximab to fludarabine and cyclophosphamide in patients with chronic lymphocytic leukaemia: a randomised, open-label, phase 3 trial. *The Lancet* 2010; **376**(9747): 1164-74.

240. DeNardo DG, Brennan DJ, Rexhepaj E, et al. Leukocyte complexity predicts breast cancer survival and functionally regulates response to chemotherapy. *Cancer discovery* 2011.

241. Shree T, Olson OC, Elie BT, et al. Macrophages and cathepsin proteases blunt chemotherapeutic response in breast cancer. *Genes & development* 2011; **25**(23): 2465-79.

242. Jinushi M, Chiba S, Yoshiyama H, et al. Tumor-associated macrophages regulate tumorigenicity and anticancer drug responses of cancer stem/initiating cells. *Proceedings of the National Academy of Sciences* 2011; **108**(30): 12425-30.

243. Mantovani A, Polentarutti N, Luini W, Peri G, Spreafico F. Role of host defense mechanisms in the antitumor activity of adriamycin and daunomycin in mice. *Journal of the National Cancer Institute* 1979; **63**(1): 61-6.
244. Moore M, Williams DE. Contribution of host immunity to cyclophosphamide therapy of a chemically-induced murine sarcoma. *International journal of cancer* 1973; **11**(2): 358-68.
245. Steele G, Pierce GE. Effects of cyclophosphamide on immunity against chemically-induced syngeneic murine sarcomas. *International journal of cancer* 1974; **13**(4): 572-8.
246. Galletti G, Scielzo C, Barboglio F, et al. Targeting macrophages sensitizes chronic lymphocytic leukaemia to apoptosis and inhibits disease progression. *Cell reports* 2016; **14**(7): 1748-60.
247. Aakanksha Bansal RN, Elena Izquierdo-Alvarez, Daniela Vorholt, Henning Feldkötter, Hendrik Nolte PL, Reinhard Büttner, Markus Krüger, Christian P. Pallasch and Björn Schumacher. ATM-mediated DNA damage response in macrophages primes phagocytosis and immune checkpoint regulation. [www.biorxiv.com](http://www.biorxiv.com); 2020.
248. Vogel DY, Glim JE, Stavenuiter AW, et al. Human macrophage polarization in vitro: maturation and activation methods compared. *Immunobiology* 2014; **219**(9): 695-703.
249. Krombach F, Münzing S, Allmeling A-M, Gerlach JT, Behr J, Dörger M. Cell size of alveolar macrophages: an interspecies comparison. *Environmental health perspectives* 1997; **105**(Suppl 5): 1261.
250. Petty HR. Influence of Neuroendocrine Mediators on Phagocyte Function: WAYNE STATE UNIV DETROIT MI DEPT OF BIOLOGICAL SCIENCES, 1988.
251. Liberale L, Dallegri F, Montecucco F, Carbone F. Pathophysiological relevance of macrophage subsets in atherogenesis. *Thromb Haemost* 2017; **117**(1): 7-18.

252. Wang LX, Zhang SX, Wu HJ, Rong XL, Guo J. M2b macrophage polarization and its roles in diseases. *J Leukoc Biol* 2019; **106**(2): 345-58.
253. Gensel JC, Zhang B. Macrophage activation and its role in repair and pathology after spinal cord injury. *Brain Res* 2015; **1619**: 1-11.
254. Freeman GJ, Long AJ, Iwai Y, et al. Engagement of the PD-1 immunoinhibitory receptor by a novel B7 family member leads to negative regulation of lymphocyte activation. *J Exp Med* 2000; **192**(7): 1027-34.
255. Langer CJ, Gadgeel SM, Borghaei H, et al. Carboplatin and pemetrexed with or without pembrolizumab for advanced, non-squamous non-small-cell lung cancer: a randomised, phase 2 cohort of the open-label KEYNOTE-021 study. *Lancet Oncol* 2016; **17**(11): 1497-508.
256. Socinski MA, Jotte RM, Cappuzzo F, et al. Atezolizumab for First-Line Treatment of Metastatic Nonsquamous NSCLC. *N Engl J Med* 2018; **378**(24): 2288-301.
257. Benoit M, Desnues B, Mege JL. Macrophage polarization in bacterial infections. *J Immunol* 2008; **181**(6): 3733-9.
258. Lasser A. The mononuclear phagocytic system: a review. *Human pathology* 1983; **14**(2): 108-26.
259. Schulz D, Severin Y, Zanotelli VRT, Bodenmiller B. In-Depth Characterization of Monocyte-Derived Macrophages using a Mass Cytometry-Based Phagocytosis Assay. *Sci Rep* 2019; **9**(1): 1925.
260. Allavena P, Chieppa M, Monti P, Piemonti L. From pattern recognition receptor to regulator of homeostasis: the double-faced macrophage mannose receptor. *Crit Rev Immunol* 2004; **24**(3): 179-92.
261. Storm G, Steerenberg PA, Emmen F, van Borssum Waalkes M, Crommelin DJA. Release of doxorubicin from peritoneal macrophages exposed in vivo to doxorubicin-containing liposomes. *Biochimica et Biophysica Acta (BBA) - General Subjects* 1988; **965**(2): 136-45.

262. Reichner JS, Fitzpatrick PA, Wakshull E, Albina JE. Receptor-mediated phagocytosis of rat macrophages is regulated differentially for opsonized particles and non-opsonized particles containing  $\beta$ -glucan. *Immunology* 2001; **104**(2): 198-206.
263. Yamamori T, Inanami O, Nagahata H, Cui Y-D, Kuwabara M. Roles of p38 MAPK, PKC and PI3-K in the signalling pathways of NADPH oxidase activation and phagocytosis in bovine polymorphonuclear leukocytes. *FEBS Letters* 2000; **467**(2-3): 253-8.
264. Zuliani JP, Gutiérrez JM, Teixeira C. Signalling pathways involved in zymosan phagocytosis induced by two secreted phospholipases A2 isolated from Bothrops asper snake venom in macrophages. *International Journal of Biological Macromolecules* 2018; **113**: 575-82.
265. Fritz G, Henninger C. Rho GTPases: Novel Players in the Regulation of the DNA Damage Response? *Biomolecules* 2015; **5**(4).
266. Ninković J, Roy S. Morphine Decreases Bacterial Phagocytosis by Inhibiting Actin Polymerization through cAMP-, Rac-1-, and p38 MAPK-Dependent Mechanisms. *The American Journal of Pathology* 2012; **180**(3): 1068-79.
267. Zhang X, Liu Z, Xu B, Sun Z, Gong Y, Shao C. Neferine, an alkaloid ingredient in lotus seed embryo, inhibits proliferation of human osteosarcoma cells by promoting p38 MAPK-mediated p21 stabilization. *Eur J Pharmacol* 2012; **677**(1-3): 47-54.
268. Ehrke MJ, Cohen SA, Mihich E. Selective effects of Adriamycin on murine host defense systems. *Immunological reviews* 1982; **65**(1): 55-78.

## 8 Appendices

### 8.1 Supplemental Data

#### 8.1.1 Supplemental WB

The results for p53 induction in macrophages through Mafosfamide and Doxorubicin treatment, shown in 5.2, were validated by additional WBs. These were performed on a different day with a different culture of J774A.1 following the same protocol (see 4.2.3). The concentration of 5 $\mu$ M was not used in these experiments. The same tendency in the induction of p53 for higher doses of the chemotherapeutics was seen.

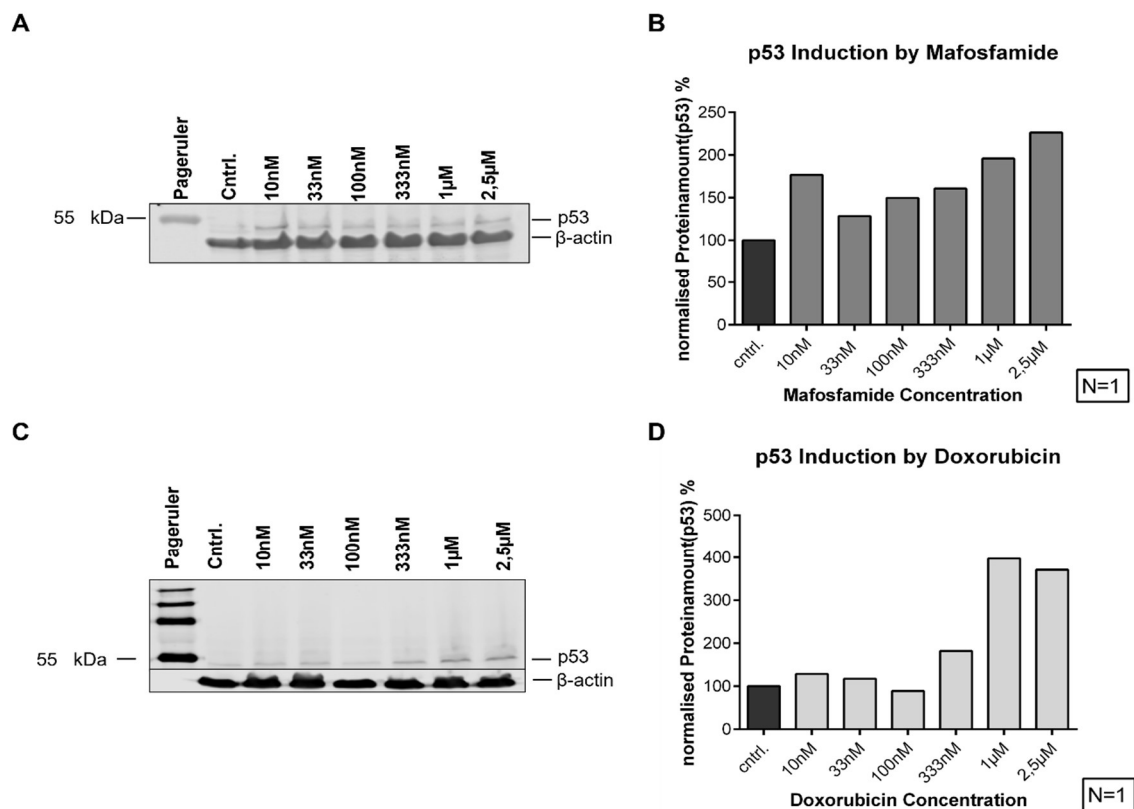


**Figure 18: Induction of p53 by Mafosfamide and Doxorubicin**

J774A.1 were treated with different concentrations of Mafosfamide and Doxorubicin, lysed, separated according to molecular weight by SDS-PAGE and blotted onto a nitrocellulose membrane via WB. The blot with p53 and  $\beta$ -actin staining is shown for Mafosfamide (**A**) and Doxorubicin (**C**). For Doxorubicin two scans had to be utilized, because the  $\beta$ -actin staining was too intense to display the p53 staining on the same scan. p53 fluorescence was normalised to  $\beta$ -actin and compared to normalised p53 levels of the untreated control (**B** and **D**). The results of one WB are shown here.

### 8.1.2 Supplemental figure of bacteria to macrophage ratio dependency

In Figure 10 not all significances were shown, due to clarity reasons. The following figure shows every significance, which was calculated with the obtained data.

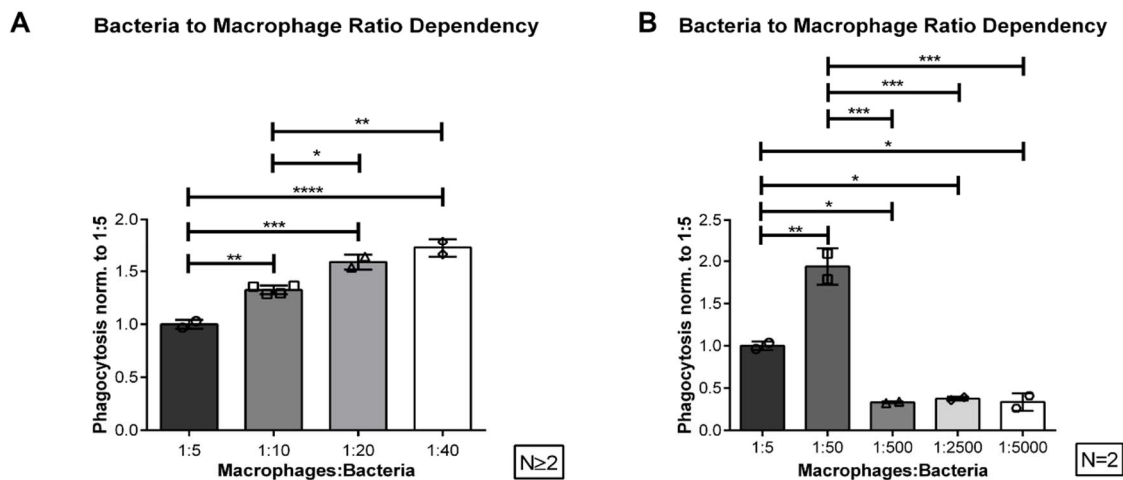


**Figure 19: Dependency of the phagocytic capacity on the bacteria to macrophage ratio with all calculated significances**

J774A.1, plated out in the same concentration, were incubated with different amounts of bacteria, resulting in macrophage to bacteria ratios as labelled. The double positive cell rate, for dsRED and the VioGreen anti-CD11b antibody, was measured and then normalised to the double positive cell rate of the 1:5 ratio. Ratios varied from 1:5 to 1:5000 (A, B). Data are expressed as mean +/- SD. The experiment was performed once with at least 2 biological replicates per condition, leading to a sample size of N≥2 or N=2. (\*=p<0.05; \*\*=p<0.01; \*\*\*=p<0.001; \*\*\*\*=p<0.0001)

### 8.1.3 Supplemental figure of bead to macrophage ratio dependency

In Figure 14 not all significances were shown, due to clarity reasons. The following figure shows every significance, which was calculated with the obtained data.

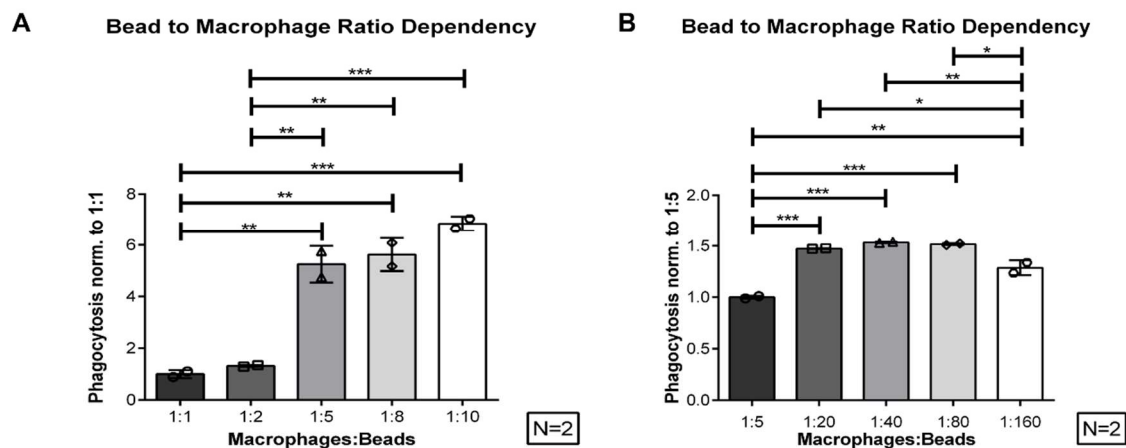


**Figure 20: Impact of the bead to macrophage ratio on the phagocytosis of J774A.1 with all calculated significances**

J774A.1 were plated out in the same concentrations, before being incubated with different amounts of pH-sensitive beads. The double positive cells, for CypHer5E and the VioGreen anti-CD11b antibody, were measured and then normalised to the bead to macrophage ratio of 1:1 (A) or 1:5 (B). Data are expressed as mean +/- SD. The experiment was performed once with two biological replicates, resulting in a sample size of N=2. (\*=p<0.05; \*\*=p<0.01; \*\*\*=p<0.001; \*\*\*\*=p<0.0001)

## 8.1.4 Modification to the BCG-phagocytosis assay

### 8.1.4.1 Method

To even out the differences in the bacteria to macrophage ratio in between the different conditions, a modification of the BCG-phagocytosis assay was developed. Macrophages and bacteria were prepared as described in 4.2.5.1. According to macrophage counts in previous experiments, different bacteria amounts were added, in 100µl 7H9 medium, to each condition with the intent of accomplishing a ratio of 5 bacteria per macrophage in every condition. After adding the bacteria, the experiment was continued as described in 4.2.5.1. The bacteria to macrophage ratio for each condition was calculated by dividing the bacteria amount, which was added to the condition, by the macrophage count of the respective condition, which was obtained via FACS.

### 8.1.4.2 Results

In this modification the added bacteria amount for each condition was adapted to previous macrophage counts in earlier experiments to balance the bacteria to macrophage ratios in between the different conditions and reach a bacteria to

macrophage ratio of 5 to 1 (see 8.1.4.1). The respective chemotherapeutics were used in a concentration of 5 $\mu$ M. In Figure 21 two separate experiments, in which the modification was utilized, are shown to illustrate the problems, which arose with this modification. In the first experiment Mafosfamide and Doxorubicin treatment did not show a significant effect on the normalised phagocytosis with means of 0.9 for Mafosfamide and 1.1 for Doxorubicin, compared to the untreated control (Figure 21 A). The differences in the bacteria to macrophage ratio were reversed compared to unmodified BCG-phagocytosis assays and displayed a significant difference between the untreated control and the treated conditions (Figure 21 B; see **Figure 9 B**, Figure 11 B, D). The mean bacteria to macrophage ratio for the untreated control was 6.8 bacteria per macrophage, for 5 $\mu$ M Mafosfamide it was 1.5 and 5 $\mu$ M Doxorubicin showed a ratio of 1.6 (Figure 21 B). A significant increase in the normalised phagocytosis was seen in the second experiment with means of 1.9 for 5 $\mu$ M Mafosfamide and 2 for 5 $\mu$ M Doxorubicin (Figure 21 C). The bacteria to macrophage ratio did not display significant differences, but was also reversed as described for the first experiment. The untreated control showed a mean bacteria to macrophage ratio of 3.7 bacteria per macrophage, 5 $\mu$ M Mafosfamide and 5 $\mu$ M Doxorubicin displayed a ratio of 1.9 and 1.7 respectively (Figure 21 D). The reversed bacteria to macrophage ratio led to the question of how consistent the macrophage counts were in between different experiments.

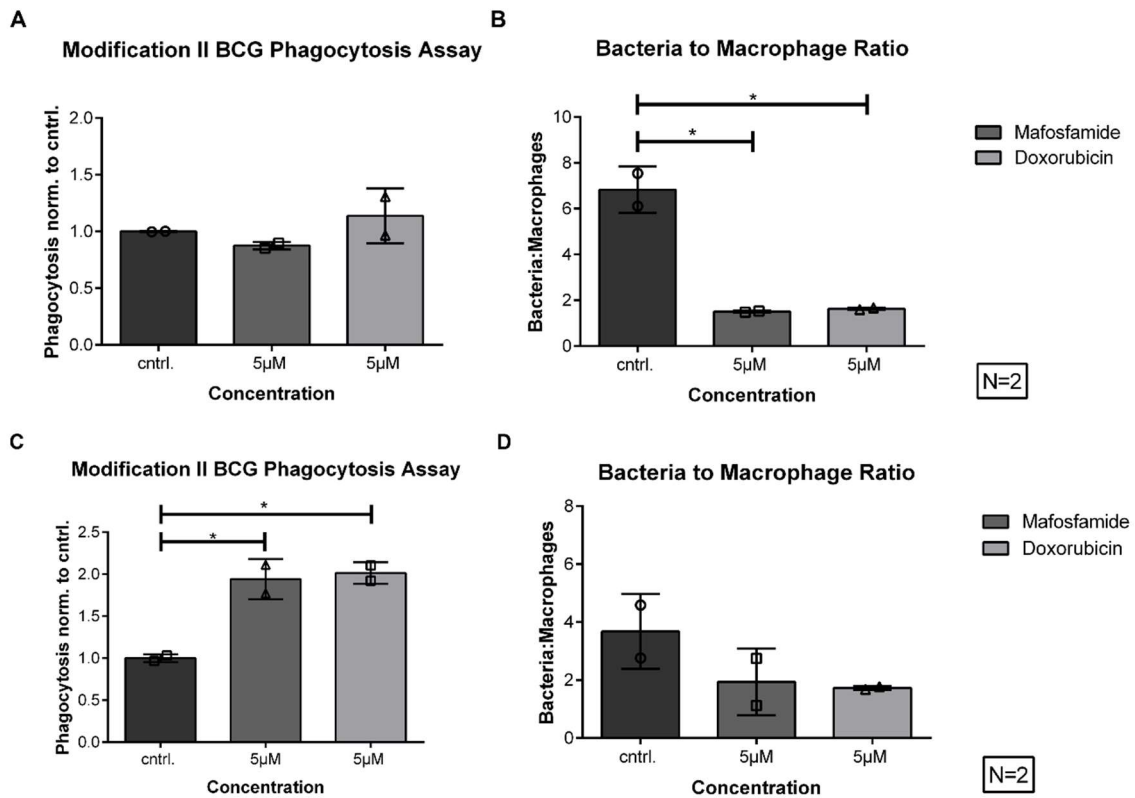


**Figure 21: Modification of the BCG-phagocytosis assay led to adverse effect on bacteria to macrophage ratio**

J774A.1 were treated with 5 $\mu$ M Mafosfamide or Doxorubicin before being used for a BCG-phagocytosis assay. The bacteria amount added to each condition was altered in respect to macrophage counts in previous experiments. The rate of double positive cells, for dsRED and the VioGreen anti-CD11b antibody, was identified and then normalised to the double positive cell rate of the respective control (A, C). Macrophage cell count and number of used bacteria per condition were put into relation, resulting in the bacteria to macrophage ratio (B, D). Data are expressed as mean +/- SD. The experiments were performed once with two biological replicates, leading to a sample size of N=2. (\*=p<0.05; \*\*=p<0.01; \*\*\*=p<0.001; \*\*\*\*=p<0.0001)

To elucidate the fluctuations of macrophage cell counts in between different BCG-phagocytosis assays, the mean cell counts for the untreated control, 5 $\mu$ M Mafosfamide and 5 $\mu$ M Doxorubicin of different experiments are displayed in separate graphs. A high standard deviation of the cell counts was observed for every condition with extremes ranging from 521340 cells per well to 47476 cells for the untreated control, 79708 to 8616 cells for 5 $\mu$ M Mafosfamide and 46316 to 8176 cells for 5 $\mu$ M Doxorubicin (Figure 22 A, B, C). This offered some explanation for the problems, which arose with the described modification.

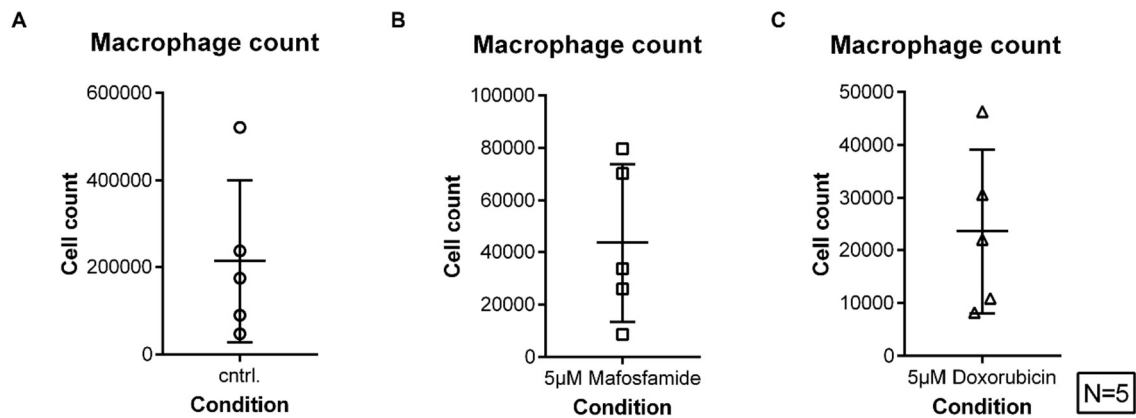


**Figure 22: Macrophage cell counts of different BCG-phagocytosis assays**

Macrophage cell counts from different experiments are displayed. The cell counts were obtained by flowcytometry at the end of the respective BCG-phagocytosis assay and are displayed as mean of two biological replicates from the same experiment for the untreated control, 5µM Mafosfamide and 5µM Doxorubicin (**A**, **B**, **C**). Data are expressed as mean +/- SD and N=5.

#### 8.1.4.3 Discussion

To eliminate the influence of the varying bacteria to macrophage ratios, in between the different conditions, on the phagocytic capacity, a modification of the BCG-phagocytosis assay was tested. For this modification the added bacteria amounts were adapted for each condition according to macrophage counts of the respective condition in previous experiments. Through this modification the bacteria to macrophage ratios were reversed, leading to higher ratios for the untreated control than the treated conditions. For one experiment a significant increase in the phagocytic capacity after treatment was still seen, which endorsed the impact of chemotherapy on macrophages seen in the other experiments (see 5.7, 5.11, 8.1.4.2). Because the bacteria to macrophage ratios were still differing and were lower than the intended ratio of 5 bacteria per macrophage for the treated conditions, it could not be cancelled out that the phagocytic capacity of the treated macrophages exceeded the number of bacteria added to the respective conditions, potentially leading to inaccurately low phagocytosis rates. An explanation for the inaccurate equalization of the bacteria to macrophage ratios was found, after looking at the macrophage counts of the respective conditions in different experiments. It was apparent that the macrophage counts of one condition vary in between different experiments,

which could be caused by fluctuating levels of adhesive capability of the macrophages in between the experiments, varying generation cycles or unknown external reasons. Leading to the recognition that the macrophage counts cannot be predicted reliably from one experiment to the other, this modification of the BCG-phagocytosis assay was discontinued, because of impracticability and the existence of a more feasible modification (see 4.2.5.4).

## 8.2 List of Tables

<b>Table 1: Recipe for separating and stacking gel .....</b>	<b>52</b>
--	-----------

### 8.3 List of Figures

<b>Figure 1: Polarisation states of macrophages (modified from<sup>74</sup>)</b> .....	23
<b>Figure 2: Role of the TME in preventing tumors, tumorigenesis and tumor progression<sup>102</sup></b> .....	29
<b>Figure 3 Extract of the DNA damage response pathway</b> .....	35
<b>Figure 4 Viability Assay of J774A.1 treated with different concentrations of Mafosfamide and Doxorubicin.</b> .....	61
<b>Figure 5: Induction of p53 and pp53 by Mafosfamide</b> .....	63
<b>Figure 6: Induction of p53 and pp53 by Doxorubicin</b> .....	64
<b>Figure 7: Microscopy pictures of untreated and treated J774A.1 macrophages with pH-sensitive beads</b> .....	66
<b>Figure 8: Analysis of microscopy pictures</b> .....	68
<b>Figure 9: Mafosfamide and Doxorubicin increased the non-opsonised phagocytosis of J774A.1 macrophages</b> .....	70
<b>Figure 10: Dependency of the phagocytic capacity on the bacteria to macrophage ratio</b> .....	71
<b>Figure 11: Lower Mafosfamide and Doxorubicin concentrations increased the non-opsonised phagocytosis of murine macrophages</b> .....	73
<b>Figure 12: Mafosfamide and Doxorubicin increased the phagocytic capacity of murine macrophages independent from the bacteria to macrophage ratio.</b> .....	74
<b>Figure 13: Effect of conditioned media on the phagocytic capacity of J774A.1</b> .....	76
<b>Figure 14: Impact of the bead to macrophage ratio on the phagocytosis of J774A.1</b> .....	77
<b>Figure 15: 5µM Mafosfamide and Doxorubicin increased pH-sensitive bead phagocytosis by murine macrophages</b> .....	78
<b>Figure 16: Lower concentrations of Mafosfamide and Doxorubicin increase phagocytosis of pH-sensitive beads by murine macrophages</b> ...	79
<b>Figure 17: Mafosfamide and Doxorubicin increased the phagocytic capacity of murine macrophages in a modified pH-sensitive bead phagocytosis assay</b> .....	81
<b>Figure 18: Induction of p53 by Mafosfamide and Doxorubicin</b> .....	125

<b>Figure 19: Dependency of the phagocytic capacity on the bacteria to macrophage ratio with all calculated significances .....</b>	<b>126</b>
<b>Figure 20: Impact of the bead to macrophage ratio on the phagocytosis of J774A.1 with all calculated significances.....</b>	<b>127</b>
<b>Figure 21: Modification of the BCG-phagocytosis assay led to adverse effect on bacteria to macrophage ratio .....</b>	<b>129</b>
<b>Figure 22: Macrophage cell counts of different BCG-phagocytosis assays .....</b>	<b>130</b>